UCSF
UC San Francisco Electronic Theses and Dissertations

Title
Object size classification and sensorimotor decision making in the larval zebrafish

Permalink
https://escholarship.org/uc/item/7h41t528

Author
Barker, Alison Joyce

Publication Date
2015

Peer reviewed|Thesis/dissertation

eScholarship.org Powered by the California Digital Library
University of California

Object size classification and sensorimotor decision making in the larval zebrafish

by

Alison J Barker

DISSERTATION

Submitted in partial satisfaction of the requirements for the degree of

DOCTOR OF PHILOSOPHY

in

Neuroscience

in the

GRADUATE DIVISION

of the

UNIVERSITY OF CALIFORNIA, SAN FRANCISCO

Copyright 2015

by

Alison J. Barker

Acknowledgements:

First and foremost I thank Herwig Baier for his continued support and scientific guidance.

I thank the members of my thesis committee, David Copenhagen, Michael Stryker and Michael Brainard for their advice and counsel. I especially thank Russell Fernald for agreeing to serve as my external committee member.

I thank all members of the Baier lab past and present, especially Joe Donovan and Alessandro Filosa for collaborative efforts and discussions and Tod Thiele and Duncan Mearns for being enthusiastic and engaging desk mates. I thank Michael Stryker and Jonathan Horton for their inspiring class on the Neurobiology of Vision which early in my graduate career reaffirmed my decision to study visual neuroscience. I thank my first mentor at UCSF, Erik Ullian and past and present members of the Ullian lab as well as the professors who gave me the opportunity to rotate through their labs: Christoph Schreiner, Linda Wilbrecht and Michael Stryker. I thank Rob Froemke, Sunil Gandhi and Cris Niell for their direct mentorship.

I was fortunate to experience the new unique situation of splitting my PhD research across two countries in two institutes. I thank members of the Max Planck Institute of Neurobiology in Martinsried, Germany who welcomed me with friendship and scientific camaraderie.

I thank my classmates, members of the NS09 entering class for their friendship and intelligence. I am greatly indebted to the efforts of Louis Reichardt and the administration of the Neuroscience

Program and Graduate School, Pat Veitch, Carrie Huckaba, Lucita Nacionales and Rick Wyllie who helped negotiate the many and varied administrative hurdles of a transatlantic PhD.

Finally I thank my family and dedicate this work to them.

Work in this thesis has been previously published in the following two manuscripts. Project conception and implementation were supervised by Herwig Baier who in collaboration with Alison Barker wrote the manuscripts. The text of Chapter 2 and Chapter 3 is a reprint of the material as it appears in “Sensorimotor Decision Making in the Zebrafish Tectum”. The co-author listed in this publication directed and supervised the research that forms the basis for the dissertation/thesis. In Chapter 4, Figure 30 is reprinted from “SINs and SOMs: neural microcircuits for size tuning in the zebrafish and mouse visual pathway”.

Barker, A.J., and Baier, H. (2013). SINs and SOMs: neural microcircuits for size tuning in the zebrafish and mouse visual pathway. Front. Neural Circuits *7*, 89.

Barker, A.J., and Baier, H. (2015). Sensorimotor Decision Making in the Zebrafish Tectum. Curr Biol. 25, 2804–2814.

This work was supported by an NSF Graduate Research Fellowship and the Max Planck Society.

Object size classification and sensorimotor decision making in the larval zebrafish

Alison J Barker

Abstract

An organism's survival depends on its success in evading threats and acquiring resources. These basic needs require that sensory information be processed to maximize behavioral outputs in a given environment. The appropriate classification of visual objects can be used to drive context specific behavior (e.g. avoiding potential threats or pursuing potential food sources). In this work using the larval zebrafish as a model, I explore two central questions: How is visual information classified? Where along the visuomotor pathway is "positive" or "negative" value assigned to perceived objects? This work succeeds in linking visual perception (evaluation of object size) to action selection (deciding between approach and avoidance). Chapter 2 describes the development of behavioral paradigms to evaluate object size classification. A free swimming assay for the larval zebrafish was developed that elicited both approach and avoidance through the presentation of moving dots of different sizes. This assay was used to identify neural components mediating both approach and avoidance behaviors. Chapters 3 and 4 investigate the roles of specific neuronal populations that contribute to the implementation of size-mediated behaviors. A significant advance is the identification of a population of glutamatergic interneurons residing in the optic tectum which are components of a neural pathway for approach towards small objects. Ablation of these neurons results in a shift from approach to avoidance when small moving dots are presented. Conversely activating these interneurons enhances approaches to small dots. These results suggests that neural circuits in the optic tectum are actively involved in object classification which biases behavioral output towards approach or avoidance.

Table of Contents

Acknowledgements….....iii

Abstract.....vi

List of Figures……...viii

Chapter 1……1
General Introduction

Chapter 2……..……13
Object size classification in the larval zebrafish, behavioral readouts for decision-making

Chapter 3……..……37
Sensorimotor decision-making in the zebrafish tectum

Chapter 4……..……64
Investigating the role of the SINs in size selective behaviors

Chapter 5……...74
General Discussion

Chapter 6…….. 78
Materials and Methods

List of Figures

Figure 1……3
Figure 2……5
Figure 3……9
Figure 4……16
Figure 5……17
Figure 6……18
Figure 7……19
Figure 8……19
Figure 9……21
Figure 10……22
Figure 11……23
Figure 12……24
Figure 13……24
Figure 14……26
Figure 15……28
Figure 16……29
Figure 17……30
Figure 18……31
Figure 19……39
Figure 20……41
Figure 21……43
Figure 22……44
Figure 23……44
Figure 24……45
Figure 25……47
Figure 26……48
Figure 27……49
Figure 28……52
Figure 29……53
Figure 30……65
Figure 31……66

Figure 32.....67
Figure 33.....69
Figure 34.....69
Figure 35.....76
Figure 36.....88
Figure 37.....89
Figure 38.....90
Figure 39.....91

Chapter 1: General Introduction

Extracting visual features relevant for behavior

How we interact with our environments is shaped by the type and quality of sensory information we receive. Neuroscientists have long been driven to understand how our brains are able to process this information to drive behavior. Understanding our interaction with the visual world presents a unique set of questions: How is the visual environment characterized by the brain? Are ecologically relevant features or objects overly represented? How sparse or complete is this representation? Where does it reside in the brain? A critical first step is understanding how the features of the visual world are detected. In vertebrates the retina is the first processor of visual information and itself a highly complex information filter. Entering light passes through the lens to the back of the eye where it is absorbed by the photoreceptors. The signal received by the photoreceptors is processed by the intricate intraretinal circuit and arrives at the retina's output neurons, the retinal ganglion cells (RGCs) (Kandel et al., 2000). Early experiments in the retina by Hartline and Barlow identified the center-surround receptive field (RF)s of the RGCs (Barlow, 1953; Hartline, 1938, 1940a, 1940b, Kuffler, 1953). The center-surround RF structure allows the retina to extract information about contrast and movement across the visual area it samples.

The realization that the retina was tuned to extract specific visual features led to the identification of additional types of specialized RGCs. Lettvin reported four types of RGCs in the frog retina: "the contrast detector", "the convexity detector", "the moving-edge detector" and the "dimming detector" (Lettvin et al., 1959). At the same time, Hubel and Wiesel began their now famous experiments in the cat visual cortex, discovering that visual cortical neurons act as local edge detectors. In contrast to the spots of light that optimally drove RGC firing, neurons in V1 were tuned to the orientation of moving bars (Hubel and Wiesel, 1959). This provided the

framework for the feature selectivity of neurons in the visual system. RGCs are tuned to extract certain features, such as motion, size, color, and contrast. These visual streams are later combined to generate representations of the visual world, allowing the brain to extract salient features of the visual environment. While many of these characterizations were initially oversimplified, the shift in intellectual framework was revolutionary.

Working in amphibians, *Rana pipiens* and *Bufo bufo*, David Ingle and Jörg-Peter Ewert began to link visual perception to behavior. They were motivated by the hypothesis that certain visual features were essential for "unlocking" fixed behavioral repertoires. Indeed, they found just this. Ewert reported that toads reliably responded to a moving black disk with approach and orienting behaviors at small sizes (<16°) and with avoidance behaviors at larger sizes (> 30°). (See Figure 1, Ewert, 1970; Ingle, 1968). By combining careful behavioral analysis, lesion, and electrical stimulation studies, Ewert and Ingle independently characterized unique features for approach and avoidance behaviors, including a size dependence of the stimulus, and localized these behaviors to the optic tectum and caudal thalamus (Ewert, 1970, 1997; Ewert and Ingle, 1971; Ingle, 1968, 1973a, 1973b, 1977). Electrical stimulation across the optic tectum and pretectum generated orienting and avoidance behaviors respectively in the absence of visual stimuli. Regions in the rostral tectum were able to elicit both orienting and avoidance, defining an anatomical boundary between "prey catching" and "avoidance" inducing brain regions (Ewert, 1970).

This body of work also established that pretectal areas provide inhibitory modulation of tectally driven behaviors as ablations of pretectal areas and caudal thalamus resulted in indiscriminate prey capture attempts. Animals with these lesions would no longer selectively target small objects, but rather anything in the visual field. One striking result of these studies was that while the angular velocity and contrast of the visual stimuli could be described by retinal output, the size dependence could not, suggesting that additional mechanisms such as spatial

summation were required in the tectum or other brain regions to generate behavioral size selectivity (Ewert, 1970). Despite these advances in localizing brain regions and activity in these regions to visual stimuli parameters releasing specific behaviors, detailed analysis of neuronal subtypes was limited by techniques for identifying and reliably labeling neuronal subsets in the tectum.

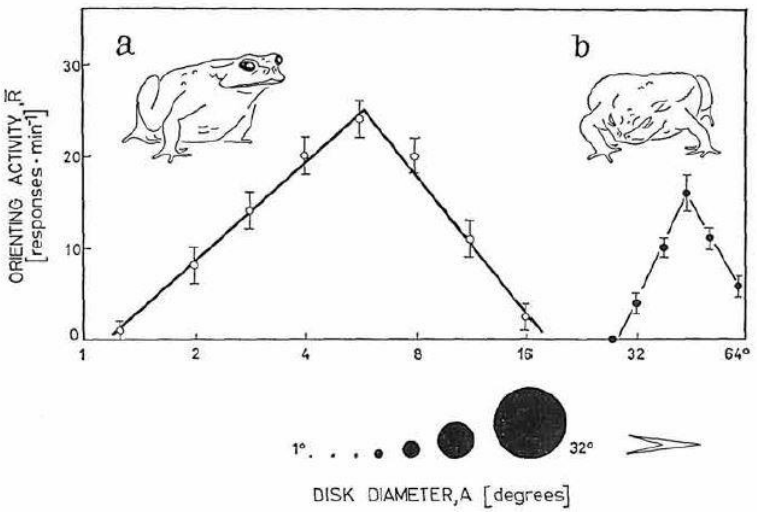

Figure 1: Behavioral tuning curves for orienting and avoidance behaviors in the common toad (*Bufo bufo*). A moving black disk of increasing diameter elicits approach at small sizes (a, <16°, optimal range 4-8°) and avoidance at larger sizes (b, >30°). [Figure reprinted from (Ewert, 1970)].

Currently, genetic advances have allowed for the opportunity to examine the brain with cell-type specificity, and provide possibilities for more detailed circuit analysis (Arenkiel and Ehlers, 2009). Work in non-teleost species continued to identify “feature detectors”. Notably, the identification of “approach sensitive/looming” detectors and “aerial predator” detectors in the mouse retina (Münch et al., 2009; Zhang et al., 2012). Currently there are ~20-30 types of identified RGCs in most mammals each with the capacity for unique feature detection (Field and

Chichilnisky, 2007; Sanes and Masland, 2015). RGC projection patterns in various brain regions have been extensively mapped and characterization of the circuits underlying motion detection and orientation selectivity has advanced greatly (Borst et al., 2010; Chapman and Stryker, 1992; Dhande and Huberman, 2014; Huberman et al., 2008) . However, how these representations are decoded by the brain to generate behavior is still largely unknown.

Retinal projections in the larval zebrafish

There are ten retinorecipient areas in the zebrafish brain, termed arborization fields (AF)1-10, with the largest and most studied being AF10, the optic tectum (Figure 2, Burrill and Easter, 1994; Robles et al., 2014). Many of these arborization fields are homologous to regions in the mammalian brain (e.g. AF10, the superior colliculus and AF1, the suprachiasmatic nucleus) (Nevin et al., 2010). These conserved projections make the zebrafish an attractive model organism for studying visual processing streams. However, identification of RGC subtypes in the zebrafish has lagged behind efforts in the mouse and other species (Field and Chichilnisky, 2007; Sanes and Masland, 2015). Recently, an anatomical classification of RGC projections was performed in the larval zebrafish revealing ~14 RGC types (Robles et al., 2014). The classification of RGC subtypes was based on distinct dendritic morphology and stratification patterns within the retina. Many of these types are morphologically similar to those reported in mice (~30 types, Sanes and Masland, 2015) and primate (~17 types, Field and Chichilnisky, 2007). Due to the small size and transparency of the zebrafish larva, the axonal projections of RGC subtypes could also be analyzed. When unique projection patterns were considered in combination with dendritic morphology, the number of possible RGC subtypes increased to ~82. While many RGC axons send collaterals to extratectal arborization fields, 97% of these axons continue to the tectum. Further experiments are needed to test if these ~82 RGC subtypes have distinct functional properties, tile the retina and/or share gene expression profiles, standard parameters for neuronal

cell type identification (Sanes and Masland, 2015). However, this work marks a significant step forward in revealing the complexity of the retinal output streams.

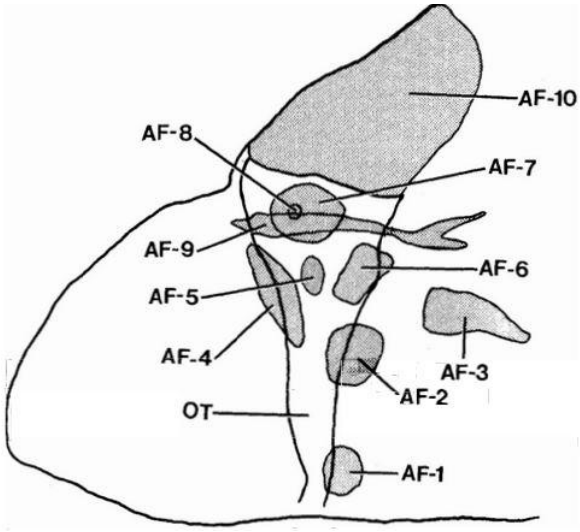

Figure 2: Schematic of RGC axon arborization fields (AFs) in the 6-7 dpf larval zebrafish. 10 AFs are identified. The largest is the optic tectum, AF10. [Figure reprinted from (Burrill and Easter, 1994)].

There is now evidence that AFs receive dedicated retinal input for specific visual features and thus contribute to specialized behaviors. Ablation and imaging studies of AF7 demonstrated a role of projections to this region in prey capture (Semmelhack et al., 2014). A similar study determined AF6 and AF8 as well as specific layers of AF10, the stratum fibrosum et griseum superficiale (SFGS)2-6 are involved in visually mediated escape behaviors in response to looming and dimming stimuli (Temizer et al., 2015). These studies imaged activity in RGC axons arborizing in AFs and focused ablations on active neuropil regions. It remains to be determined how the resident neurons in these AFs process information from the RGC axons and drive behavior. It is especially important to investigate the functional output of these AFs as 97% of RGC axons sending collaterals to pretectal AFs continue to the tectum and other work has demonstrated that the tectum is required for both prey capture and visually mediated avoidance (Dong et al., 2009; Gahtan et al., 2005).

Organization of the optic tectum

The optic tectum possesses both a laminar and retinotopic organization. A retinotopic map, creates a point-by-point mapping of visual space unto the tectum such that the relative spatial positon of objects in the visual environment is matched in the brain. RGCs in the nasal retina project axons to the posterior tectum, temporally positioned RGCs, to the anterior tectum. On the perpendicular axis, dorsally positioned RGCs project to the lateral tectum and ventrally positioned RGCs to the medial tectum. In the zebrafish 100% of the RGC axons cross at the optic chiasm, maps in each tecta represent the visual field seen by the contralateral eye (Luo, 2015). This retinotopic map of the visual world preserves information about the spatial position of objects in the visual environment.

In addition to the A-P and M-L mapping of retinal inputs the tectum is a highly layered structure with each RGC axon choosing a specific lamina (Huberman et al., 2010; Nevin et al., 2010; Robles et al., 2013). The tectum is not an exclusively retinorecipient brain region; afferents from the telencephalon, the torus longitudinalis, the torus semicircularis, and the nucleus isthmi have all been reported in several teleost species (Pérez-Pérez et al., 2003; Xue et al., 2003). The visual layers in the tectum can be roughly divided into four main partitions, the stratum opticum (SO), the stratum fibrosum et griseum superficiale (SFGS), the stratum griseum centrale (SGC), and the interface between the stratum album centrale and the stratum periventriculare SAC/SPV. The SO and SFGS can be further subdivided into SO1-2 and SFGS 1-6 (Robles et al., 2013). These layers comprise the neuropil. The final subdivision of the tectum is the stratum periventriculare (SPV) where the cell bodies of the resident tectal neurons, periventricular neurons (PVNs) are located. PVNs can be divided into two broad classes, periventricular interneurons (PVINs) with both axons and dendrites restricted to the tectum and the periventricular projection neurons (PVPNs) which send efferents outside of the tectum. With the exception of a recently identified population of interneurons which sit within the superficial layers of the tectal neuropil

the cell bodies of all PVNs are located in the SPV. All local synaptic connections within the tectum are localized to the neuropil which in addition to receiving retinal and other sensory information contains the PVN neurites (Nevin et al., 2010).

Classification of neuronal subtypes in the optic tectum has been limited. Based on a comprehensive Golgi study in the adult goldfish ~ 15 morphological types may be expected in the tectum (Meek and Schellart, 1978). Early electrophysiological studies suggest at least four distinct functional cell types in the adult zebrafish tectum (Sajovic and Levinthal, 1982a). More recently in larval zebrafish functional imaging studies have begun to classify the response properties of tectal neurons (Del Bene et al., 2010; Gabriel et al., 2012; Niell and Smith, 2005; Preuss et al., 2014; Robles et al., 2011). Three populations of direction-selective PVNs have been identified, those tuned to caudal to rostral motion, rostral to caudal motion and downward-upward motion. Neurons with rostral-caudal and caudal-rostral tuning are bistratified but project to different layers within the SFGS. Rostral-caudal tuned PVNs are more superficially stratified and also stratified in the SO. The up-down preferring PVN class was found to make a single broader projection in the deeper layers of the neuropil (Gabriel et al., 2012). Two studies have characterized a morphologically identifiable population of interneurons tuned to object size (Del Bene et al., 2010; Preuss et al., 2014). Additional studies describe tectal neurons with distinct size, direction and orientation tuning, but did provide morphological information about these populations (Niell and Smith, 2005; Preuss et al., 2014). However in all of these studies, neurons were not tested for additional stimuli, and thus it is unclear if neurons are exclusively tuned to a single parameter such as size or if for example, neurons preferring small objects may also show a direction preference.

Size tuning in the optic tectum

The first comprehensive study to map size tuning in the zebrafish optic tectum was undertaken by Sajovic and Levinthal in two landmark papers in 1982. They recorded responses to a wide array of visual stimuli in the optic tectum of adult zebrafish (Sajovic and Levinthal, 1982a, 1982b). A striking finding was that tectal receptive fields (25-39°) while larger in absolute size than the RGC receptive fields (7-13°) providing their input, could be tuned to much smaller objects (0.5-2.8°). A small moving white dot of ~3° within a larger ~30° receptive field of a tectal neuron gave stronger neural responses than the activation of the full receptive field. The ethological benefit of the complex tectal receptive field is clear. Smaller objects match the size of the preferred food source of the zebrafish and thus a brain structure composed of neurons specialized for the detection of small food objects against background provides a potential survival advantage. The complex structure of the tectal receptive field, suggested that inputs from the retina might be compared or pooled within the tectum. Such a mechanism might: (1) increase the accuracy with which an object's spatial position could be determined (2) allow for movement of a small object to be resolved within a larger field or (3) provide a more accurate measure of the size of an object through the comparison of multiple retinal inputs. While the potential advantages of this RF structure were numerous, the more compelling question remained- how are the receptive fields of tectal neurons structured to gain this complex and ethologically specialized tuning?

Recent work from Semmelhack et al., suggests that RGC tuning may be more finely tuned. (Optimal tuning is reported at 3° versus the 7-13° reported by Sajovic and Levinthal). Differences may result from the age and relative size of the fish. Sajovic and Levinthal used adult zebrafish and Semmelhack and colleagues, larvae. In another study using larval zebrafish, Bianco et al found that 13.2° dots were more effective that 3.5° dots in driving eye convergence, a hallmark of prey capture (Bianco and Engert, 2015). Yet how this information is transformed in the resident tectal neurons remains unknown. Earlier work by Niell and Smith demonstrated that at 84 hours

post fertilization (hpf) tectal neurons show a preferred tuning to 12° over 6° dots and no tuning to 3°. By 9 days post fertilization (dpf) clear tuning to 3° dots is observed, despite average receptive field sizes of 40 ± 4° (Niell and Smith, 2005). Taken together these results suggest that the tectum contributes to size processing. While size classification is one aspect of sensory processing. A remaining question is where and how valence "positive" and "negative" information is assigned to a given stimuli. (See Figure 3).

In this thesis, I developed a behavioral assay that utilized a single visual parameter, size, to elicit distinct behavioral responses, approach and avoidance in the larval zebrafish. The duality of the behavior assay allowed me to ask: (1) how is visual information, specifically information about object size classified? (2) where in the brain does this classification occur? And later (3) where along the visuomotor pathway is "positive" or "negative" value assigned to visual objects? (Figure 3). Using genetically restricted *Gal4* driver lines I was able to manipulate selective populations of neurons and directly assay how they contributed to the behavioral decision to approach or avoid a moving object.

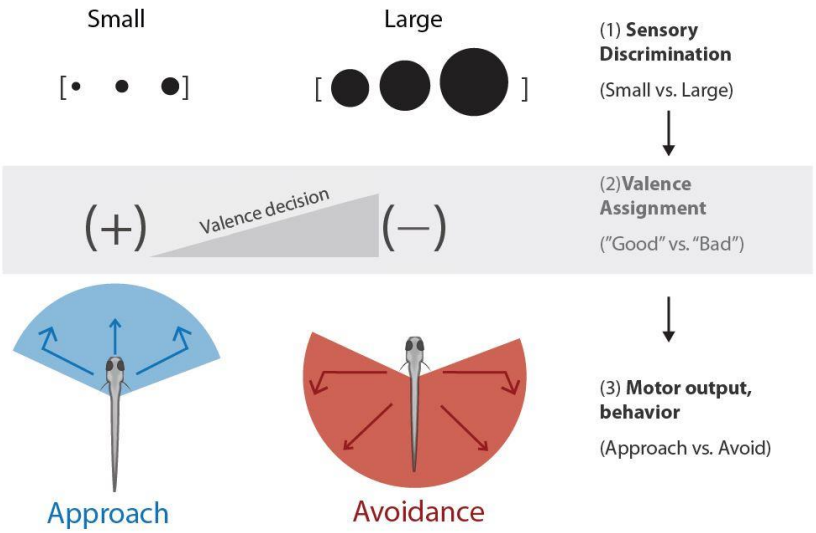

Figure 3: The aim of this thesis is to investigate how sensory information, here object size, is characterized by the brain to generate behavioral outputs (approach vs. avoidance). A secondary consideration is where along the visuomotor pathway valence ("good" vs "bad" quality of the stimulus) is assigned.

References

Arenkiel, B.R., and Ehlers, M.D. (2009). Molecular genetics and imaging technologies for circuit-based neuroanatomy. Nature *461*, 900–907.

Barlow, H.B. (1953). Summation and inhibition in the frog's retina. J. Physiol. *119*, 69–88.

Bianco, I.H., and Engert, F. (2015). Visuomotor transformations underlying hunting behavior in zebrafish. Curr. Biol. CB *25*, 831–846.

Borst, A., Haag, J., and Reiff, D.F. (2010). Fly motion vision. Annu. Rev. Neurosci. *33*, 49–70.

Burrill, J.D., and Easter, S.S. (1994). Development of the retinofugal projections in the embryonic and larval zebrafish (Brachydanio rerio). J. Comp. Neurol. *346*, 583–600.

Chapman, B., and Stryker, M.P. (1992). Origin of orientation tuning in the visual cortex. Curr. Opin. Neurobiol. *2*, 498–501.

Del Bene, F., Wyart, C., Robles, E., Tran, A., Looger, L., Scott, E.K., Isacoff, E.Y., and Baier, H. (2010). Filtering of visual information in the tectum by an identified neural circuit. Science *330*, 669–673.

Dhande, O.S., and Huberman, A.D. (2014). Retinal ganglion cell maps in the brain: implications for visual processing. Curr. Opin. Neurobiol. *24*, 133–142.

Dong, W., Lee, R.H., Xu, H., Yang, S., Pratt, K.G., Cao, V., Song, Y.-K., Nurmikko, A., and Aizenman, C.D. (2009). Visual avoidance in Xenopus tadpoles is correlated with the maturation of visual responses in the optic tectum. J. Neurophysiol. *101*, 803–815.

Ewert, J.P. (1970). Neural mechanisms of prey-catching and avoidance behavior in the toad (Bufo bufo L.). Brain. Behav. Evol. *3*, 36–56.

Ewert, J.P. (1997). Neural correlates of key stimulus and releasing mechanism: a case study and two concepts. Trends Neurosci. *20*, 332–339.

Ewert, J.P., and Ingle, D. (1971). Excitatory effects following habituation of prey-catching activity in frogs and toads. J. Comp. Physiol. Psychol. *77*, 369–374.

Field, G.D., and Chichilnisky, E.J. (2007). Information processing in the primate retina: circuitry and coding. Annu. Rev. Neurosci. *30*, 1–30.

Gabriel, J.P., Trivedi, C.A., Maurer, C.M., Ryu, S., and Bollmann, J.H. (2012). Layer-specific targeting of direction-selective neurons in the zebrafish optic tectum. Neuron *76*, 1147–1160.

Gahtan, E., Tanger, P., and Baier, H. (2005). Visual prey capture in larval zebrafish is controlled by identified reticulospinal neurons downstream of the tectum. J. Neurosci. Off. J. Soc. Neurosci. *25*, 9294–9303.

Hartline, H.K. (1938). The response of single optic nerve fibers of the vertebrate eye to illumination of the retina. Am. J. Physiol. *121*, 400–415.

Hartline, H.K. (1940a). The receptive fields of optic nerve fibers. Am. J. Physiol. *130*, 690–699.

Hartline, H.K. (1940b). The effects of spatial summation in the retina on the excitation of the fibers of the optic nerve. Am. J. Physiol. *130*, 700–711.

Hubel, D.H., and Wiesel, T.N. (1959). Receptive fields of single neurones in the cat's striate cortex. J. Physiol. *148*, 574–591.

Huberman, A.D., Feller, M.B., and Chapman, B. (2008). Mechanisms underlying development of visual maps and receptive fields. Annu. Rev. Neurosci. *31*, 479–509.

Huberman, A.D., Clandinin, T.R., and Baier, H. (2010). Molecular and cellular mechanisms of lamina-specific axon targeting. Cold Spring Harb. Perspect. Biol. *2*, a001743.

Ingle, D. (1968). Visual Releasers of Prey-Catching Behavior in Frogs and Toads. Brain. Behav. Evol. *1*, 500–518.

Ingle, D. (1973a). Two visual systems in the frog. Science *181*, 1053–1055.

Ingle, D. (1973b). Disinhibition of tectal neurons by pretectal lesions in the frog. Science *180*, 422–424.

Ingle, D. (1977). Detection of stationary objects by frogs (Rana pipiens) after ablation of optic tectum. J. Comp. Physiol. Psychol. *91*, 1359–1364.

Kandel, E.R., Schwartz, J.H., and Jessell, T.M. (2000). Principles of neural science (New York: McGraw-Hill, Health Professions Division).

Kuffler, S.W. (1953). Discharge patterns and functional organization of mammalian retina. J Neurophysiol. 16(1):37-68.

Lettvin, J.Y., Maturana, H.R., McCulloch, W.S., and Pitts, W.H. (1959). What the frog's eye tells the frog's brain. Proc. Inst. Radio Eng. *47*, 1940–1951.

Luo, L. (2015). Principles of neurobiology (New York, NY: Garland Science).

Meek, J., and Schellart, N.A. (1978). A Golgi study of goldfish optic tectum. J. Comp. Neurol. *182*, 89–122.

Münch, T.A., da Silveira, R.A., Siegert, S., Viney, T.J., Awatramani, G.B., and Roska, B. (2009). Approach sensitivity in the retina processed by a multifunctional neural circuit. Nat. Neurosci. *12*, 1308–1316.

Nevin, L.M., Robles, E., Baier, H., and Scott, E.K. (2010). Focusing on optic tectum circuitry through the lens of genetics. BMC Biol. *8*, 126.

Niell, C., and Smith, S. (2005). Functional Imaging Reveals Rapid Development of Visual Response Properties in the Zebrafish Tectum. Neuron *45*, 941–951.

Pérez-Pérez, M.P., Luque, M.A., Herrero, L., Núñez-Abades, P.A., and Torres, B. (2003). Afferent connectivity to different functional zones of the optic tectum in goldfish. Vis. Neurosci. *20*, 397–410.

Preuss, S.J., Trivedi, C.A., Vom Berg-Maurer, C.M., Ryu, S., and Bollmann, J.H. (2014). Classification of Object Size in Retinotectal Microcircuits. Curr. Biol. CB.

Robles, E., Smith, S.J., and Baier, H. (2011). Characterization of genetically targeted neuron types in the zebrafish optic tectum. Front. Neural Circuits *5*, 1.

Robles, E., Filosa, A., and Baier, H. (2013). Precise lamination of retinal axons generates multiple parallel input pathways in the tectum. J. Neurosci. Off. J. Soc. Neurosci. *33*, 5027–5039.

Robles, E., Laurell, E., and Baier, H. (2014). The Retinal Projectome Reveals Brain-Area-Specific Visual Representations Generated by Ganglion Cell Diversity. Curr. Biol. CB.

Sajovic, P., and Levinthal, C. (1982a). Visual cells of zebrafish optic tectum: mapping with small spots. Neuroscience *7*, 2407–2426.

Sajovic, P., and Levinthal, C. (1982b). Visual response properties of zebrafish tectal cells. Neuroscience *7*, 2427–2440.

Sanes, J.R., and Masland, R.H. (2015). The types of retinal ganglion cells: current status and implications for neuronal classification. Annu. Rev. Neurosci. *38*, 221–246.

Semmelhack, J.L., Donovan, J.C., Thiele, T.R., Kuehn, E., Laurell, E., and Baier, H. (2014). A dedicated visual pathway for prey detection in larval zebrafish. eLife *3*.

Temizer, I., Donovan, J.C., Baier, H., and Semmelhack, J.L. (2015). A Visual Pathway for Looming-Evoked Escape in Larval Zebrafish. Curr. Biol. CB *25*, 1823–1834.

Xue, H.-G., Yamamoto, N., Yang, C.-Y., Kerem, G., Yoshimoto, M., Imura, K., and Ito, H. (2003). Fiber connections of the torus longitudinalis and optic tectum in holocentrid teleosts. J. Comp. Neurol. *462*, 194–212.

Zhang, Y., Kim, I.-J., Sanes, J.R., and Meister, M. (2012). The most numerous ganglion cell type of the mouse retina is a selective feature detector. Proc. Natl. Acad. Sci. U. S. A. *109*, E2391–E2398.

Chapter 2: Object size classification in the larval zebrafish, behavioral readouts for decision-making

2.1 Introduction

In recent years, numerous behavioral assays for the larval zebrafish have been developed based on natural behaviors. Transition into the laboratory setting has been largely motivated by available genetic lines (Baier and Scott, 2009) and imaging technologies unique to the transparent larva, which allow for neural activity, especially on a network level, to be linked directly to behavior (Feierstein et al., 2015). Here I briefly outline the status of several behavioral paradigms and the motivations for the current work.

Innate behaviors in response to optic flow: OMR and OKR

The larval zebrafish like many organisms employs several behaviors to compensate for whole-field motion within its environment (Borst et al., 2010; Kubo et al., 2014; Portugues et al., 2014; Roeser and Baier, 2003; Schoonheim et al., 2010). These behaviors are innate and robust. The optokinetic reflex (OKR) is composed of a smooth eye pursuit and a quick saccade, allowing for an object moving across the visual field to be tracked and subsequently for a quick reset of eye position. The net result is image stabilization on the retina. In contrast, the optomotor response (OMR) is a whole body locomotor response to optic flow; a fish will adjust its swimming direction to compensate for perceived motion in the environment, thus stabilizing itself in space. Both responses can be elicited in the laboratory setting with the presentation of sine-wave gratings and both develop early, making them valuable tools for studying visuomotor transformations. OKR is fully functional by 80 hours post fertilization (hpf), while OMR develops

between 5-7 days post fertilization (dpf) (Portugues and Engert, 2009). These behaviors do not require the tectum (Roeser and Baier, 2003).

Behavioral studies of prey capture

Zebrafish begin tracking and hunting prey objects as soon as they are able to swim (Borla et al., 2002; Neuhauss, 2003; Orger et al., 2004). Detailed kinematic analysis of tail (Bianco et al., 2011; Borla et al., 2002; McElligott and O'Malley, 2005; Patterson et al., 2013; Semmelhack et al., 2014) pectoral fin (McClenahan et al., 2012) and eye movements (Bianco et al., 2011; Bianco and Engert, 2015) reveal prey capture events are composed of stereotyped action patterns. Prey capture precedes in three discrete stages, 1) orientation towards the prey, including an eye convergence, 2) directed pursuit movements towards the prey and 3) capture of the prey (predatory strike) (Bianco et al., 2011; Budick and O'Malley, 2000). Two distinct movements, J-turns for orientation and forward swims for approach can be reliably identified in free-swimming (McElligott and O'Malley, 2005) and head-fixed preparations (Bianco et al., 2011; Semmelhack et al., 2014; Trivedi and Bollmann, 2013). The latter has allowed for neural imaging to be combined with behavior and has identified anterior regions in the optic tectum (Muto et al., 2013) and pretectal areas specifically, arborization field 7 (AF7) as brain regions involved in prey capture (Fajardo et al., 2013; Semmelhack et al., 2014). Both live prey such as paramecia and virtual stimuli have been successfully used in laboratory settings to study prey capture behaviors.

Behavioral studies of collision avoidance and visually-mediated escape

Similar to the strong ethological need for recognizing and tracking food objects, large threatening objects need to be avoided. On the opposite side of the size spectrum, several studies have quantified avoidance and escape behaviors (Budick and O'Malley, 2000; Temizer et al.,

2015). Recent work by Temizer et al., 2015 identified pretectal areas AF6 and AF8 and the retinorecipient layers SFGS2-SFGS6 as responsive to looming and dimming stimuli. Interestingly layers SFGS2-SFGS5 appear to respond preferentially to looming parameters when compared to overall dimming. Strikingly these regions do not overlap with the retinorecipient layers tuned for prey capture although more detailed analysis is needed.

Despite these strides, more work is needed to identify intratectal circuits and their constituent cell types that process size information and lead to behavioral outputs. Work by Muto et al. and Bianco and Engert has identified tectal regions that are active during prey capture but have not reliably identified their cell properties or synaptic partners (Bianco and Engert, 2015; Muto et al., 2013). Since these studies have examined the tuning of exclusively small moving objects it is possible that size processing of small and large objects is shared among tectal circuitry or pooled after segregated inputs arrive from the retina. To address these possibilities I sought to develop a behavioral assay that evaluated both approach and avoidance. This behavioral assay could then serve as a platform for rapidly screening cell types contributing to size discrimination behaviors using pharmacogenetic tools in combination with *Gal4* driver lines with limited brain (tectal) expression (Figure 4).

2.2 Developing a behavioral assay for size discrimination in the larval zebrafish

A behavioral assay for testing size discrimination was developed for free-swimming larval zebrafish. Larvae were exposed to moving dots of constant velocity and maximal contrast (black dots on a white background). For behavioral trials, a single larva was placed in a transparent plastic chamber above a computer screen. Visual stimuli were generated on the computer screen, and a high-speed camera recorded the larva's movements from above (Figure 5A). For each behavioral trial, a single larva was presented with dots of seven distinct sizes (each dot size was

presented nine times before the dot size was changed). The initial position of the dots and the order in which dots of different sizes were presented was pseudo-randomly ordered. Dot sizes ranged from 1° to 50° of the larva's visual field.

Aim of this Chapter:

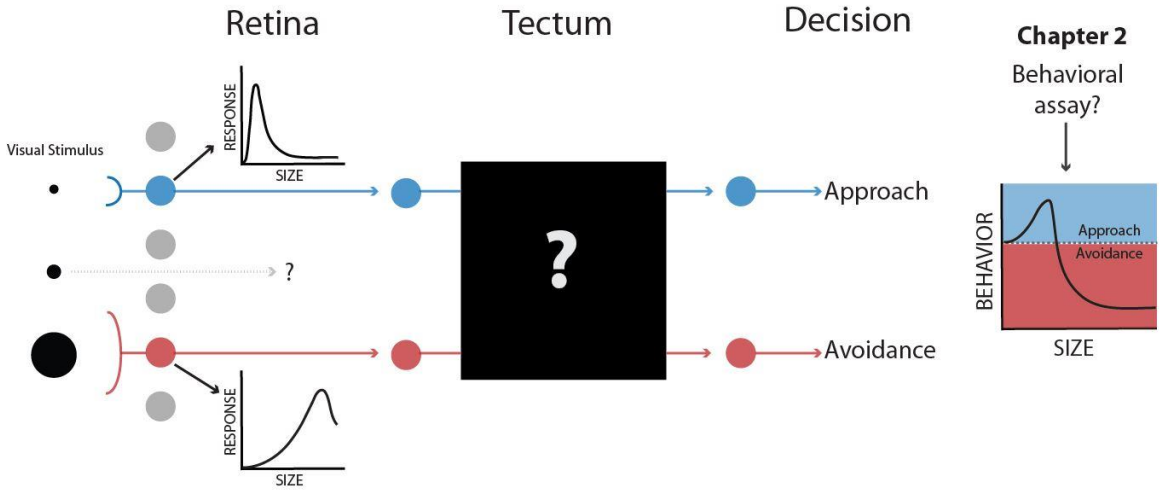

Figure 4: Studies from Semmelhack et al., 2014 and Temizer et al., 2015, suggest the identity of dedicated "small" and "large/looming" RGC pathways. Cell types in the tectum that process this information are largely unknown (with the exception of the SINs, see Del Bene et al., 2010; Preuss et al., 2014 and see Chapter 4). The identity of tectal neurons involved in size processing is investigated in Chapter 3. This chapter focuses on the development of a behavioral readout to assay sensorimotor decisions based on the size of the visual stimulus.

Approach and avoidance were readily distinguishable by both the direction and speed of the larva's movement (Figure 5B). Approach behaviors typically persisted across 3-4 frames of the video acquisition (60 Hz), with the direction of movement towards the dot. This resulted in a reorientation and sustained pursuit of the dot (Figure 6A), often involving J-turns, a hallmark of prey capture behavior (Bianco et al., 2011; Budick and O'Malley, 2000; McElligott and O'Malley, 2005; Patterson et al., 2013; Semmelhack et al., 2014; Trivedi and Bollmann, 2013). In contrast,

avoidance behaviors were markedly faster (always less than 2 frames at 60 Hz) and further characterized by swimming away from the direction of the dot's motion (Figure 6B). (Fish and dot trajectories for single behavioral trials are shown in Figures 7 and 8). While individual trajectories were varied, approaches consistently resulted in the final position of the fish overlapping with that of the dot. During avoidance maneuvers, the fish moved rapidly away from the projected position of the dot with its final position never overlapping with the end position of the dot.

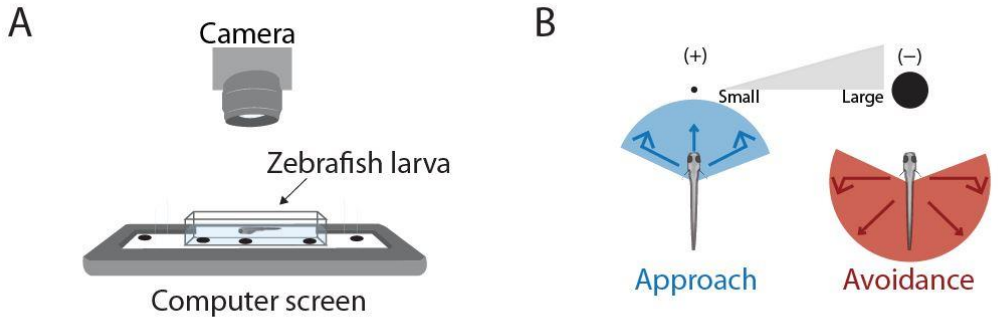

Figure 5: A visually-mediated behavioral paradigm for size discrimination. (**A**) Schematic of behavioral set-up. (**B**) Schematic of behavioral paradigm. Moving dots entering the central visual field of the larva are scored for their ability to generate behavioral responses. Neutral interactions are scored when the fish has no response to the dot (no change in direction or speed, or no overall movement). An approach interaction is scored when the larva changes direction to match the trajectory of the moving dot (denoted in blue in the schematic). An avoidance interaction is scored when the larva changes its direction to avoid the dot's trajectory of motion (denoted in red in the schematic).

To quantify each dot-larva interaction, the following two behavioral indices were used: a response index (R.I.) = (the number of approaches minus the number of avoidances) divided by (the total number of larva-dot interactions) and a valence index (V.I.) = (the number of approaches minus the number of avoidances) divided by (the number of approaches plus the number of avoidances). In both indices, approach is assigned a positive value (maximum possible response equal to 1) and avoidance a negative value (maximum possible response equal to -1; Figure 9). The R.I. considers each time the fish encounters a dot, including trials where the dot does not elicit a

behavioral response. This metric allowed us to assess the overall strength of the stimulus in eliciting a behavior as well as the direction of the behavior, towards or away from the dot (Figure 9A). In contrast, the V.I. provides a measure of the value assigned to the stimulus regardless of the strength of the behavioral response (Figure 9C). In some cases we also analyzed the overall fraction of behavioral responses to each stimulus (fraction of behavioral responses = total number of avoidances plus total number of approaches)/ total number of larva-dot interactions).

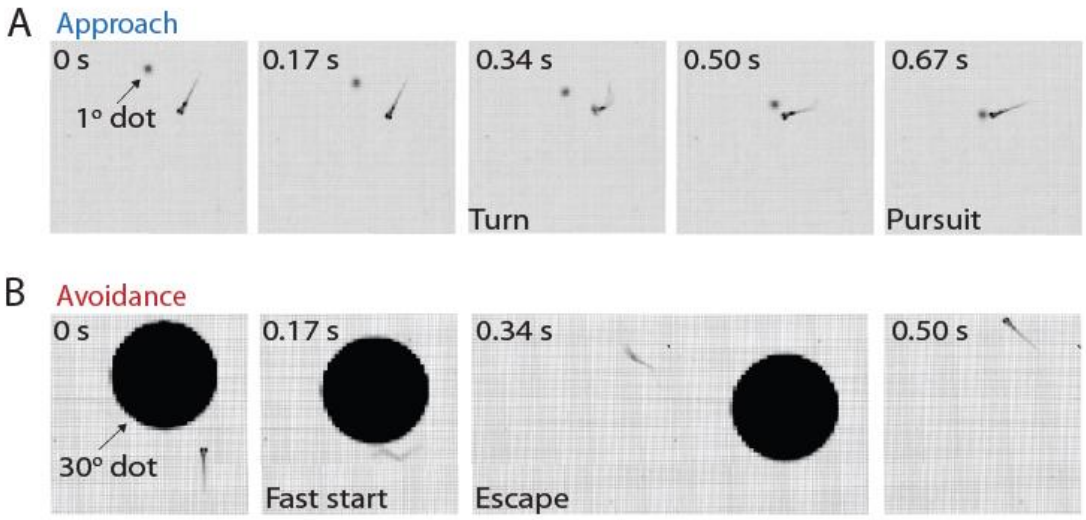

Figure 6: (**A**) Frame-by-frame example of approach behavior. As the small dot (here 1°) enters its visual field, the larva re-positions its body towards the dot. (**B**) In response to a large moving dot (here 30°) the larva makes a rapid movement away from the trajectory of the dot.

With increasing dot size, behavior switches from approach to avoidance

At 7 dpf small moving dots (<5°) elicited mainly approaches, and large dots (>10°) avoidances. In the narrow range between 5° and 10°, the behavior transitioned from approach to avoidance (Figure 9A, C). During this transitional range, the behavioral responses were highly

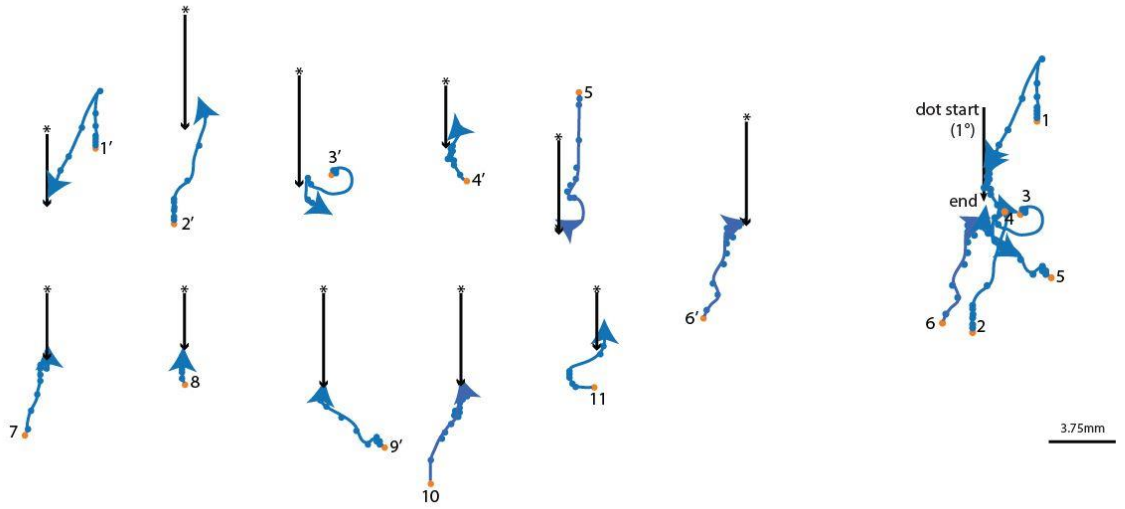

Figure 7: Examples of frame-by-frame trajectories of 11 approach behaviors. In each example, a black arrow denotes the movement of a 1° dot during the behavioral event and the asterisk the starting point of the dot. The starting position of the fish is denoted with an orange circle and subsequent positions with blue circles along a blue line denoting the complete trajectory of the fish with an arrow denoting the direction of the fish's movement. For each example, between 10 and 15 consecutive frames of the video recording were plotted until the behavior was complete. Apostrophes denote traces that are included in the overlay.

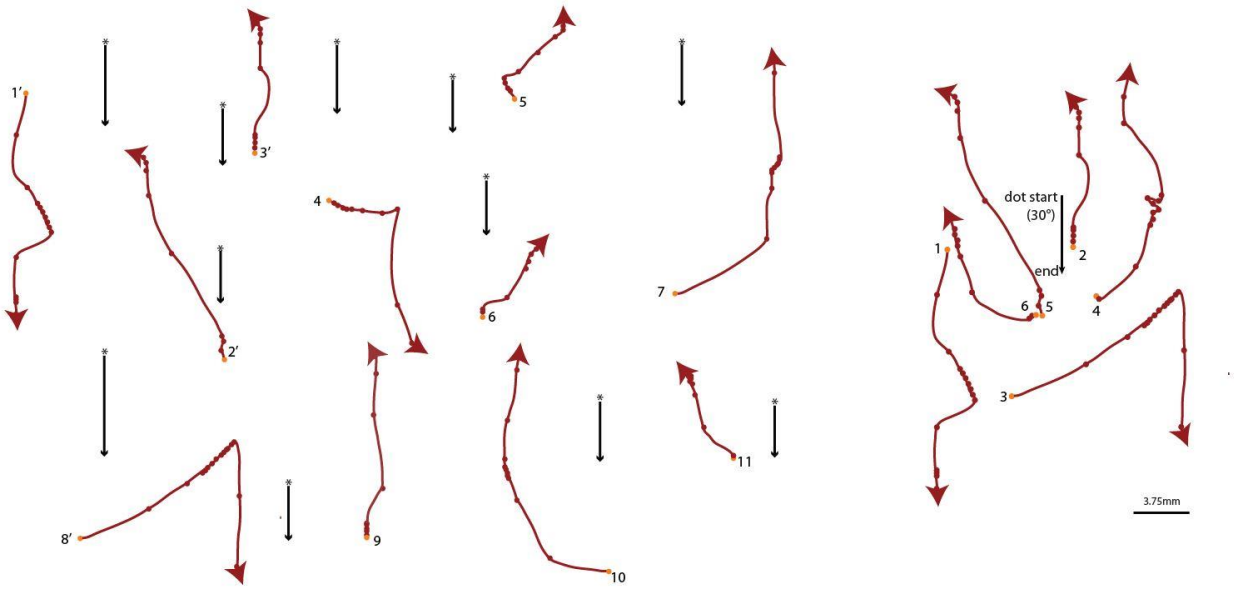

Figure 8: Examples of frame-by-frame trajectories of 11 avoidance behaviors in response to a 30° dot. Same notation as in Figure 7, except that trajectories are drawn in red. Apostrophes denote traces that are included in the overlay.

variable. When larvae were presented with 5° dots, both behavioral indices exhibited the largest variance (SEM± 0.10 for R.I.; SEM ± 0.27 for V.I.) and hovered around zero (not significantly different from zero, $p = 0.4384$; one-sample, t-test), suggesting that this size represents an ambiguous stimulus to the 7 dpf fish larvae. To better resolve the transition range, we subjected a subset of nine fish to an expanded stimulus set (1°, 2°, 3°, 4°, 5°, 7°, 9° and 10° dot sizes were presented). Preference for approach behaviors was observed for 1°, 2° and 3° dots. Near equal propensities for avoidance and approach (and therefore highly variable behavior) occurred for 4°, 5°, 7° and 9° dots. At 10°, the sign of the R.I. and V.I. changed to a significantly negative value, indicating that, at this size, avoidances predominated (Figure 9B,D). A clear transition between approach and avoidance is observed in all fish. However, the dot size that represented the approach-avoidance transition and the overall strength of the behavioral response showed variability across the entire tested population. Variability for a single fish across trials was generally low. The behavioral data for all 37 7 dpf fish is displayed in Figure 10 to fully illustrate the range of behavioral responses across the population.

Size tuning curves adjust with increasing body size

To assess at which age the behavior arises and to investigate if size preferences change in older larva, additional experiments were performed at 4, 5, and 15 dpf (Figure 11A). As the fish ages its body size increases. One interesting hypothesis is that as the body size of the larva increases its optimal size range for “prey” and “predator” adjusts accordingly, such that previous ambiguously classified “small-medium” sized objects may now be edible and previously threatening “medium-large” sized objects may now be less aversive. Shortly after hatching (4 dpf), larvae already exhibited a biphasic psychometric function, indicating that the observed size preferences are innate. Interestingly, older larvae (15 dpf) consistently approached dots of 5°,

which were ambiguous to 7 dpf larvae. This suggests that the behavioral transition point moves to larger sizes, concomitant with the fish growing in size. As predicted, the classification of “edible” previously ambiguously classed objects is revised to reflect the increased body size of the larvae.

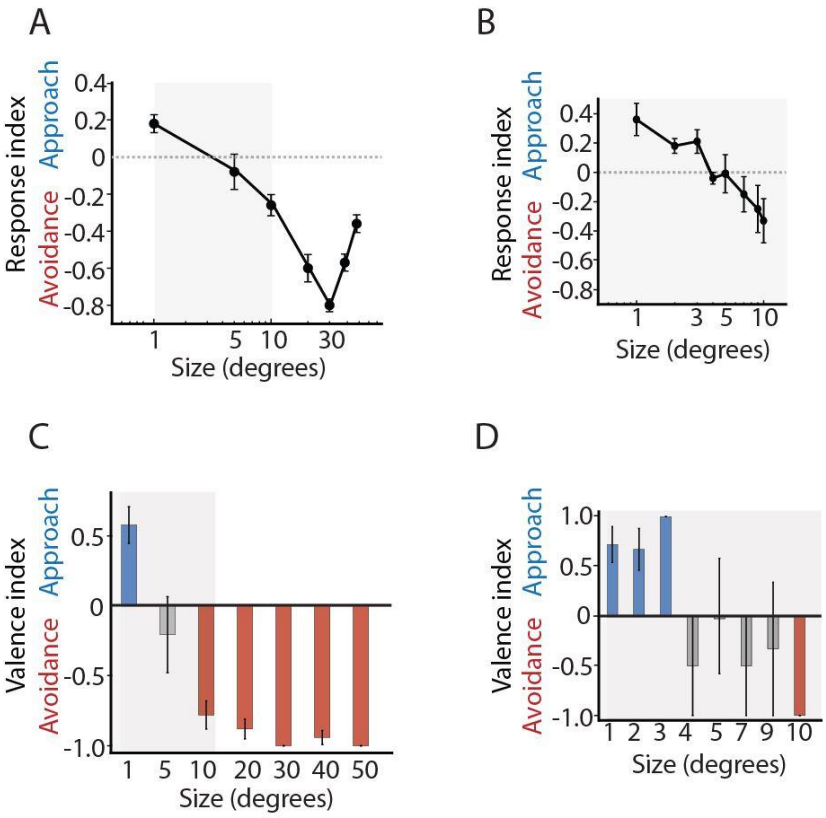

Figure 9: (**A**) Behavioral size discrimination tuning curve (n= 37 larvae; 7 dpf). Behavioral responses to moving dots of a given size are plotted as a response index (R.I., see text). The transition between approach and avoidance occurs around 5°-10°, with the smallest dot size presented 1°, generating approach responses. Avoidance responses peak around 30° and taper off towards 50°. (**B**) Finer resolution of the size discrimination tuning curve for small and medium sizes (shaded gray area in (A), n= 9 fish of the 37 included in (A)). (**C**) Same larvae as shown in (A) plotted using a valence index (V.I.; see text). At 1° dot sizes, there is strong preference for approach. A slight preference for avoidance is observed in response to 5° dots, with increasing preference (almost to maximal values) for sizes greater than 10°. (**D**) Same data in (B) plotted using the V.I. as in (C).

When evaluating the fraction of behavioral responses performed at different ages, fish were significantly less likely to respond to 10° dots at 7 dpf (Figure 11B). Larger dots (40° and 50°) were less likely to drive a response at 15 dpf when compared to 5 dpf and 7 dpf larvae. This

may represent a decrease in the saliency of the stimulus as the size of the fish increases rendering dots of 40° and 50° to be perceived as less threatening.

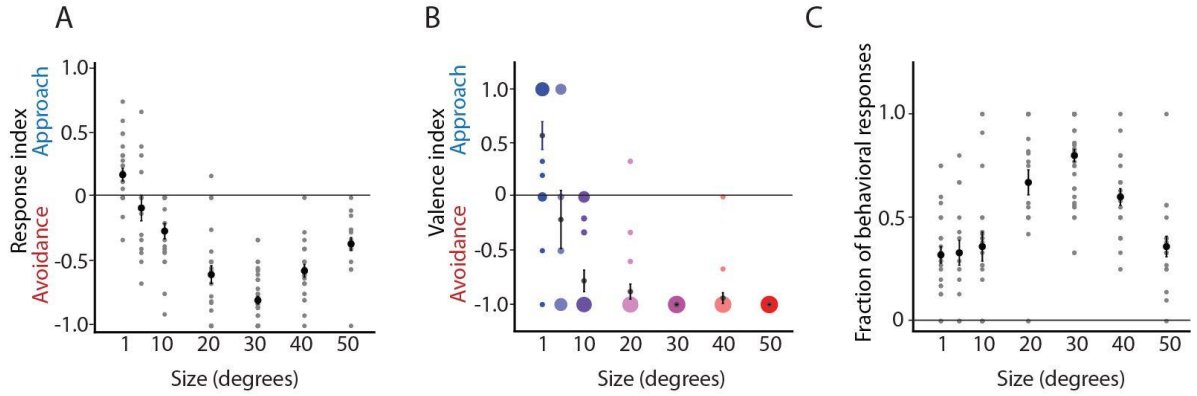

Figure 10: (**A**) Behavioral responses of all fish in the size discrimination experiments shown in Figure 9 (n=37; 7 dpf; TL background). Response values for single fish are shown in gray, average values for each size in black (error bars are ± SEM). (**B**) Valence characterization of all behavioral responses of fish shown in (A). The diameter of the data point is proportional to the fraction of fish responding with the designated valence score. (The data points for 30° and 50° dots represent the maximal dot diameter with 100% of fish displaying the plotted score of -1.0). (**C**) The fraction of behavioral responses for all fish shown in (A). Response values for single fish are shown in gray, average values for each size in black (error bars are ± SEM).

Habituation and order of stimulus presentation do not diminish behavioral outcomes

One consideration in the development of the behavioral assay was the potential for behavioral response saturation. To test the response rate and the response valence (approach vs. avoidance) we performed several experiments in which fish were repeatedly exposed to dots of the same size across multiple trials. Each behavioral trial consisted of nine dot presentations and fish were exposed to four consecutive trials. When a single dot size (30°) was tested no change in the valence of the stimulus response was observed (Figure 12A), all dots generated a maximum V.I. of (-1). We did observe a decrease in the overall behavioral response rate across trials (Figure 12B). This decrease was strongest between trials 1 and 2 and continued to decrease, albeit more moderately, across the remaining trials. Despite the trend towards

decreased responsiveness this effect was not significant (one-way ANOVA, Tukey's correction, p=0.167, p = 0.307 t1 vs t2).

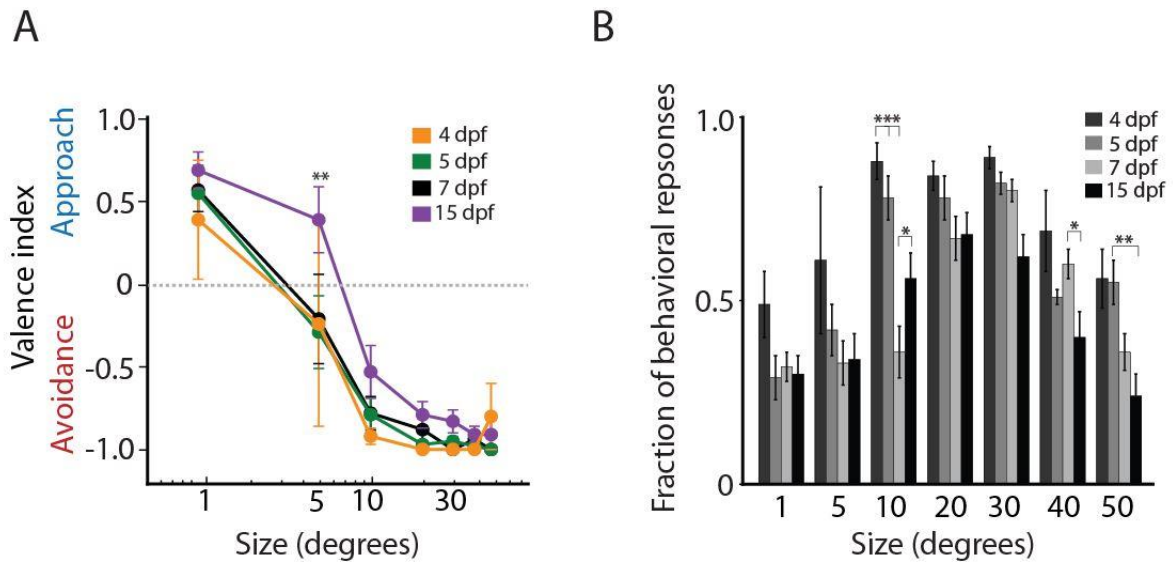

Figure 11: (**A**) V.I. tuning curves for three additional ages 4, 5, and 15 dpf. Data from 7 dpf (Figure 9A, C) are included here for comparison. (4 dpf: n=5, orange line; 5 dpf: n=18, green line; 7 dpf: n=37, black line; 15 dpf: n=18, purple line). At 15 dpf larvae are significantly more likely to approach 5° dots (p=0.004, 7 dpf vs. 15 dpf; p=0.0003, 5 dpf vs 15 dpf, two-way, ANOVA with Tukey's correction). (**B**) The fraction of behavioral responses for larvae shown in (A). For 10° dots, responses are the most variable across all sizes. At larger sizes, behavioral responses decreased at 15 dpf compared to 5 dpf and 7 dpf. For both panels, error bars are ± SEM

In addition to testing for changes in behavioral responses across trials we also examined intra-trial variability. For each behavioral trial seven different size dots were presented. The order in which dots of each size was presented was pseudorandomly ordered, yet it was important to test if the order in which dots of a given size were presented affected the behavioral response rate or the valence of the response. To examine this possibility we performed another set of behavioral experiments and compared the R.I. for 30° dots when they were presented as the first, second or fifth stimulus (Figure 13). No significant changes in the R.I. were observed (p = 0.452, one-way ANOVA, Tukey's correction).

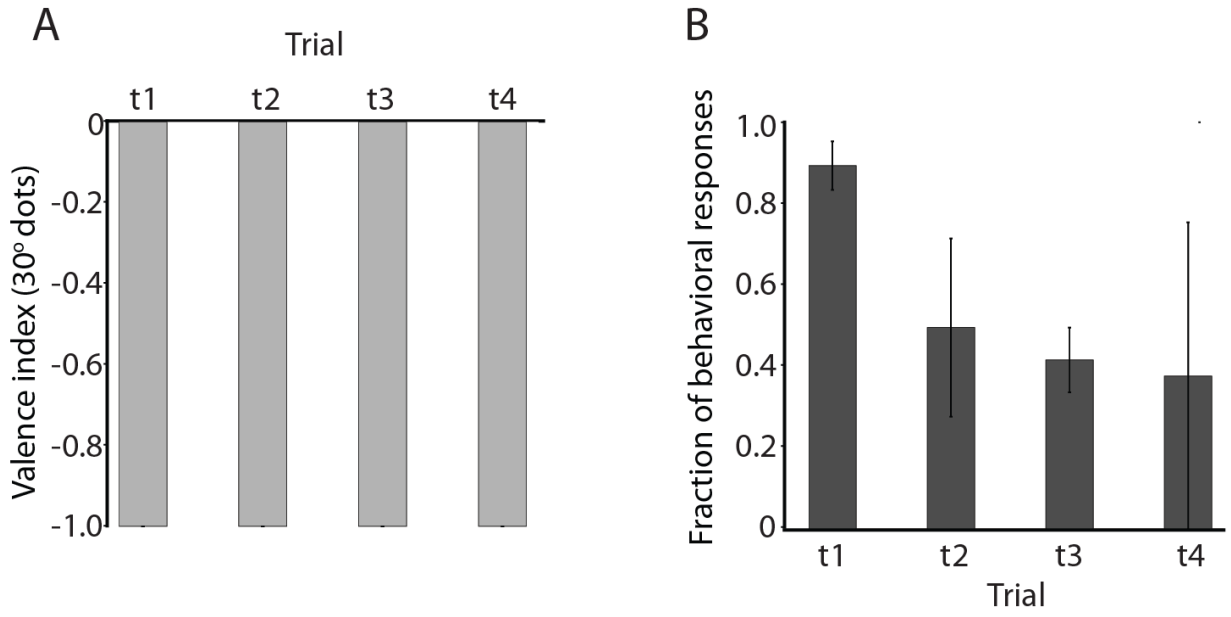

Figure 12: (**A**) Valence index is unchanged across subsequent trials. (**B**) The fraction of behavioral respones decreases between all trials, with the greatest change between the first and second trial (one-way ANVOA, Tukey's correction p = 0.307 t1 vs. t2).

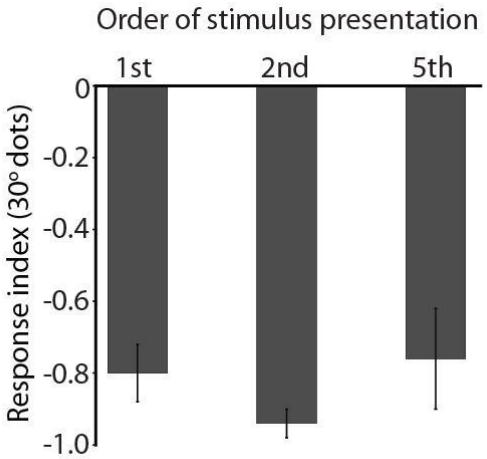

Figure 13: R.I. for 30° dots presented as the 1st, 2nd or 5th stimulus during the behavioral trial. No significant differences in R.I. are observed (p =0.452, one-way ANOVA, Tukey's correction.

The retina is required for visually evoked avoidance and approach behaviors

Changes in overall luminance detected through the pineal gland and deep brain photoreceptors are capable of driving phototaxis (Fernandes et al., 2012; Jamieson and Roberts, 2000). To test contributions of such non-retinal photodetection mechanisms to the behaviors examined here, we employed three methods to attenuate or eliminate RGC input. In a first set of experiments nitroreductase was used to remove, RGCs (see Methods chapter Figure 36). *Atoh7:Gal4-VP16* transgenic fish were crossed to carriers of *UAS:Nitroreductase (Nfsb)-mChry* and treated with metronidazole (MTZ) at 5 dpf. *Atoh7* is a promoter that labels all RGCs (Kay et al., 2001). Within a few hours, MTZ is converted by nitroreductase into a cytotoxic compound resulting in the cell-autonomous death of cells expressing it (Pisharath et al., 2007). Fish were treated with MTZ for 12 hours and allowed to recover for 24 hours, before behavior was performed at 7 dpf. Ablation of RGCs resulted in a flattening of the behavioral response curve showing no significantly different responses from the curve expected for a blind fish (i.e. R.I. = 0 for all sizes) (Figure 14A, uncorrected p = 0.741, 0.436, 0.254, 0.068, 0.039, 0.012, 0.229 for sizes 1°-50°; one-sample t test with Bonferroni correction). When the ablated RGC condition was compared to control conditions with matched genotype and no MTZ treatment or with *Atoh7:Gal4-VP16* transgenic fish crossed to carriers of *UAS:Dendra* and treated with MTZ to control for drug only effects, there was a highly significant flattening of the behavioral response curve (two-way ANOVA with Tukey's correction, $F(2,225)$, $p < 0.0001$). The overall fraction of behavioral responses was significantly reduced in RGC ablated conditions for larger dot sizes 20°-50° (Figure 14C). While the overall behavioral rate was not reduced in ablated conditions for dots sizes between 1°-10° the R.I. curve was flattened suggesting that while some behavioral events remained these were equally distributed between approach and avoidance and that the larvae were therefore unable to properly resolve the visual stimulus. It is possible that the MTZ-mediated ablation was not complete due to suboptimal drug delivery or that labeling of RGCs was not

complete due to variegation within the *Gal4* or *UAS* lines used. To control for these possibilities we performed an additional experiment, surgically removing the eyes of the larvae before assaying behavior.

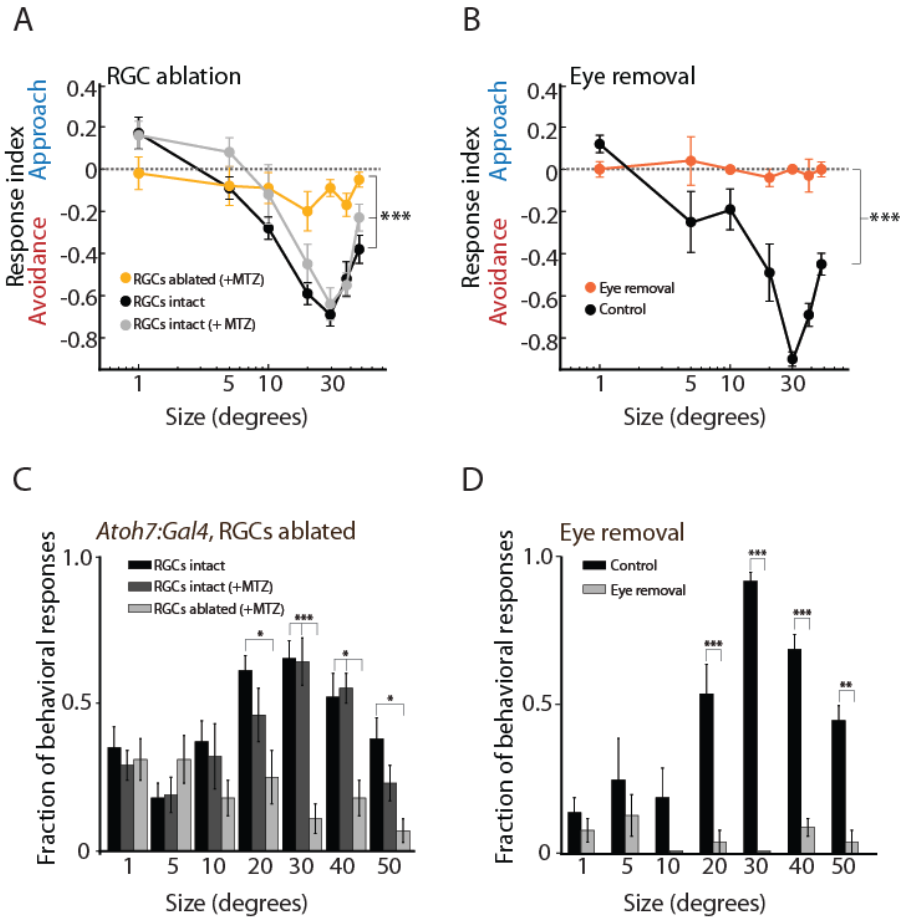

Figure 14: RGCs contribute to size discrimination. (**A**) Size discrimination tuning curves of *Atoh7:Gal4, UAS:Nfsb-mChry* ablated fish (n = 14, yellow) and control conditions (*Atoh7:Gal4, UAS:Nfsb-mChry* with no MTZ treatment, n = 20, black; *Atoh7:Gal4, UAS:Dendra* with MTZ treatment, n = 10, gray). When RGCs are ablated, values are not significantly different from zero ($p > 0.07$ for all sizes except 30° ($p = 0.039$) and 40° ($p = 0.012$), one-sample t test, Bonferroni correction). (**B**) Tuning curves of enucleated and control siblings (enucleated, n=7, orange; control, n=10, black). Under enucleated conditions, values are not different from zero ($p > 0.30$ for all sizes, one-sample t test, Bonferroni correction). (**C**) Fraction of behavioral responses decreased at larger sizes in RGC-ablated conditions. (adjusted $p = 0.013$; $p < 0.0001$, $p < 0.0001$; $p = 0.005$, 0.01; $p = 0.011$ for 20°, 30°, 40°, 50° respectively, two-way, ANOVA with Bonferroni correction; first p value corresponds to MTZ and no MTZ comparison, second p value to Nitroreductase +MTZ and Dendra + MTZ comparison) (**D**) Fraction of behavioral responses decreased at all sizes under enucleated conditions. (adjusted $p = 0.0002$; $p < 0.0001$; $p < 0.0001$; $p = 0.005$ for 20°, 30°, 40°, 50° respectively, two-way, ANOVA with Bonferroni correction). For all panels error bars are $\pm$ SEM. * = $p < 0.05$, ** = $p < 0.005$, *** = $p < 0.0005$.

Surgically enucleated fish similarly did not respond to dots of any size (Figure 14B, R.I. not significantly different from zero at any size, uncorrected p = 1.000, 0.786, 0.374, 0.423, 0.391, 0.718, 0.391 for sizes 1°-50° respectively; one-sample t test with Bonferroni correction) and responses were significantly reduced compared to control conditions in which wild type, eye intact siblings were subjected to the behavior (two-way ANOVA with Bonferroni correction, $F(1,62)= 84.55$, $p < 0.0001$). In these experiments, the fraction of behavioral responses decreased across all sizes (Figure 14D, reaching significance for sizes 20°-50°).

Testing blind mutants: *Lakritz* fish

Finally, we examined one additional method for eliminating RGCs. Specification of RGCs occurs during the first wave of retinal neurogenesis and requires the action of the transcription factor Ath5. The previous identification of the *lakrtiz*^{th241}*(lak)* mutant which encodes Ath5 provided us with a means for testing size discrimination behaviors in larvae that have never possessed RGCs as opposed to larvae in which RGCs were ablated or removed at later developmental time points (Kay et al., 2001). We tested *lak* mutants and *het* and *wt* siblings on our behavioral assay (Figure 15). As expected we found a complete flattening of the behavioral tuning curve with R.I.s not significantly different from zero for all sizes (Figure 15A, adjusted p = 0.14, 0.39, 0.97, 0.44, 0.26, 0.35, 0.26 for sizes 1°-50° respectively, one-sample t test, Bonferroni correction). As with other RGC removal conditions the *lak* behavioral curve was significantly different from control conditions ($p <0.0001$, $F (1,129) = 68.90$, two-way ANOVA, Bonferroni correction). Similar to other RGC manipulations the fraction of behavioral responses diminished across all sizes (Figure 15B, reaching significance for dot sizes between 20°-50°).

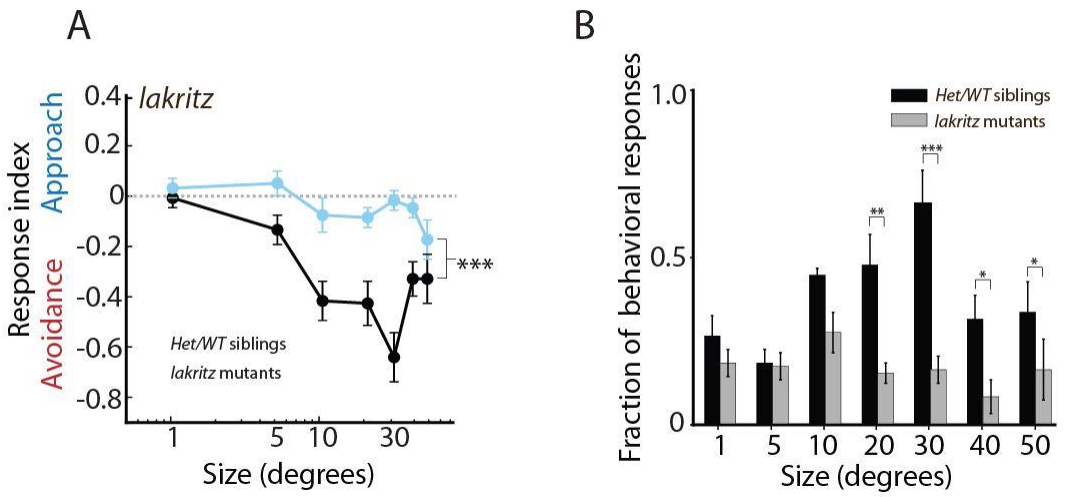

Figure 15: (**A**) R.I. curves for *lak* mutants and *het*/*wt* siblings. *Lak* mutants (n= 14, blue) show a flattening of the response curve that is not significantly different from zero ($p \geq 0.14$ for all sizes, one-sample t test, Bonferroni correction) but is significantly reduced compared to control conditions (n=16, black line, $p<0.0001$, two-way ANOVA, Bonferroni correction). (**B**) The fraction of behavioral responses is reduced in *lak* mutants compared to *het*/*wt* conditions, especially at larger sizes (reaching significance at 20°-50°). For all panels error bars are $\pm$ SEM. * = $p < 0.05$, ** = $p < 0.005$, *** = $p < 0.0005$.

The optic tectum is required for visually evoked avoidance and approach behaviors

While more than 95% of retinal ganglion cell (RGC) axons make synaptic connections in the tectum, visually guided behaviors can be mediated by other retinorecipient brain areas (Kubo et al., 2014; Roeser and Baier, 2003). To test the contribution of the tectum in our behavioral assay, we crossed the *Gal4s1013t* enhancer trap line, previously characterized to drive broad expression in the optic tectum (Scott and Baier, 2009), to a *UAS* line expressing tetanus-toxin light chain (TeTxLC) fused to CFP (Figure 16A). (Cell ablation with nitroreductase cannot be employed here because of weak muscle expression in the *Gal4s1013t* line). Silencing of tectal neurons resulted in a complete loss of behavior with no response values significantly different from zero (Figure 16B, one-sample t test with Bonferroni correction, uncorrected p =0.391, 0.391, 0.374, 0.500, 0.482, 0.226, 0.215 for sizes 1°-50° respectively). The fraction of behavioral responses decreased at all sizes except 50°, reaching significance at sizes between 10°-30°

(Figure16C). In combination with the RGC ablation manipulations, these experiments firmly establish the retinotectal pathway as necessary for both visually mediated approach and avoidance behaviors.

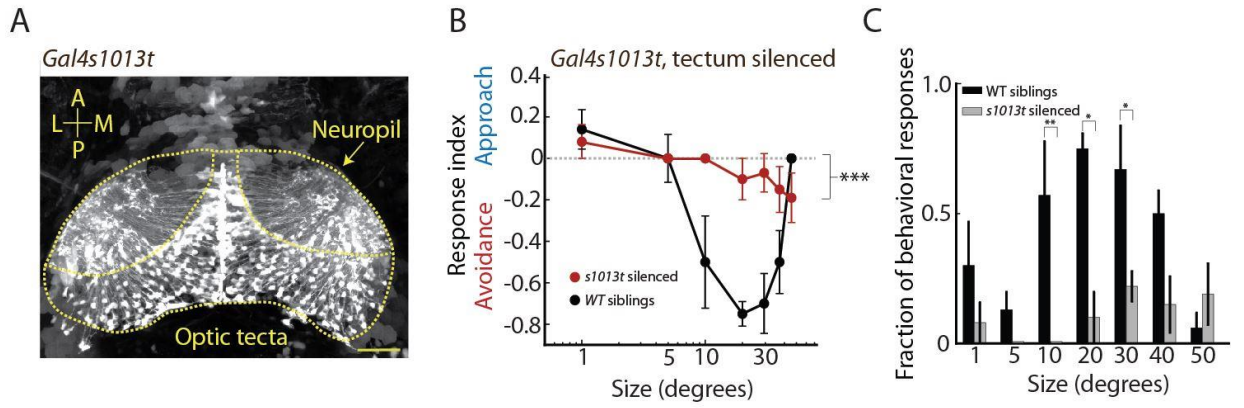

Figure 16: Neurons in the tectum contribute to size discrimination. (**A**) Expression pattern of *Gal4s1013t* shown in a 5 dpf larvae-expressing *UAS:EGFP*. *Gal4s1013t* labels a large portion, but not all, of the tectal neurons. (**B**) Tuning curve in *Gal4s1013t* silenced larvae. When compared to WT siblings, *Gal4s1013t, UAS:TeTxLC-CFP* larvae showed a marked reduction in R.I., with no responses significantly different from zero (experimental, n=7, red; control, n= 4, black; p > 0.200 for all sizes, one-sample t test, Bonferroni correction). (**C**) Fraction of behavioral responses is reduced at all sizes except for the largest size, 50° when a large proportion of tectal neurons are silenced (adjusted p =0.005; p =0.013; p =0.024 for 10°, 20°, 30° respectively, two-way, ANOVA with Bonferroni correction). Scale bars = 50 µm; A = anterior, P = posterior, L = lateral, M = medial. Hatched yellow lines denote the optic tecta for each image. Neuropil is indicated in the right tectum with a yellow arrow. For all panels error bars are ± SEM. * = p < 0.05, ** = p < 0.005, *** = p < 0.0005.

Visual acuity defects can be assayed by our behavioral paradigm

Our size discrimination assay proved effective in eliciting both approach and avoidance behaviors in response to moving dots of different sizes and proved sensitive to extreme visual defects, yet we wondered if our assay would be able to detect more subtle effects on visual acuity. To test this we again turned to available mutant lines. The *blumenkohl*^{tz257}*(blu)* mutant displays characterized deficits in visual perception resulting from a mutation in the vesicular glutamate transporter *vglut2a* (Smear et al., 2007). When tested on the size discrmination assay *blu* and *het/wt* siblings displayed distinct tuning curves with the *blu* tuning curve shifted towards larger sizes. Notably approach was observed in response to 5° and 10° dots and at large sizes

avoidance to 20°-50° dots was slightly depressed (Figure 17). In combination with the known acuity defects these results suggest larger dots are being msiclassified at the earliest stages of visual processing; RGC detection of 1°-10° dots is impaired such that 5° and 10° are now approached when previously avoided. The underlying mechanisms are not yet known and are not addressed at this time.

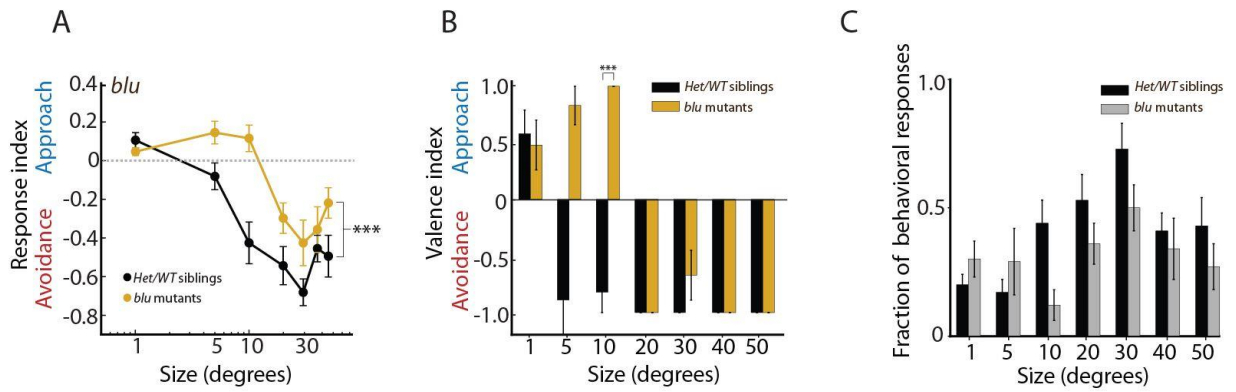

Figure 17: (**A**) Behavioral tuning curve for *blu* and *wt/het* control larvae. The behavioral response curve shifts to larger sizes in *blu* mutants (*blu,* n= 24, gold, p<0.0001, two-way ANOVA, Bonferroni correction) when compared to *het/wt* siblings (n= 18, black). (**B**) The V.I. for *blu* mutants shows a switch in valence to approach for 5° and 10° dot sizes (p = 0.119 at 5°, p < 0.0001 at 10°, Fisher's exact test). Valence classification at other sizes remains unchanged. (**C**) The fraction of behavioral responses remains unchanged at all sizes, with the exception of a slight but not statistically significant decrease at 10° (p = 0.095 at 10° for all other sizes p > 0.54, two-way ANOVA with Bonferroni correction). For all panels error bars are ± SEM. * = p < 0.05, ** = p < 0.005, *** = p < 0.0005.

Next we designed a slight modification in the visual stimulus to allow for an increased testing of visual acuity defects. As the zebrafish larvae ages its visual acuity increases as reflected in its increased success at prey capture (Budick and O'Malley, 2000). Thus a sensitive assay should see improvements in discrimination of smaller sized dots at later developmental time points. To test this we devised a new stimulus set combining the optimal dots sizes for driving approach and avoidance as empricially determined in this work (see Figure 9A), 1° and 30° respectively. We used 30° as an outer diameter and superimposed 1° dots of varying spacing (inter-dot-distance, IDI) inside the outer 30° diameter. We could then ask via behavioral output whether the larvae perceived the dot as a solid object of 30° diameter thus generating an

avoidance or was able to distinquish that the object was not continuous (Figure 18). We found that 6dpf larvae are more likely to avoid stimuli with IDI values of 2 and 3 and less likley to approach stimuli with IDI values of 5 when compared to 7dpf and 8dpf larvae. This is conistent with an increase in visual acuity from 6 to 8 dpf.

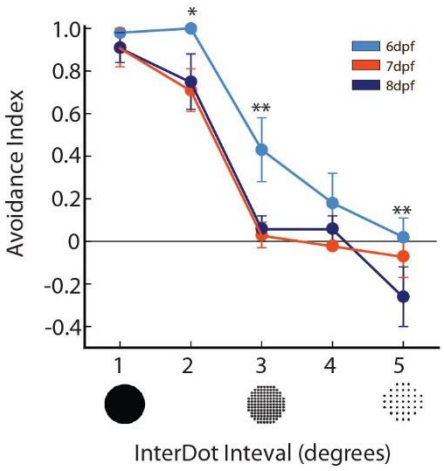

Figure 18: The ability of larvae to discriminate between large and small dots in an embedded stimulus is significantly increased between 6-8 dpf (p=0.04 at IDI=2 (6dpf vs 7dpf); p= 0.02, 0.004 at IDI =3 (6dpf vs 7dpf and 6dpf vs 8dpf); p= 0.006 at IDI=5 (6dpf vs 8dpf); two-way ANOVA, Bonferonni correction).

2.3 Discussion

This chapter focused on the development of a behavioral assay to test size discrimination in the larval zebrafish. In a single assay we can elicit both approach and avoidance behaviors in response to moving dots of varying size. The size dependence of this response transition allowed us to investigate neural substrates contributing to each behavior. In a first set of experiments we confirmed the necessity of the retinotectal projection for both approach and avoidance. We employed pharmacogenetic, surgical and genetic technologies to eliminate the acitivty of RGCs or resident tectal neurons. All of these manipulations significantly reduced behavioral response curves at all sizes. Additionally we confirmed the assay is sensitive to changes in visual acuity through the use of the *blumenkohl* mutant and through modifications to the stimulus paramters.

How successful is our assay? Can we relate our findings to repsonse rates ocurring in response to real prey and predators? As a first assessment we can compare our behavioral

response rates to previously published data. We observe a behavioral response rate of 32% (SEM ± 0.04%) for 1° dots in 7 dpf larvae. The behavioral response rate for small moving dots is similar to that published in a virtual assay by Bianco et al., 2011 where 22% of small dot presentations and 24% of large dot presentations reliably elicited behavior. In this study "large" dots were ~10°. In our assay we observed a behavioral response rate of 36% (SEM ± 0.07) for 10° dots and much larger response values for larger sizes (e.g. responses rates for 20°, 30°, 40° dots were all greater than 60%, with responses to 50° dots dropping to ~36%). In response to looming stimuli (expanding between 2°-48°), Temizer et al., 2015 reported an escape probability of greater than 80%. It is likely that some differences between our results and those previously reported may be due to differences in the speed or contrast of the stimulus. For our assay we kept a constant speed for all sizes. By these measures our assay succeeds in reliably eliciting responses. While our behavioral response rates are within the range of rates reported by other virtual assays eliciting approach and avoidance it is important to note, there is some divergence between the size, contrast and speed parameters reported for optimal stimuli.

We find that ~1-3° dots elicit approach and dot sizes greater than 10° reliably elicit avoidance. For dot sizes between 4°-9° we observe a high variability of the response valence with no clear behavioral preference for approach or avoidance. Between 4-6 dpf the measured visual acuity of the larval zebrafish is ~3.1°, slightly less than the optimal value expected by photoreceptor spacing (~2.1°) (Haug et al., 2010). Based on this calculation we would predict that the maximal resolution achieved by the the retina is that of a ~3°dot. However, it is possible that enhanced acuity may occur through further processing of retinal inputs in the tectum which were not considered in the visual acuity calculation performed by Haug and colleagues. The Haug et al. study used OKR to test visual acuity which has been shown to be a tectum-independent behavior (Roeser and Baier, 2003). It is possible that OKR and tectally-mediated behaviors, such as prey capture have different visual acuity requirements.

Experiments in adult zebrafish have demonstrated that 0.5° dots can be resolved by tectal neurons (Sajovic and Levinthal, 1982b). Calcium imaging studies in the 9 dpf larval zebrafish show a large number of cells tuned for 3° dots but smaller sizes were not tested (Niell and Smith, 2005). One recent study in a head-restrained preparation for larval zebrafish reports 3° dots as optimal for inducing prey capture related tail movements but these movements were also observed for smaller sizes (Semmelhack et al., 2014). Another head-fixed preparation used 2° stimuli to elicit prey capture-like swims (Trivedi and Bollmann, 2013). In a virtual environment using free swimming larvae, Bianco et al., 2011 reported 1°, 3°, and 5° dots were sufficient to induce orienting turns toward a moving dot, with the greatest turning seen for 1° dots. Several studies have examined prey capture in response to live prey (e.g. paramecia). The average size of a paramecium is ~150-300μm. Several studies have approximated the visual angle of a parmecium to range from 2°-8° and 3.2°-11.9° from the first fixation to the final approach (Semmelhack et al., 2014; Smear et al., 2007; Trivedi and Bollmann, 2013). Our behavioral results are consistent with these results.

Two final parameters must be considered in evaluating our assay, the speed and contrast of the stimuli. Various studies examining prey capture have used small white dots on a dark background (Bianco et al., 2011; Semmelhack et al., 2014; Trivedi and Bollmann, 2013), while others employ the inverse stimuli, black dots on a light background (Bianco and Engert, 2015). For approach behaviors both small white and small black dots can reliably initiate approach behaviors. However, large white dots are very poor drivers of avoidance (Temizer et al., 2015). This result was supported by our pilot experiments where avoidance of white dots was very low compared to black dots. In pilot experiments we chose a stimulus speed capable of eliciting both approach and avoidance (42°/s). This falls within the range of reported values for free swimming assays where larvae were found to perform equally well to dot speeds of 30°/s and 60°/s, but adjusted the speed of their response accordingly (Bianco et al., 2011). The speed of live prey was

measured between ~20°/s and ~67°/s depending on the swim bout during the capture sequence (Trivedi and Bollmann, 2013). Finally two head-fixed preparations found different optimal speeds 30°/s (Bianco and Engert, 2015) and 90°/s (Semmelhack et al., 2014), for eliciting distinct components of the prey capture sequence. It is important to note these studies also reported different optimal sizes for eliciting prey capture behaviors and used contrast inverted stimuli, yet importantly, our stimulus speed falls within the range of these values. The optimal angular expansion rate for looming induced avoidance has been reported to be 20°/s in a head-restrained preparation (Temizer et al., 2015). In all assays the direction of the virtual/real prey or potential threat dictated the direction of the behavioral response either toward or away from the dot. We also observed these effects.

References

Baier, H., and Scott, E.K. (2009). Genetic and optical targeting of neural circuits and behavior--zebrafish in the spotlight. Curr. Opin. Neurobiol. *19*, 553–560.

Bianco, I.H., and Engert, F. (2015). Visuomotor transformations underlying hunting behavior in zebrafish. Curr. Biol. CB *25*, 831–846.

Bianco, I.H., Kampff, A.R., and Engert, F. (2011). Prey capture behavior evoked by simple visual stimuli in larval zebrafish. Front. Syst. Neurosci. *5*, 101.

Borla, M.A., Palecek, B., Budick, S., and O'Malley, D.M. (2002). Prey capture by larval zebrafish: evidence for fine axial motor control. Brain. Behav. Evol. *60*, 207–229.

Borst, A., Haag, J., and Reiff, D.F. (2010). Fly motion vision. Annu. Rev. Neurosci. *33*, 49–70.

Budick, S.A., and O'Malley, D.M. (2000). Locomotor repertoire of the larval zebrafish: swimming, turning and prey capture. J. Exp. Biol. *203*, 2565–2579.

Del Bene, F., Wyart, C., Robles, E., Tran, A., Looger, L., Scott, E.K., Isacoff, E.Y., and Baier, H. (2010). Filtering of visual information in the tectum by an identified neural circuit. Science *330*, 669–673.

Fajardo, O., Zhu, P., and Friedrich, R.W. (2013). Control of a specific motor program by a small brain area in zebrafish. Front. Neural Circuits *7*, 67.

Feierstein, C.E., Portugues, R., and Orger, M.B. (2015). Seeing the whole picture: A comprehensive imaging approach to functional mapping of circuits in behaving zebrafish. Neuroscience *296*, 26–38.

Fernandes, A.M., Fero, K., Arrenberg, A.B., Bergeron, S.A., Driever, W., and Burgess, H.A. (2012). Deep brain photoreceptors control light-seeking behavior in zebrafish larvae. Curr. Biol. CB *22*, 2042–2047.

Haug, M.F., Biehlmaier, O., Mueller, K.P., and Neuhauss, S.C. (2010). Visual acuity in larval zebrafish: behavior and histology. Front. Zool. *7*, 8.

Jamieson, D., and Roberts, A. (2000). Responses of young Xenopus laevis tadpoles to light dimming: possible roles for the pineal eye. J. Exp. Biol. *203*, 1857–1867.

Kay, J.N., Finger-Baier, K.C., Roeser, T., Staub, W., and Baier, H. (2001). Retinal ganglion cell genesis requires lakritz, a Zebrafish atonal Homolog. Neuron *30*, 725–736.

Kubo, F., Hablitzel, B., Dal Maschio, M., Driever, W., Baier, H., and Arrenberg, A.B. (2014). Functional architecture of an optic flow-responsive area that drives horizontal eye movements in zebrafish. Neuron *81*, 1344–1359.

McClenahan, P., Troup, M., and Scott, E.K. (2012). Fin-tail coordination during escape and predatory behavior in larval zebrafish. PloS One *7*, e32295.

McElligott, M.B., and O'Malley, D.M. (2005). Prey tracking by larval zebrafish: axial kinematics and visual control. Brain. Behav. Evol. *66*, 177–196.

Muto, A., Ohkura, M., Abe, G., Nakai, J., and Kawakami, K. (2013). Real-time visualization of neuronal activity during perception. Curr. Biol. CB *23*, 307–311.

Neuhauss, S.C.F. (2003). Behavioral genetic approaches to visual system development and function in zebrafish. J. Neurobiol. *54*, 148–160.

Niell, C., and Smith, S. (2005). Functional Imaging Reveals Rapid Development of Visual Response Properties in the Zebrafish Tectum. Neuron *45*, 941–951.

Orger, M.B., Gahtan, E., Muto, A., Page-McCaw, P., Smear, M.C., and Baier, H. (2004). Behavioral screening assays in zebrafish. Methods Cell Biol. *77*, 53–68.

Patterson, B.W., Abraham, A.O., MacIver, M.A., and McLean, D.L. (2013). Visually guided gradation of prey capture movements in larval zebrafish. J. Exp. Biol. *216*, 3071–3083.

Pisharath, H., Rhee, J.M., Swanson, M.A., Leach, S.D., and Parsons, M.J. (2007). Targeted ablation of beta cells in the embryonic zebrafish pancreas using E. coli nitroreductase. Mech. Dev. *124*, 218–229.

Portugues, R., and Engert, F. (2009). The neural basis of visual behaviors in the larval zebrafish. Curr. Opin. Neurobiol. *19*, 644–647.

Portugues, R., Feierstein, C.E., Engert, F., and Orger, M.B. (2014). Whole-brain activity maps reveal stereotyped, distributed networks for visuomotor behavior. Neuron *81*, 1328–1343.

Preuss, S.J., Trivedi, C.A., Vom Berg-Maurer, C.M., Ryu, S., and Bollmann, J.H. (2014). Classification of Object Size in Retinotectal Microcircuits. Curr. Biol. CB.

Roeser, T., and Baier, H. (2003). Visuomotor behaviors in larval zebrafish after GFP-guided laser ablation of the optic tectum. J. Neurosci. Off. J. Soc. Neurosci. *23*, 3726–3734.

Sajovic, P., and Levinthal, C. (1982). Visual response properties of zebrafish tectal cells. Neuroscience *7*, 2427–2440.

Schoonheim, P.J., Arrenberg, A.B., Del Bene, F., and Baier, H. (2010). Optogenetic localization and genetic perturbation of saccade-generating neurons in zebrafish. J. Neurosci. Off. J. Soc. Neurosci. *30*, 7111–7120.

Scott, E.K., and Baier, H. (2009). The cellular architecture of the larval zebrafish tectum, as revealed by gal4 enhancer trap lines. Front. Neural Circuits *3*, 13.

Semmelhack, J.L., Donovan, J.C., Thiele, T.R., Kuehn, E., Laurell, E., and Baier, H. (2014). A dedicated visual pathway for prey detection in larval zebrafish. eLife *3*.

Smear, M.C., Tao, H.W., Staub, W., Orger, M.B., Gosse, N.J., Liu, Y., Takahashi, K., Poo, M.-M., and Baier, H. (2007). Vesicular glutamate transport at a central synapse limits the acuity of visual perception in zebrafish. Neuron *53*, 65–77.

Temizer, I., Donovan, J.C., Baier, H., and Semmelhack, J.L. (2015). A Visual Pathway for Looming-Evoked Escape in Larval Zebrafish. Curr. Biol. CB *25*, 1823–1834.

Trivedi, C.A., and Bollmann, J.H. (2013). Visually driven chaining of elementary swim patterns into a goal-directed motor sequence: a virtual reality study of zebrafish prey capture. Front. Neural Circuits *7*, 86.

Chapter 3: Sensorimotor decision making in the zebrafish tectum

3.1 Summary

An animal's survival depends on its ability to correctly evaluate sensory stimuli and select appropriate behavioral responses. When confronted with ambiguous stimuli, the brain is faced with the task of selecting one action, while suppressing others. Although conceptually simple, the site and substrate of this elementary form of decision making is still largely unknown. Zebrafish larvae respond to a moving dot stimulus in either of two ways; a small object (potential prey) evokes approach, whereas a large object (potential predator) is avoided. The classification of object size relies on processing in the optic tectum. We genetically identified a population of cells, largely comprised of glutamatergic tectal interneurons with non-stratified morphologies that are specifically required for approach towards small objects. When these neurons are ablated, we found that the behavioral response is shifted; small objects now tend to elicit avoidance. Conversely, optogenetic facilitation of neuronal responses with channelrhodopsin (ChR2) enhances approaches to small objects. Calcium imaging in head-fixed larvae shows that a large proportion of these neurons are tuned to small sizes. Their receptive fields are shaped by input from retinal ganglion cells (RGCs) that are selective for prey identity. We propose a model in which valence-based decisions arise, at a fundamental level, from competition between dedicated sensorimotor pathways in the tectum.

Introduction

In many predatory vertebrates, small moving objects elicit pursuit and capture movements (Bianco et al., 2011; Budick and O'Malley, 2000; Gahtan et al., 2005; Muto et al., 2013; Patterson et al., 2013; Roeser and Baier, 2003; Semmelhack et al., 2014; Trivedi and Bollmann, 2013). Conversely, large or looming objects frequently trigger escape (Dong et al., 2009; Ewert, 1970; Ingle, 1973; Temizer et al., 2015). In the zebrafish brain, visual objects are processed in the optic tectum (Del Bene et al., 2010; Niell and Smith, 2005; Preuss et al., 2014; Sajovic and Levinthal, 1982a, 1982b). Recent studies demonstrated that information about object size can be transmitted directly to tectal neurons from retinal ganglion cells (RGCs) (Del Bene et al., 2010; Preuss et al., 2014; Semmelhack et al., 2014). Yet it remains unclear how size information is further processed by local tectal circuitry and, critically, how it is evaluated to generate distinct behavioral outputs.

In birds and mammals, the optic tectum (OT) and its homologous mammalian structure, the superior colliculus (SC), control orienting behavior through direct target selection and through the weighing of stimulus value. Notably, in barn owls, the tectum is an integral part of midbrain circuitry that assigns priority between competing stimuli (Mysore and Knudsen, 2011). In primates, activity within the SC is required for target selection during saccadic eye movements (Gardner and Lisberger, 2002; Krauzlis et al., 2013; Kustov and Robinson, 1996; McPeek and Keller, 2004; Schiller and Stryker, 1972; Wurtz and Goldberg, 1972a, 1972b, 1972c, 1972d). However, because these studies rely predominantly on electrophysiological recordings and relatively unspecific perturbations, very little is known about the contributions of individual cell types to these behavioral functions. A genetically accessible system may help bridge this gap, provided these animals show sufficiently complex decision making behavior. Here we introduce zebrafish larvae as such a system.

We assay sensorimotor action selection in larval zebrafish by the presentation of small and large moving objects, such that the behavioral output is a direct report of whether the stimulus was classified as “positive” (edible) or “negative” (threatening). This behavioral paradigm, combined with calcium imaging, pharmacogenetic lesions and optogenetic manipulations, allowed us to investigate how neural circuits in the tectum generate valence decisions based on the classification of visual stimuli by size (Figure 19). We provide evidence that a genetically identified population of tectal neurons, belonging to the non-stratified periventricular interneuron (nsPVIN) class (Nevin et al., 2010), biases behavior toward approach at small sizes.

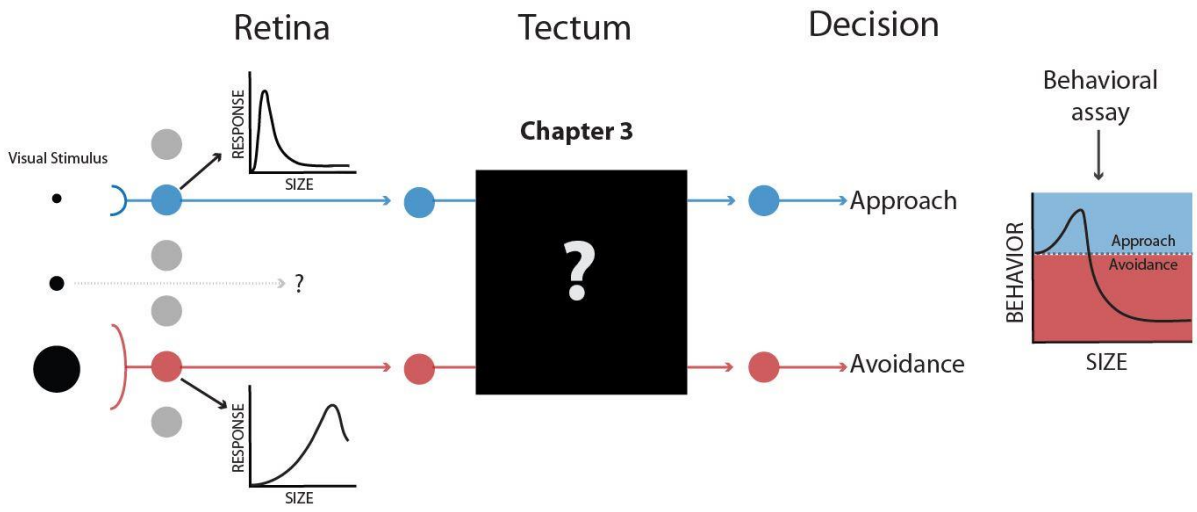

Figure 19: A behavioral assay was developed (Chapter 2) to test how sensory discrimination, distinguishing between small and large objects leads to dedicated behavioral outputs approach vs. avoidance. In this Chapter, this assay is used to investigate tectal circuitry that contributes to the decision to avoid or approach a visual object.

3.2 Testing neuronal populations underlying sensorimotor decision making

Ablation of Superficial Interneurons (SINs) impairs large object avoidance

The SINs are GABAergic neurons positioned within the superficial layers of the optic tectum and have been reported to receive size-tuned retinal inputs (Del Bene et al., 2010; Preuss et al., 2014). A substantial fraction of the SINs are labeled in the *Gal4s1156t* enhancer trap line (Figure 20A, see Methods Chapter Figure 37) (Scott and Baier, 2009). This driver line, however, labels additional GABAergic cell types in the periventricular layer, preventing us from using either nitroreductase or TeTxLC. We therefore used a pulsed infrared (2-photon) laser to selectively ablate between 2 and 12 SINs in both tectal hemispheres. Following ablation, larvae were allowed to recover overnight and behavioral experiments were performed on the following day (7 dpf). All larvae were subsequently imaged to confirm the successful and exclusive removal of SINs.

In SIN-ablated larvae, behavioral responses were impaired, particularly to large sizes. At 30°, the strength of the behavioral response was significantly decreased, with the R.I. shifted to less negative values (Figure 20B, 'SIN ablated' R.I. = -0.44; 'Non-ablated' R.I. = -0.74) (adjusted p= 0.04 at 30°, two-way ANOVA, Bonferroni correction). Responses to small dots were also diminished, although to a lesser extent. Fish in which a large number of SINs were ablated tended to show greater behavioral deficits than fish with more restricted lesions, although individuals with the same number of cells targeted could vary in the extent of their impairment (see Methods Chapter, Figure 37). This heterogeneity suggests that other factors, such as SIN subtype identity (Preuss et al., 2014) and position in the tectum, may contribute to their functional relevance. Importantly we found no difference in the fraction of approaches or avoidances in SIN-ablated larvae. Rather, these fish were less responsive across the entire range of sizes, consistent with a role for SINs in stimulus detection (Figure 20C, D).

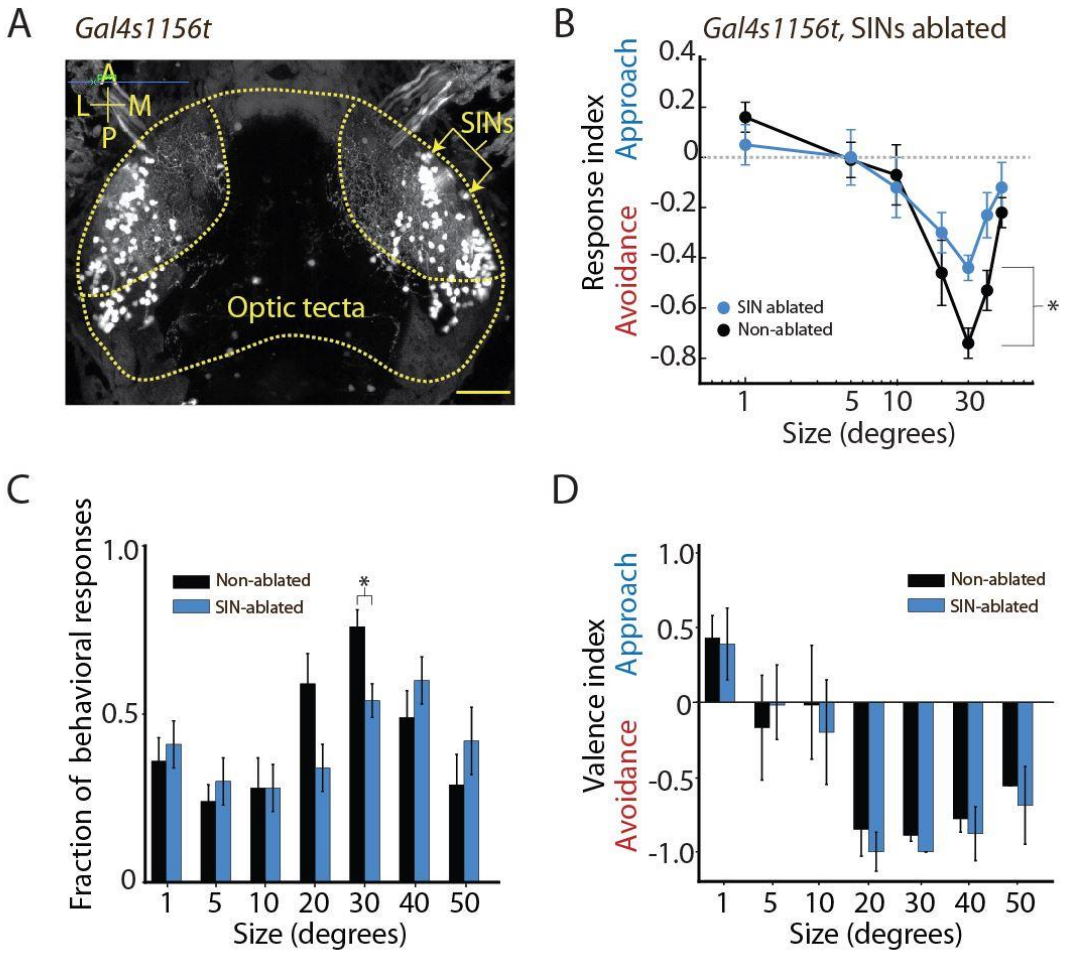

Figure 20: (**A**) Expression pattern of *Gal4s1156t*, *UAS:Kaede*, labeling a subset of the SINs (yellow arrows), as well as additional tectal neurons. (**B**) Tuning curves for SIN-ablated fish (n = 16, blue) and control larvae (n = 16, black). SIN-restricted ablations were performed in *Gal4s1156t*, *UAS:Kaede* larvae using a 2-photon laser. The R.I. is significantly reduced at 30° (two-way ANOVA with Bonferroni correction, p at 20° = 0.068; p at 30° = 0.040). (**C**) SIN-ablated larvae show fewer behavioral responses (two-way ANOVA with Bonferroni correction, uncorrected p at 30° = 0.004, same larvae as in (B)). (**D**) SIN-ablated larvae have an unchanged V.I. (Ablated, n = 25, gray; Non-ablated, n =16, black; two-way ANOVA, Bonferroni correction, same larvae as in (B)). Scale bar = 50µm; A = anterior, P = posterior, L = lateral, M = medial. Hatched yellow lines denote the optic tecta. Neuropil is indicated in the right tectum with a yellow arrow. For all panels error bars are $\pm$ SEM. * =$p < 0.05$.

Ablation of *Gal4mpn354* neurons shifts responses from approach to avoidance

In the newly generated gene trap line *Gal4mpn354*, labeling is largely restricted to the dorsal tectum and the cerebellum, with occasional expression in trunk musculature of the larval body axis (Figure 21A, see Methods Chapter Figure 38, 39). Due to variegation in the expression pattern, it is possible to select for larvae in which labeling is largely restricted to the tectum. Ablations of *Gal4mpn354* cells in fish expressing nitroreductase selectively disrupted behavioral responses to small sizes (Figure 21B; two-way ANOVA with Tukey's correction, p=0.038, p = 0.032 at 1°). The overall rate of behavioral responsiveness was unaffected (Figure 21C). For 1° dots, however, we found a shift in the sign of the V.I. from positive (approach) to negative (avoidance) when *Gal4mpn354*-ablated larvae were compared to controls (Figure 21D; p = 0.0003; Fisher's exact test performed on approach and avoidance counts), indicating that the observed change arose from both an increase in the number of avoidances and a decrease in the number of approaches to small dots.

In the above experiment, nitroreductase also removed *Gal4mpn354*-labeled cells outside of the tectum. Although these cells represent a small fraction, it is still possible that they contributed to the observed phenotype. We therefore attempted to selectively laser-ablate the labeled neurons in the tectum, leaving, e. g., the cerebellar population intact. These experiments are difficult, owing to the limited number of cells that can be reliably ablated in an individual fish without affecting its overall health and behavior. Furthermore, as will be shown below, the *Gal4mpn354* population is heterogeneous in its physiological responses, suggesting that removing a random subset will result in a diverse range of effects. Nevertheless, we succeeded in reproducing the phenotype of the nitroreductase ablation in fish in which 20 or more *Gal4mpn354* neurons were removed (Figure 22 shows a representative example). Together, these experiments strongly suggest that the tectal circuitry from which *Gal4mpn354* neurons has been removed biases the behavioral response towards approach. This effect was not seen when

only a subset of tectal neurons, labeled in the *Gal4s1038t* line, were ablated (Figure 23; two-way ANOVA, Tukey's correction). These cells are projection neurons of unknown function in the posterior tectum and are contained within the *Gal4s1013t*-labeled population (Scott and Baier, 2009). This result demonstrated that not all tectal populations contribute equally to the behaviors tested here.

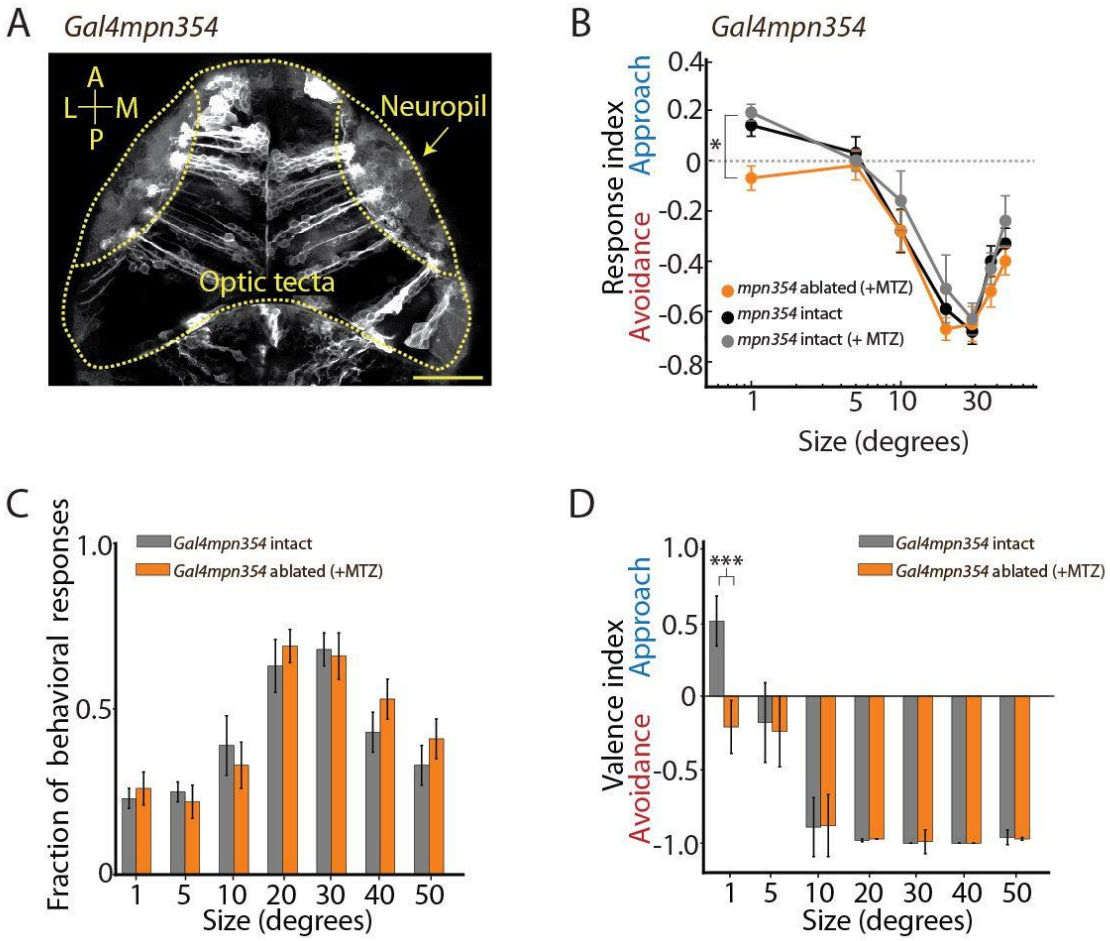

Figure 21: Ablation of *Gal4mpn354* neurons shifts behavioral responses to avoidance at small sizes. (**A**) Expression pattern in the 5 dpf optic tectum in a *Gal4mpn354*, *UAS:Dendra* fish. (**B**) R.I. of *Gal4mpn354, UAS:Nfsb-mChry* larvae (MTZ-treated, n=31, orange; no MTZ, n=24, black) and *Gal4mpn354, UAS:Dendra* (MTZ-treated, n=12, gray). Following ablation, the R.I. for a 1° dot switches from approach to avoidance (two-way ANOVA, Tukey's correction, p at 1° = 0.038, 0.032). (**C**) The fraction of behavioral responses is not changed in *Gal4mpn354* ablated larvae (P= 0.647, 0.621, 0.655 at 1°, 5°, 10° sizes respectively). (**D**) V.I. plots of fish used in (B). At 1°, V.I. is switched from approach to avoidance following ablation of *Gal4mpn354* neurons (Fisher's exact test, p at 1° = 0.0003, p= 1.00 at 5°, p=1.00 at 10°). For all panels, error bars are ± SEM. * = p < 0.05, ** = p < 0.005, *** = p < 0.0005. Scale bar = 50µm; A = anterior, P = posterior, L = lateral, M = medial. Hatched yellow lines denote the optic tecta. Neuropil is indicated in the right tectum with a yellow arrow.

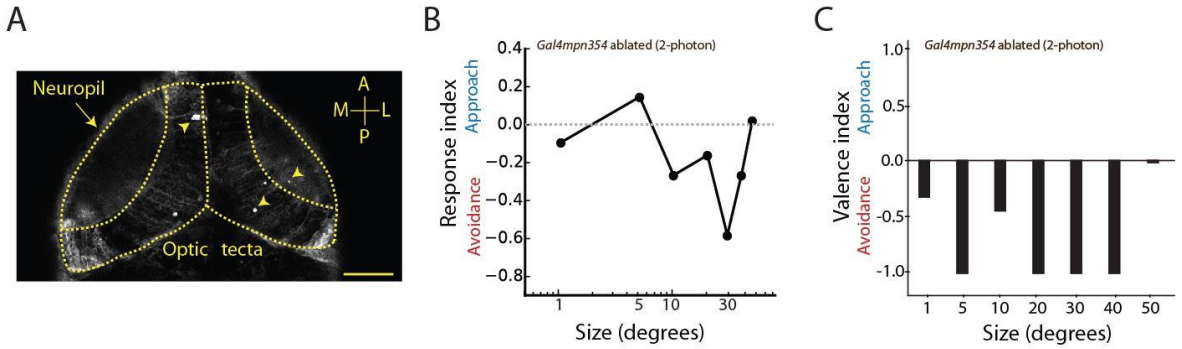

Figure 22: Targeted two-photon ablations of *Galmpn354* neurons. (**A**) Example of a fish targeted for *Gal4mpn354* single cell ablations. (Image taken the day after ablations). Arrowheads denote areas of cell debris resulting from successful cell ablations. Arrow denotes neuropil region. Optic tecta are outlined with hatched yellow lines. (**B**) The R.I. for the fish shown in (A) following ablations. (**C**) Fish with *Galmpn354* neurons ablated have increased avoidance to small dots when compared to control conditions as measured by the V.I. (same fish as in A and B). Scale bar, 50 µm. A=anterior, P=posterior, L= lateral, M = medial.

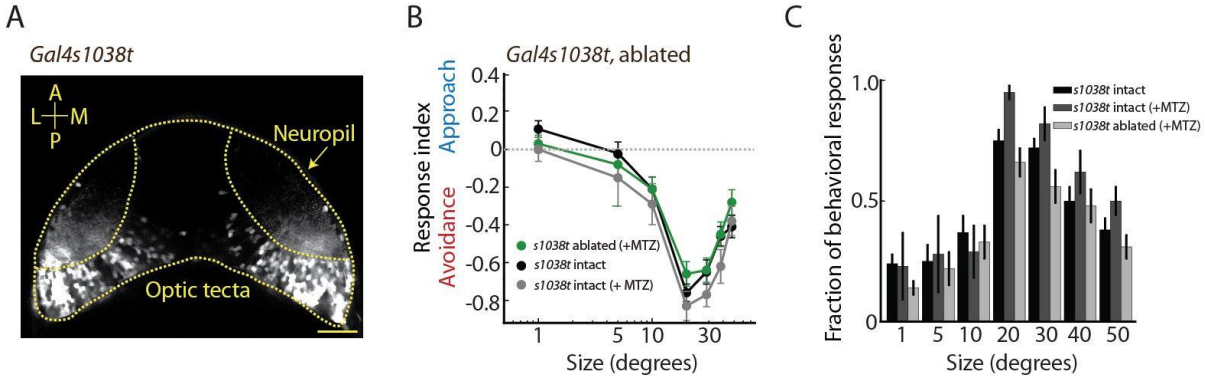

Figure 23: (**A**) Expression pattern in the optic tectum of the enhancer trap line, *Gal4s1038t* shown in a larva expressing *UAS:Kaede*. Expression is restricted to the posterior tectum. (**B**) Behavioral size discrimination tuning curves of *Gal4s1038t, UAS:Nfsb-mChry* ablated fish (green, n = 18) and control conditions (*Gal4s1038t, UAS:Nfsb-mChry* with no MTZ treatment (black, n = 26) and *Gal4s1038t, UAS:Kaede* with MTZ treatment (gray, n = 10)). No changes in the R.I. are observed in ablated larvae compared to controls (two-way, ANOVA with Tukey's correction). (**C**) The fraction of behavioral responses is not significantly different between *Gal4s1038t* ablated conditions and controls. Scale bar = 50µm; A = anterior, P = posterior, L = lateral, M = medial. Hatched yellow lines denote the optic tecta. Neuropil is indicated in the right tectum with a yellow arrow. Error bars are ± SEM.

Optogenetic activation of *Gal4mpn354* neurons facilitates approach behavior

We next asked if *Gal4mpn354* neurons were capable of actively driving approach behaviors. We transiently expressed *UAS:ChR2-mCherry* under the control of the *Gal4mpn354* driver and tested larvae positive for red (mCherry) fluorescence in our behavioral assay while a blue light LED array (475 nm) was pulsed at 10 Hz (20% duty cycle). This illumination regime is expected to activate ChR2 and facilitate spiking of *Gal4mpn354*-positive neurons. We found that global activation of *Gal4mpn354* neurons resulted in an increase in approach behaviors at the smallest size presented (Figure 24A, B). While the blue-light illumination regime reduced behavioral responses to dots of all sizes, and in some cases changed the valence index slightly inverting it at 1° for control fish and decreasing it at 10° for ChR2 expressing fish, we could not detect differences in overall behavioral responsiveness between *Gal4mpn354* larvae and *Gal4*-negative control larvae exposed to the same illumination protocol (Figure 24C). It is likely that the mildly aversive nature of the blue light stimulus is responsible for these observed effects.

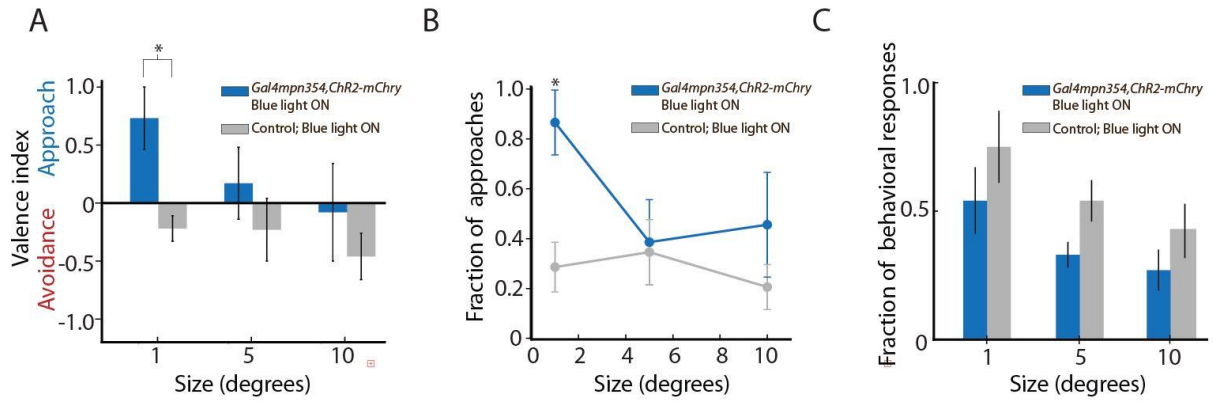

Figure 24: ChR2 activation of *Gal4mpn354* neurons enhances approach behaviors at small sizes. (**A**) The V.I. for *Gal4mpn354* neurons is shifted to approach when compared to wild type siblings exposed to the same blue light stimulation (Fisher's exact test, p= 0.015 at 1°). (**B**) The fraction of approaches is significantly increased at 1° when *Gal4mpn354* neurons are activated (unpaired t test, Bonferroni correction, uncorrected p = 0.014 at 1°). (**C**) The fraction of behavioral responses is not changed when *Gal4mpn354, UAS:ChR2-mChry* larvae are exposed to blue light or when wild type siblings are exposed to blue light. (n= 6, 4 larvae; unpaired t test, Bonferroni correction, uncorrected p =0.331, 0.07, 0.19 for 1°, 5°, 10° respectively. For all panels, error bars are $\pm$ SEM. * = $p < 0.05$.

The majority of *Gal4mpn354* neurons are narrowly tuned to object size

To test the tuning of individual *Gal4mpn354* neurons, we used a *UAS:GCaMP6s* line to drive the expression of the genetically encoded calcium indicator, GCaMP6s, as a readout of neural activity (Chen et al., 2013). Using a custom-built two-photon microscope, we imaged neural activity in head-restrained larvae while presenting visual stimuli (Figure 25A, B). A miniature OLED screen positioned directly in front of the larva presented moving bars of varying widths. To prevent light from the OLED screen from reaching the PMTs, two magenta filters were placed over the screen, and the total luminance of the stimulus was reduced by presenting a gray moving bar on a black background. A horizontally moving vertical bar was chosen to ensure activation of the entire elevation (vertical axis) of the visual field. With this configuration, we could reliably elicit strong calcium responses to the stimulus. An example of the raw calcium response in a 1° tuned cell is shown in Figure 25B. We initially imaged young larvae (5 dpf). In 72 cells recorded from 10 larvae, we found that half of the cells (52%) were narrowly tuned to one of the presented sizes. Interestingly, almost a third of the neurons (31%) were dually tuned, responding to both small and large stimuli, but not to intermediate sizes (Figure 25C-E).

To rule out that sampling any subset of tectal neurons might lead to a similar size tuning distribution, we imaged the responses of *Gal4s1038t* fish crossed to *UAS:GCaMP6s* (Figure 26A). In 38 cells from 5 larvae, we found a significantly different distribution of size-tuned neurons (Mann-Whitney U test, $p = 0.0478$). Overall the number of cells responding to the visual stimuli was much lower in *Gal4s1038t* when compared to *Gal4mpn354* larvae, and the vast majority of neurons labeled in *Gal4s1038t* were tuned to sizes between 10°-40° (Figure 26B, C). Neurons preferring small sizes or dually tuned neurons were largely absent in the *Gal4s1038t* population. The mean population responses, were significantly different between *Gal4mpn354* and *Gal4s1038t* populations (Figure 26D-F, Mann-Whitney U test, $p = 0.0478$).

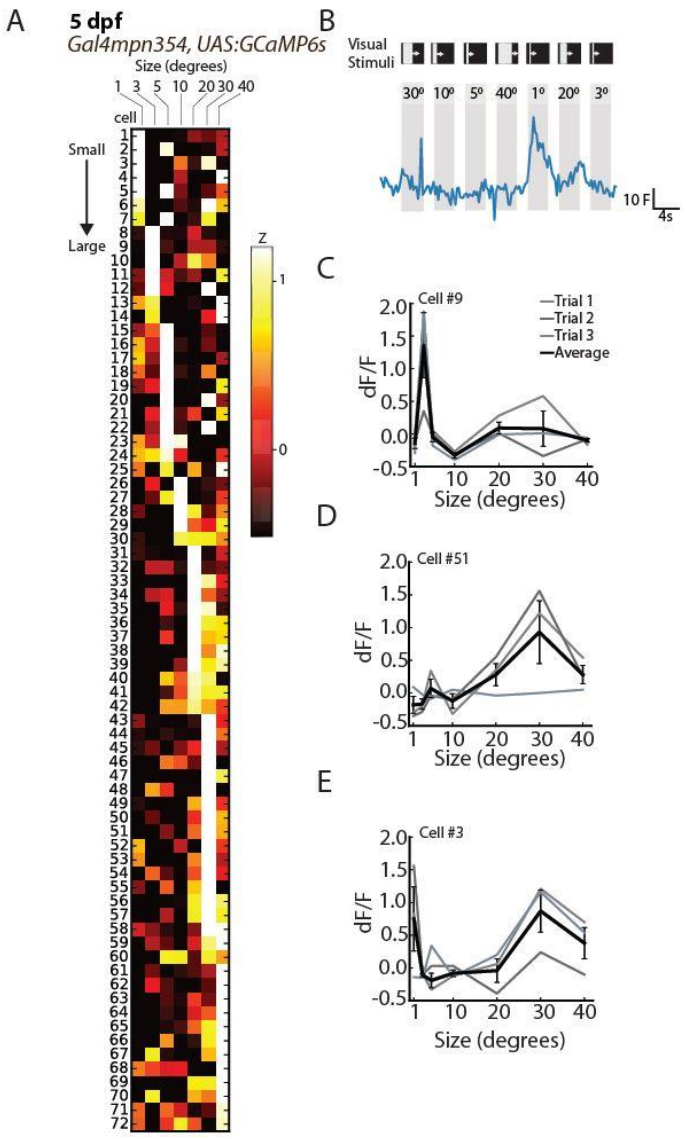

Figure 25: Two-photon GCaMP6s imaging reveals tuning properties of *Gal4mpn354* neurons. (**A**) Complete size-tuning profiles for *Gal4mpn354, UAS:GCaMP6s* neurons (72 cells recorded in 10 larvae, 5 dpf). To normalize raw calcium transients, Z-scores were calculated for each cell. Cells were presented with each stimulus 3-4 times in pseudo-randomized order. (**B**) Raw calcium response to a single trial of a cell tuned to a 1º bar. Each bar stimulus (shaded in gray) lasts for 4s and is preceded by a 2s period of stimulus off. (**C-E**) Examples of size tuning for 3 cells. dF/F values are plotted for each size presentation across three trials (shown in gray scale). Average tuning for the cell is shown in black. (**C**) Example of a cell tuned to a 3° bar. (**D**) Example of a cell tuned to a 30° bar. (**E**) Example of a dually tuned cell responding to both 1° and 30°. For all panels error bars are ± SEM.

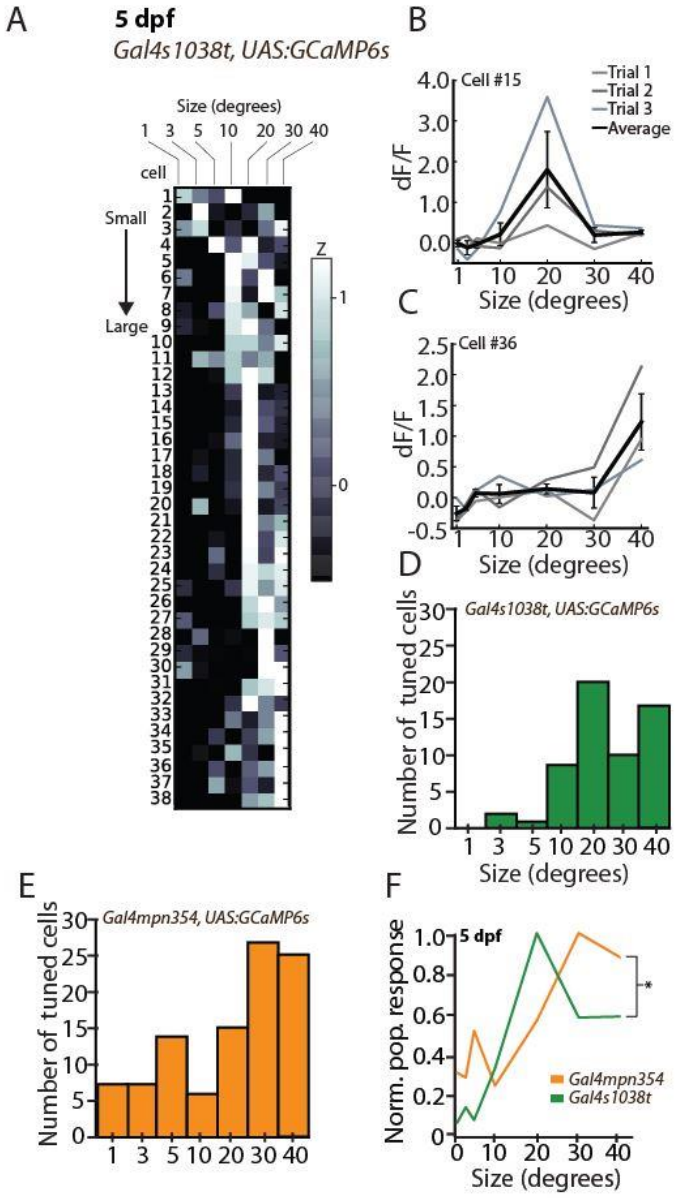

Figure 26: Two-photon GCaMP6s imaging reveals that *Gal4mpn354* and *Gal4s1038t* lines label functionally distinct subsets of tectal neurons. (**A**) Complete size-tuning profiles for *Gal4s1038t, UAS:GCaMP6s* neurons (38 cells recorded in 5 larvae, 5 dpf). (**B**) Example of cell tuned to 20°. (**C**) Example cell tuned to 40°. Notation as above in Figure 25. (**D**) Frequency histogram of all tunings represented in the imaged *Gal4s1038t, UAS:*GCaMP6s larvae. (**E**) Frequency histogram of all tunings represented in the imaged *Gal4mpn354, UAS:*GCaMP6s larvae. (**F**) Normalized population responses. The distribution between the two populations is significantly different (Mann-Whitney U, $p = 0.0478$). For all panels error bars are $\pm$ SEM. * = $p < 0.05$.

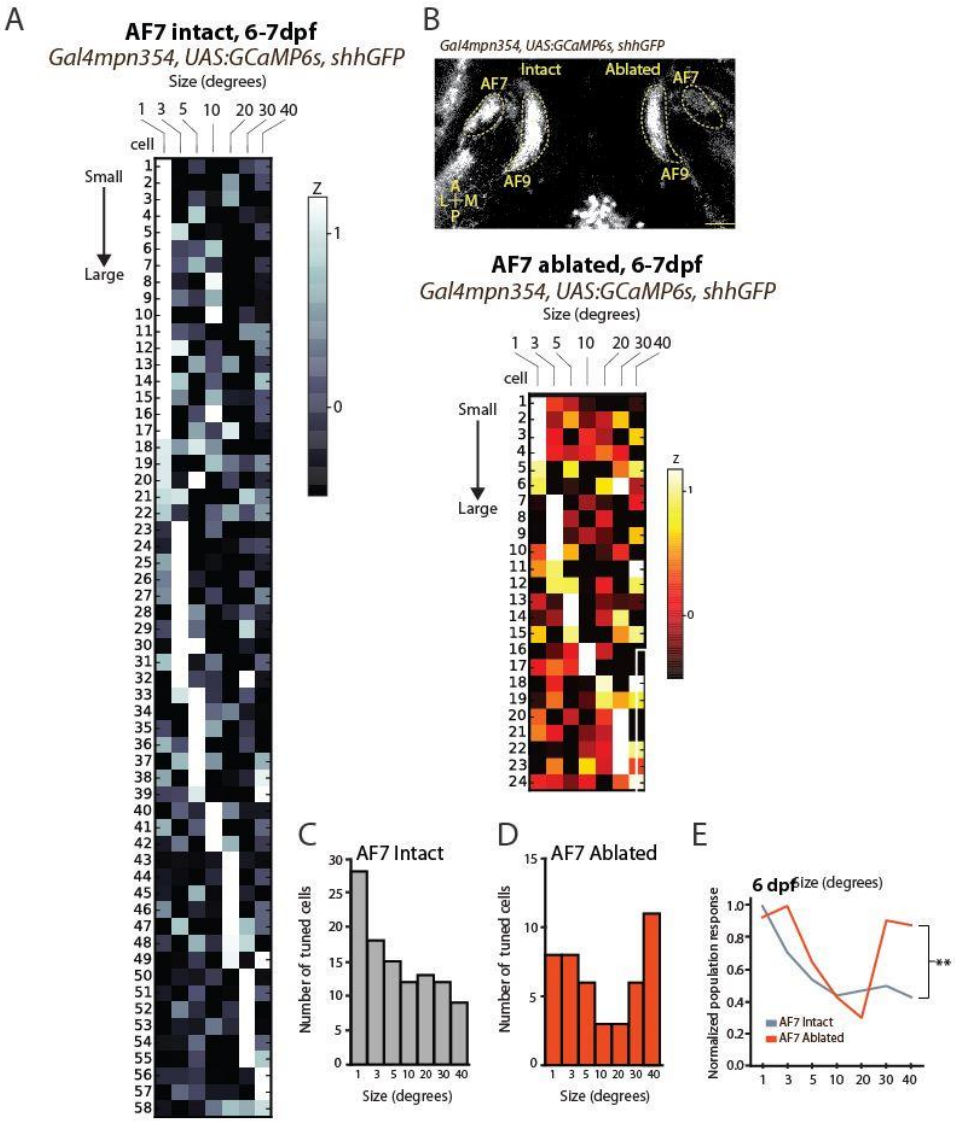

Figure 27: AF7 lesion shifts the population tuning of *Gal4mpn354* neurons to larger sizes. Notations as in Figure 25,26. (**A, B**) Complete size-tuning profiles for *Gal4mpn354, UAS:GCaMP6s* neurons with AF7 intact (58 cells recorded in 10 larvae, 6-7 dpf) and ablated (24 cells recorded in 8 larvae, 6-7 dpf). (**B**) Example of two-photon AF7 ablation performed in *Gal4mpn354, UAS:GCaMP6s, shhGFP* fish. AF9 is also visible in the imaging plane (confocal stack 24 hours post ablation). Left side shows intact AF7 and AF9, right side ablated AF7 and intact AF9. (**C**) Frequency histogram of all tunings presented in (A). (**D**) Frequency histogram of all tunings presented in (B). (**E**) Normalized population responses. The distribution between the two populations is significantly different (Mann-Whitney U test, p =0.0012). Scale bar = 50 µm. A=anterior, P=posterior, L= lateral, M = medial. ** = $p < 0.05$.

Size tuning of *Gal4mpn354* neurons is shaped by inputs from AF7-projecting RGCs

The contribution of *Gal4mpn354* neurons to small-object approach is consistent with a role in prey capture or in the prey capture processing pathway. Between 5 and 7 dpf, prey capture behavior undergoes substantial refinement (Budick and O'Malley, 2000). Consistent with maturation of the underlying circuitry, we found a proportionately larger number of *Gal4mpn354* neurons tuned to small stimuli (1°, 3°, 5°) at 7 dpf than at 5 dpf (Figure 27A; compare with Figure 25A). We hypothesized that weakening prey-selective visual inputs would alter the tuning of *Gal4mpn354* neurons. RGCs that project to pretectal visual area AF7 and the superficial layer SO of the tectum have recently been identified as components of a prey-detection pathway (Semmelhack et al., 2014). We targeted some of the RGC afferents in AF7 for laser ablation in triple-transgenic zebrafish expressing *UAS:GCaMP6s*, driven by *Gal4mpn354*, as well as *Shh:GFP* to label all RGCs (Neumann and Nuesslein-Volhard, 2000). Size tuning was assessed by calcium imaging at 6 or 7 dpf, one day after the lesion of AF7 (Figure 27B). Interestingly, when AF7-RGCs were ablated and thus collateral inputs to the tectum weakened, the frequency distribution and mean population tuning of *Gal4mpn354* neurons were shifted to larger sizes (Figure 27C-E; Mann-Whitney U test, $p = 0.0012$). This result suggests that the AF7-RGC axons provide input to the *Gal4mpn354* neurons, biasing their responses to small, prey-like stimuli.

Most *Gal4mpn354* neurons belong to the nsPVIN class

To characterize the morphology of the *Gal4mpn354* labeled neurons, we used a highly variegated version of *UAS*-driven membrane-targeted *GFP* named "*BGUG*" (Scott et al., 2007) for single neuron labeling (Figure 28A, B). We found that *Gal4mpn354* neurons resemble the non-stratified periventricular interneurons (nsPVINs) described recently (Robles et al., 2011). These cells notably lack efferent projections and form a bushy neurite arbor straddling several deeper

layers of the stratum fibrosum et griseum superficiale (SFGS) and the stratum griseum centrale (SGC). The depth and multi-laminar targeting of their projections suggest a role in integrating visual information arriving from RGCs terminating in different layers of the tectum (Robles et al., 2011)

Most *Gal4mpn354* neurons are glutamatergic

To identify the neurotransmitter identity of the *Gal4mpn354* population we quantified co-localization of *Gal4mpn354, UAS:GCaMP6s* expression and markers of excitatory and inhibitory neurons, vesicular glutamate transporter 2a (Vglut2a) and glutamate decarboxylase (Gad1b) respectively using BAC transgenic lines (Satou et al., 2012; Satou et al., 2013). We found that 76% of *Gal4mpn354* neurons co-localized with the glutamatergic marker and 22% with the GABAergic marker (Figure 28C-E, n=6 fish, n=7, $p = 4.8 \times 10^{-7}$, two-sample, t test).

***Gal4mpn354* ablated larvae show normal OMR, impaired prey capture**

The optomotor response does not require the tectum, but does require normal vision and proper motor control. To test if our manipulations to ablate *Gal4mpn354* neurons had any general effects on visual acuity or mobility we tested *Gal4mpn354* ablated fish and control fish (*Gal4mpn354, UAS:Nfsb-mChry* with no MTZ and *Gal4mpn354, UAS:Dendra* +MTZ) for OMR. We found no significant difference across conditions (Figure 29A, $p = 0.162$, one-way ANOVA, Bonferroni correction). Ablation and optogenetic experiments suggest that *Gal4mpn354* neurons are involved in prey capture. We tested this directly by presenting *Gal4mpn354* ablated larvae and control larvae with live paramecia. After two hours (the time it took to reduce the number of

paramecia in the control conditions to 50%), the amount of paramecia captured by *Gal4mpn354* ablated fish was significantly reduced compared to controls. Paramecium levels were more similar to conditions in which no fish were added to the dish than to control conditions (Figure 29B, adjusted p >0.999 for *Gal4mpn354* ablated conditions versus "no fish added" conditions, p =0.044 for *Gal4mpn354* ablated fish versus *Gal4s1038t* ablated fish, one-way ANOVA, Bonferroni correction).

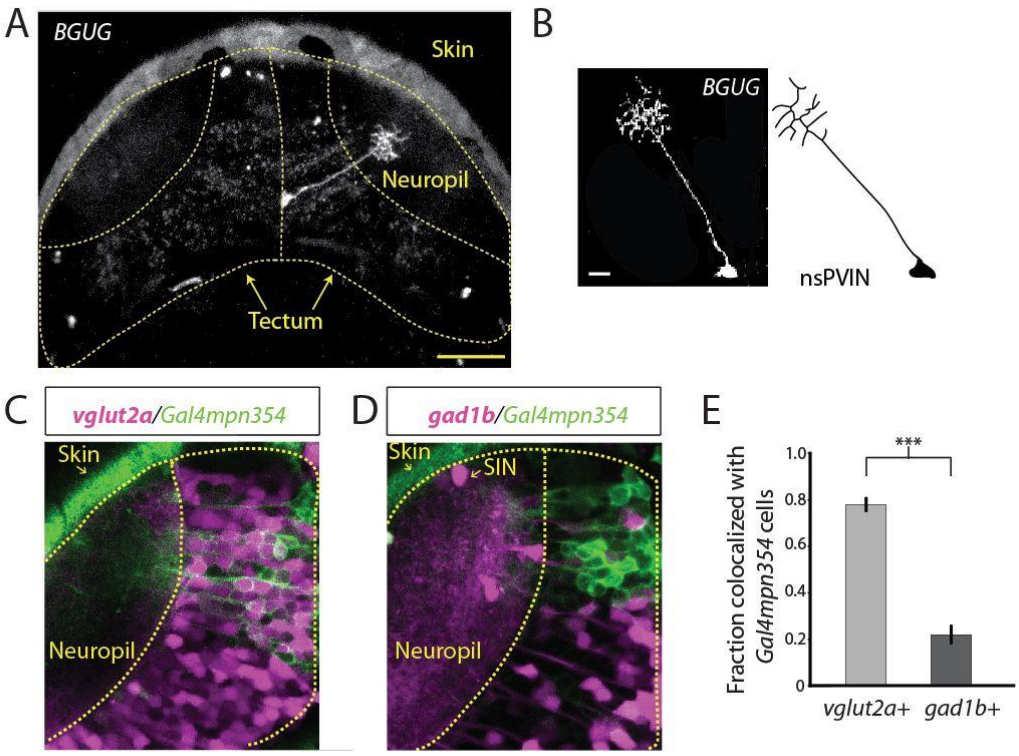

Figure 28: Most *Gal4mpn354* neurons are non-stratified periventricular interneurons (nsPVINs) (**A**) Single cell labeling of a *Gal4mpn354* neuron using the *BGUG* method. (**B**) Close-up and line drawing of the single *Gal4mpn354* neuron shown in (A). Scale bar in (A) = 50µm; in (B) = 10µm. Most *Gal4mpn354* neurons are glutamatergic (**C**) Example of co-localization of *Gal4mpn354,UAS:GCaMP6s* (green) expression and *vglut2a:loxP-DsRed-loxP-GFP* (magenta) expression. (**D**) Example of co-localization of *Gal4mpn354,UAS:GCaMP6s* (green) expression and *gad1b:loxP-DsRed-loxP-GFP* (magenta) expression. (**E**) The majority of *Gal4mpn354* labeled neurons are glutamatergic (VGlut2a; 76%). A minority are GABAergic (Gad1b; 22%). $p=4.8x10^{-7}$, unpaired t test. Hatched yellow lines denote the optic tecta. Neuropil is indicated in the right tectum and skin is also labeled. Error bars are $\pm$ SEM. *** = $p < 0.0005$.

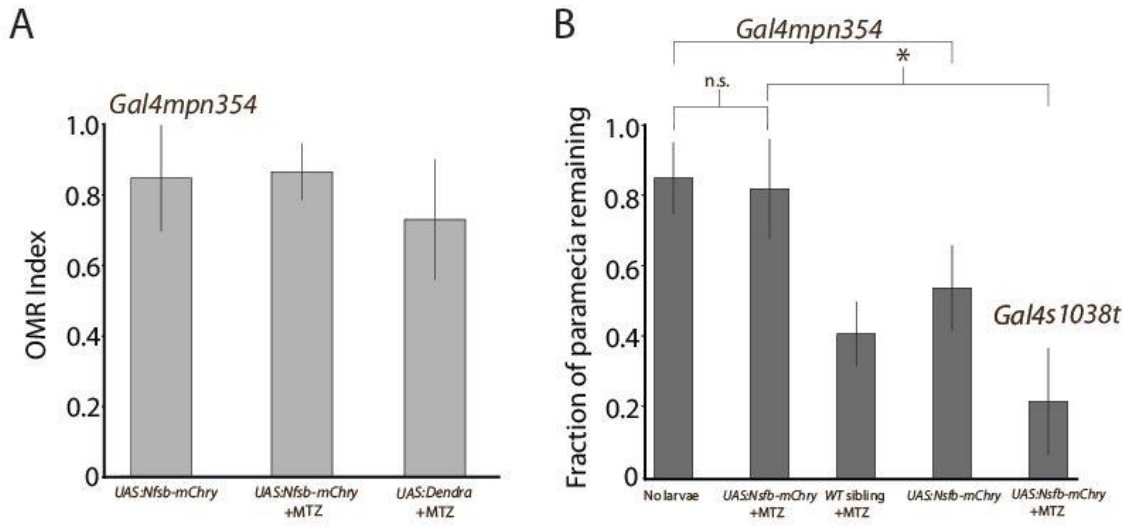

Figure 29: (**A**) Optomotor response is normal when *Gal4mpn354* neurons are ablated. OMR responses are shown for *Gal4mpn354, UAS:Nfsb-mChry* MTZ treated larvae (n =6) and controls (*Gal4mpn354, UAS:Nfsb-mChry* with no MTZ treatment (n = 6) and *Gal4mpn354, UAS:Dendra* MTZ treatment (n =5)) (one-way ANOVA, Bonferroni correction p = 0.162). (**B**) The fraction of paramecia remaining after two hours is not reduced under conditions where *Gal4mpn354* neurons are ablated (adjusted p >0.999, one-way ANOVA, Bonferroni correction). However a significant reduction is observed between *Gal4s1038t* ablated neurons and *Gal4mpn354* ablated neurons (p=0.044). For all panels, error bars are $\pm$ SEM. * = $p < 0.05$.

3.3 Discussion

To dissect the function of the optic tectum in behavioral responses to moving visual objects, we devised a rapid and quantitative behavioral assay for free-swimming zebrafish larvae. The objects presented to the larvae differed only in size, while shape, absolute speed of movement and contrast were held constant. Variations in object size were sufficient to evoke either approach or avoidance. Small dots (subtending visual angles of <5° at their nearest distance to the larva) were generally attractive, whereas large objects (≥10°) were aversive. This behavioral bifurcation is rooted in the fish larva's ecology and is innate. Approaches resemble attempts at prey capture, whereas avoidances are defensive reactions to a perceived threat, i.e., the strike of a predator or an impending collision. We confirmed this interpretation by analysis of the locomotor maneuvers

that the fish perform: Approaches were composed of extended pursuits, whereas avoidances were usually initiated by fast-start escapes. Moreover, older fish larvae approached larger dots, which younger larvae avoided, consistent with a growth-related shift in the preferred food particle size.

Consistent with previous work in birds, amphibians, mammals and fish, a series of genetic and surgical lesion experiments in zebrafish larvae demonstrated that both behaviors depend on the retina and its projections to the tectum. Extra-retinal, e. g., deep-brain (Fernandes et al., 2012) or pineal (Jamieson and Roberts, 2000), photoreception mechanisms appear to contribute very little, if at all, to avoidance of dimming or looming stimuli, at least under the conditions employed here.

An important consideration in classifying behavioral responses in a free-swimming, open-loop assay is the potential for the fish's perception of the dot size to change, and thus the risk of misclassifying a behavioral response. During the first week of life, larval zebrafish are highly myopic. In a similar behavioral configuration (with drifting gratings presented from below), responses were not observed at angles greater than 20° from the vertical plane (Orger et al., 2000). The short resolving distance of the larval fish therefore constrains the range over which objects can be perceived and thus limits possibilities for misclassification.

Both sensory discrimination and action selection have been assigned to the tectum by previous work in mammals, birds, fish and other vertebrates (Felsen and Mainen, 2008, 2012; Horwitz and Newsome, 2001; Krauzlis et al., 2004, 2012; Mysore et al., 2011). In adult goldfish, electrical stimulation of the OT evoked approach or escape depending on the strength and site of current injection (Salas et al., 1997). In the barn owl, activity patterns in the OT correlate with changing stimulus salience through rapidly and gradually changing response properties when competing stimuli are presented. This activity is likely to underlie computations that drive target

selection by biasing selection towards the most salient stimulus (Krauzlis et al., 2004; Mysore and Knudsen, 2011). In rodents, removal or acute inactivation of the SC, has been shown to bias the directional choice of rats during odor discrimination (Felsen and Mainen, 2008). Finally, in primates, a rich body of literature highlights the contributions of the SC to saccade target selection, especially in situations where distractor stimuli are present (Gardner and Lisberger, 2002; Krauzlis et al., 2004, 2013; Kustov and Robinson, 1996; Lovejoy and Krauzlis, 2010; McPeek and Keller, 2004). Taken together the studies in owls, rodents and primates suggest that neural circuits in the OT enhance the perception of target stimuli and/or suppress distractor stimuli through activity patterns that update the saliency of visual stimuli. Here we add evidence that the diminutive tectum of the larval zebrafish may have a similar dual function in sharpening sensory perception and computing behavioral outputs.

We employed our behavioral assay to test the contribution of genetically identified tectal cell types to visual size perception and valence-based behavioral decisions (Del Bene et al., 2010; Gabriel et al., 2012; Nikolaou et al., 2012; Preuss et al., 2014; Robles et al., 2011; Scott et al., 2007). The behavioral tuning curves of fish carrying genetic lesions of specific cell types, allowed us to assign a function to these cells. When SINs are ablated, we see an overall decrease in behavioral responses. This decrease is most pronounced for the stimuli that evoke avoidance, but the trend extends across the entire range of sizes. Remarkably, these deficits are not due to a change in the classification of stimuli; 30° dots are still avoided when detected. Rather, the fraction of behavioral responses is reduced; i.e., the SIN-depleted fish often ignore the moving dots. The SINs, thus, appear to be important for accurate perception of objects, perhaps by increasing visual resolving power or by enhancing stimulus-to-background contrast.

In contrast, cells within the *Gal4mpn354* population appear to have a specific role in the classification of small objects. When *Gal4mpn354* neurons are ablated, small dots tend to be

avoided rather than approached. This switch is not due to a decrease in behavioral responsiveness, suggesting that small dots are still being perceived, but are now misclassified.

Gal4mpn354-depleted larvae show normal OMR (Figure 29A). This finding excludes an unspecific effect of these cells on motor control or gross visual defects. Rather, their optogenetic activation appears to facilitate neuronal responses to potential prey objects. The ability to enhance approach, by remotely activating the *Gal4mpn354* population of neurons, and to shift approach to avoidance, by lesioning it, strongly suggests that a significant proportion of the *Gal4mpn354* neurons are components of an approach pathway. The behavioral switch may be explained by the existence of a competing avoidance circuit, which is somewhat responsive even to small objects but normally suppressed by *Gal4mpn354* neurons. When this inhibition is removed by *Gal4mpn354* ablation, tectal output may then become biased toward escape regardless of stimulus size.

Single-cell labeling of *Gal4mpn354* cells showed that they are typical tectal interneurons with neurite arbors extending into the neuropil. Morphologically, they resemble the non-stratified periventricular interneuron class (nsPVINs) previously described (Robles et al., 2011). The dendrites of the nsPVINs span multiple layers of the SFGS, which receives predominantly retinal input, and the deeper SGC. This connection might allow *Gal4mpn354* neurons to sample from multiple streams of RGC input, carrying information about different sizes of visual objects. The arborization pattern of the *Gal4mpn354* neuron might also allow for integration of both visual and nonvisual inputs arriving in deeper layers.

We have begun to explore the physiological function of the *Gal4mpn354* population by simultaneous visual stimulation and calcium imaging in a semi-restrained, “head-fixed” configuration. Using GCaMP6s, we find that the *Gal4mpn354* driver labels neurons that are each tuned to a narrow range of sizes but as a population to the full range of sizes tested (1°-40°). A

non-overlapping group of tectal cells, the posterior projection neurons labeled in the *Gal4s1038t* driver line displayed a significantly different population tuning, which was shifted to larger sizes. Although we do not yet know the behavioral function of *Gal4s1038t* neurons, this finding indicates that different tectal neurons are specialized in their size selectivity and participate in different behavioral output pathways.

Recently, our group discovered that prey capture relies on two morphological types of RGCs, which arborize in the extratectal AF7 before sending afferents to the most superficial layer of the tectum (Semmelhack et al., 2014). Here we show that ablations of AF7 neuropil, thus damaging collateral projections to the tectum, result in a shift of the population response of *Gal4mpn354* neurons from small- to large-object preference compared to larvae with an intact AF7. We do not know if the tuning of individual *Gal4mpn354* cells is altered or if many of the AF7-receptive cells become unresponsive following AF7 ablation. The fact that we see generally fewer cells responding to visual stimuli argues in favor of the latter scenario.

It is currently not possible to resolve if *Gal4mpn354* neurons are sampling AF7 input directly or if RGC afferents in AF7 which continue to the tectum are lost during AF7 ablations. It is clear that both AF7 and the tectum are required for prey capture (Gahtan et al., 2005; Semmelhack et al., 2014). It is possible that AF7 sends direct inputs into the tectum that modulate the activity of *Gal4mpn354* neurons and enhance approach. It is equally possible that *Gal4mpn354* neurons receive their small object size tuning directly from RGC inputs to the tectum. Testing direct synaptic connections via electrical stimulation protocols are unlikely to be successful due to the small size of the larval zebrafish and viral tracing techniques are currently unavailable in zebrafish.

Together, our results suggest that the tectum may discriminate objects by size through mechanisms that enhance visual resolution (via SINs and other cells) and may select appropriate

behavior through mechanisms that assign valence to pre-processed stimuli (potentially via nsPVINs (Robles et al., 2011) contained within the *Gal4mpn354* population).

Finally, in studying circuits involved in prey capture one important consideration is the metabolic state of the animal (e.g. fed or starved). Behavioral flexibility requires neural circuits to adapt to the internal state of the animal. One possible outcome of such a feedback loop might be that ambiguously classified visual stimuli will be less likely to be pursued when the fish is satiated. In future experiments it will be of interest to explore how the satiety level of the fish might affect behavioral size tuning curves and where in the brain such effects might be integrated.

Work in mammalian species has demonstrated that the prefrontal cortex (PFC) is the primary site of executive function, ensuring behavioral output matches internal goals (Miller and Cohen, 2001). A recent study demonstrated that the PFC can modulate sensory selection by directly modulating activity in the thalamus (Wimmer et al., 2015). The role of thalamus is less well understood in the zebrafish (Mueller, 2012). However, early work in the toad and frog demonstrated that the pretectum and thalamus provide inhibitory input to the tectum required for the proper gating of orienting and avoidance behaviors and there is evidence that this inhibitory feedback is in part carried by neuropeptide Y positive fibers (Ewert et al., 1999). Might neuromodulatory systems be involved in gating behavioral responses in our size discrimination assay based on internal state?

Earlier work by Ewert and colleagues demonstrated dopaminergic modulation of the final stage of prey capture. Treatment with the dopamine agonist apomorphine increased snapping in response to visual stimuli while visual discrimination was not affected and no changes in other components of prey capture, (i.e. orienting or turning) were observed (Glagow and Ewert, 1997a, 1997b). This work provided evidence that neuromodulatory pathways can influence the visuomotor transformations driving prey capture and interestingly that these circuits may act selectively on different parts of the behavioral sequence.

A recently published projectome mapping all dopaminergic and noradrenergic neurons in the larval zebrafish demonstrated that the tectum receives dopaminergic input form the pretectum and noradrenergic input from the locus coeruleus (Tay et al., 2011). Importantly this work provides a valuable foundation for future studies investigating the neuromodulation of prey capture. The tectum also receives extensive serotonergic input (Lillesaar, 2011; Yokogawa et al., 2012). The serotonergic system is known to be regulated by the hypothalamic-pituitary-adrenal (HPA) axis and its zebrafish equivalent the hypothalamic-pituitary-interrenal (HPI) axis, both regulators of appetite and satiety, making this pathway a promising candidate for modulating behavioral responses to visual stimuli in response to hunger state (Fox and Lowry, 2013; Voigt and Fink, 2015).

Acknowledgements: E. Kühn, E. Dragomir and A. Grob helped with behavioral experiments, and S. Higashijima kindly provided the *vglut2a:loxP-DsRed-loxP-GFP* and *gad1b*:*loxP-DsRed-loxP-GFP* fish lines.

References

Bianco, I.H., Kampff, A.R., and Engert, F. (2011). Prey capture behavior evoked by simple visual stimuli in larval zebrafish. Front. Syst. Neurosci. *5*, 101.

Budick, S.A., and O'Malley, D.M. (2000). Locomotor repertoire of the larval zebrafish: swimming, turning and prey capture. J. Exp. Biol. *203*, 2565–2579.

Chen, T.-W., Wardill, T.J., Sun, Y., Pulver, S.R., Renninger, S.L., Baohan, A., Schreiter, E.R., Kerr, R.A., Orger, M.B., Jayaraman, V., et al. (2013). Ultrasensitive fluorescent proteins for imaging neuronal activity. Nature *499*, 295–300.

Del Bene, F., Wyart, C., Robles, E., Tran, A., Looger, L., Scott, E.K., Isacoff, E.Y., and Baier, H. (2010). Filtering of visual information in the tectum by an identified neural circuit. Science *330*, 669–673.

Dong, W., Lee, R.H., Xu, H., Yang, S., Pratt, K.G., Cao, V., Song, Y.-K., Nurmikko, A., and Aizenman, C.D. (2009). Visual avoidance in Xenopus tadpoles is correlated with the maturation of visual responses in the optic tectum. J. Neurophysiol. *101*, 803–815.

Ewert, J.P. (1970). Neural mechanisms of prey-catching and avoidance behavior in the toad (Bufo bufo L.). Brain. Behav. Evol. *3*, 36–56.

Ewert, J.P., Buxbaum-Conradi, H., Glagow, M., Röttgen, A., Schürg-Pfeiffer, E., and Schwippert WW. (1999). Forebrain and midbrain structures involved in prey-catching behaviour of toads: stimulus-response mediating circuits and their modulating loops. Eur J Morphol. 37,172-6.

Felsen, G., and Mainen, Z.F. (2008). Neural substrates of sensory-guided locomotor decisions in the rat superior colliculus. Neuron *60*, 137–148.

Felsen, G., and Mainen, Z.F. (2012). Midbrain contributions to sensorimotor decision making. J. Neurophysiol. *108*, 135–147.

Fernandes, A.M., Fero, K., Arrenberg, A.B., Bergeron, S.A., Driever, W., and Burgess, H.A. (2012). Deep brain photoreceptors control light-seeking behavior in zebrafish larvae. Curr. Biol. CB *22*, 2042–2047.

Fox, J.H., and Lowry, C.A. (2013). Corticotropin-releasing factor-related peptides, serotonergic systems, and emotional behavior. Front Neurosci. 7.

Gabriel, J.P., Trivedi, C.A., Maurer, C.M., Ryu, S., and Bollmann, J.H. (2012). Layer-specific targeting of direction-selective neurons in the zebrafish optic tectum. Neuron *76*, 1147–1160.

Gahtan, E., Tanger, P., and Baier, H. (2005). Visual prey capture in larval zebrafish is controlled by identified reticulospinal neurons downstream of the tectum. J. Neurosci. Off. J. Soc. Neurosci. *25*, 9294–9303.

Gardner, J.L., and Lisberger, S.G. (2002). Serial linkage of target selection for orienting and tracking eye movements. Nat. Neurosci. *5*, 892–899.

Glagow M., and Ewert, J.P. (1997a). Dopaminergic modulation of visual responses in toads. I. Apomorphine-induced effects on visually directed appetitive and consummatory prey-catching behavior. J Comp Physiol A. 180, 1-9.

Glagow M., and Ewert, J.P. (1997b). Dopaminergic modulation of visual responses in toads. II. Influences of apomorphine on retinal ganglion cells and tectal cells. J Comp Physiol A. 180, 11-8.

Goldberg ME, Wurtz RH. (1972a). Activity of superior colliculus in behaving monkey. I. Visual receptive fields of single neurons. J Neurophysiol. 35, 542-59.

Goldberg ME, Wurtz RH. (1972b).Activity of superior colliculus in behaving monkey. II. Effect of attention on neuronal responses. J Neurophysiol. 35, 560-74.

Goldberg ME, Wurtz RH. (1972c). Activity of superior colliculus in behaving monkey. 3. Cells discharging before eye movements. J Neurophysiol. 35, 575-86.

Goldberg ME, Wurtz RH. (1972d). Activity of superior colliculus in behaving monkey. IV. Effects of lesions on eye movements. J Neurophysiol. 35, 587-96.

Horwitz, G.D., and Newsome, W.T. (2001). Target selection for saccadic eye movements: prelude activity in the superior colliculus during a direction-discrimination task. J. Neurophysiol. *86*, 2543–2558.

Ingle, D. (1973). Two visual systems in the frog. Science *181*, 1053–1055.

Jamieson, D., and Roberts, A. (2000). Responses of young Xenopus laevis tadpoles to light dimming: possible roles for the pineal eye. J. Exp. Biol. *203*, 1857–1867.

Krauzlis, R.J., Liston, D., and Carello, C.D. (2004). Target selection and the superior colliculus: goals, choices and hypotheses. Vision Res. *44*, 1445–1451.

Krauzlis, R.J., Dill, N., and Fowler, G.A. (2012). Dissociation of pursuit target selection from saccade execution. Vision Res. *74*, 72–79.

Krauzlis, R.J., Lovejoy, L.P., and Zénon, A. (2013). Superior colliculus and visual spatial attention. Annu. Rev. Neurosci. *36*, 165–182.

Kustov AA, Robinson DL.(1996). Shared neural control of attentional shifts and eye movements. Nature. 384, 74-7.

Lillesaar, C. (2011).The serotonergic system in fish. . J Chem Neuroanat. 41, 294-308.

Lovejoy, L.P., and Krauzlis, R.J. (2010). Inactivation of primate superior colliculus impairs covert selection of signals for perceptual judgments. Nat. Neurosci. *13*, 261–266.

McPeek, R.M., and Keller, E.L. (2004). Deficits in saccade target selection after inactivation of superior colliculus. Nat. Neurosci. *7*, 757–763.

Miller, E.K. and Cohen, J.D. (2001). An integrative theory of prefrontal cortex function. Annu Rev Neurosci. 24, 167-202.

Mueller, T. (2012). What is the Thalamus in Zebrafish? Front Neurosci., 6:64.

Muto, A., Ohkura, M., Abe, G., Nakai, J., and Kawakami, K. (2013). Real-time visualization of neuronal activity during perception. Curr. Biol. CB *23*, 307–311.

Mysore, S.P., and Knudsen, E.I. (2011). The role of a midbrain network in competitive stimulus selection. Curr. Opin. Neurobiol. *21*, 653–660.

Mysore, S.P., Asadollahi, A., and Knudsen, E.I. (2011). Signaling of the strongest stimulus in the owl optic tectum. J. Neurosci. Off. J. Soc. Neurosci. *31*, 5186–5196.

Neumann, C.J., and Nuesslein-Volhard, C. (2000). Patterning of the zebrafish retina by a wave of sonic hedgehog activity. Science *289*, 2137–2139.

Nevin, L.M., Robles, E., Baier, H., and Scott, E.K. (2010). Focusing on optic tectum circuitry through the lens of genetics. BMC Biol. *8*, 126.

Niell, C., and Smith, S. (2005). Functional Imaging Reveals Rapid Development of Visual Response Properties in the Zebrafish Tectum. Neuron *45*, 941–951.

Nikolaou, N., Lowe, A.S., Walker, A.S., Abbas, F., Hunter, P.R., Thompson, I.D., and Meyer, M.P. (2012). Parametric functional maps of visual inputs to the tectum. Neuron *76*, 317–324.

Orger, M.B., Smear, M.C., Anstis, S.M., and Baier, H. (2000). Perception of Fourier and non-Fourier motion by larval zebrafish. Nat. Neurosci. *3*, 1128–1133.

Patterson, B.W., Abraham, A.O., MacIver, M.A., and McLean, D.L. (2013). Visually guided gradation of prey capture movements in larval zebrafish. J. Exp. Biol. *216*, 3071–3083.

Preuss, S.J., Trivedi, C.A., Vom Berg-Maurer, C.M., Ryu, S., and Bollmann, J.H. (2014). Classification of Object Size in Retinotectal Microcircuits. Curr. Biol. CB.

Robles, E., Smith, S.J., and Baier, H. (2011). Characterization of genetically targeted neuron types in the zebrafish optic tectum. Front. Neural Circuits *5*, 1.

Roeser, T., and Baier, H. (2003). Visuomotor behaviors in larval zebrafish after GFP-guided laser ablation of the optic tectum. J. Neurosci. Off. J. Soc. Neurosci. *23*, 3726–3734.

Sajovic, P., and Levinthal, C. (1982a). Visual cells of zebrafish optic tectum: mapping with small spots. Neuroscience *7*, 2407–2426.

Sajovic, P., and Levinthal, C. (1982b). Visual response properties of zebrafish tectal cells. Neuroscience *7*, 2427–2440.

Salas, C., Herrero, L., Rodriguez, F., and Torres, B. (1997). Tectal codification of eye movements in goldfish studied by electrical microstimulation. f. Neuroscience *78*, 271–288.

Satou, C., Kimura, Y., and Higashijima, S. (2012). Generation of multiple classes of V0 neurons in zebrafish spinal cord: progenitor heterogeneity and temporal control of neuronal diversity. J. Neurosci. Off. J. Soc. Neurosci. *32*, 1771–1783.

Satou, C., Kimura, Y., Hirata, H., Suster, M.L., Kawakami, K., and Higashijima, S. (2013). Transgenic tools to characterize neuronal properties of discrete populations of zebrafish neurons. Dev. Camb. Engl. *140*, 3927–3931.

Schiller P.H. and Stryker M. (1972). Single-unit recording and stimulation in superior colliculus of the alert rhesus monkey. J Neurophysiol. 35, 915-24.

Scott, E.K., and Baier, H. (2009). The cellular architecture of the larval zebrafish tectum, as revealed by gal4 enhancer trap lines. Front. Neural Circuits *3*, 13.

Scott, E.K., Mason, L., Arrenberg, A.B., Ziv, L., Gosse, N.J., Xiao, T., Chi, N.C., Asakawa, K., Kawakami, K., and Baier, H. (2007). Targeting neural circuitry in zebrafish using GAL4 enhancer trapping. Nat. Methods *4*, 323–326.

Semmelhack, J.L., Donovan, J.C., Thiele, T.R., Kuehn, E., Laurell, E., and Baier, H. (2014). A dedicated visual pathway for prey detection in larval zebrafish. eLife *3*.

Tay, T,L., Ronneberger, O., Ryu, S., Nitschke, R., Driever, W. (2011). Comprehensive catecholaminergic projectome analysis reveals single-neuron integration of zebrafish ascending and descending dopaminergic systems. Nat Commun. 171.

Temizer, I., Donovan, J.C., Baier, H., and Semmelhack, J.L. (2015). A Visual Pathway for Looming-Evoked Escape in Larval Zebrafish. Curr. Biol. CB.

Trivedi, C.A., and Bollmann, J.H. (2013). Visually driven chaining of elementary swim patterns into a goal-directed motor sequence: a virtual reality study of zebrafish prey capture. Front. Neural Circuits *7*, 86.

Voigt, J.P., and Fink, H. (2015). Serotonin controlling feeding and satiety. Behav Brain Res. 277,14-31.

Wimmer, R.D., Schmitt, L.I., Davidson, T.J., Nakajima, M., Deisseroth, K., and Halassa, M.M. (2015). Thalamic control of sensory selection in divided attention. Nature.;526, 705-9.

Yokogawa, T., Hannan, M.C., and Burgess, H.A. (2012). The dorsal raphe modulates sensory responsiveness during arousal in zebrafish. J. Neurosci. Off. J. Soc. Neurosci. *32*, 15205–15215.

Chapter 4: Investigating the role of the SINs in size selective behaviors

4.1 Introduction

In addition to a screening approach using *Gal4* driver lines available in our lab (described in Chapter 3), we took a candidate approach to identify the cellular components underlying size selectivity by testing a previously identified population of neurons with proposed roles in size filtering. The **S**uperficial **In**terneurons (SINs) are GABAergic interneurons with cells bodies in the most superficial layers of the optic tectum (Del Bene et al., 2010). They were first identified in the *Gal4s1156t* driver line (Scott and Baier, 2009). Initial characterization of their size tuning properties demonstrated that the SINs were more responsive to a full screen flash than a 3° black bar moving across the visual field. As the size of the moving bar was increased, the calcium response in the SINs also increased suggesting a preferred tuning for large objects.

Further, when activity in SINs was silenced through the expression of tetanus-toxin light chain (TeTxLC), prey capture activity was impaired in a live paramecia capture assay. This was an intriguing result especially when considered with additional findings in the same work, which identified a preferred tuning for smaller objects in the deeper layers of the tectal neuropil compared to the superficial layers. Critically no superficial vs. deep difference in neural activity was seen at the level of RGC axons, only in populations of tectal periventricular neurons (PVNs), positing the existence of a tectal mechanism for extracting size information from retinal inputs. When SINs were ablated, the small object tuning was decreased in the deeper neuropil layers. The mapping of size-tuned inputs across the depth of the tectal neuropil, suggested a superficial-to-deep size filtering mechanism that was mediated in part by the inhibitory drive provided by SINs. Vertical transmission of neural activity through the tectal layers had been previously suggested by work in another teleost species (Kinoshita et al., 2002; Kinoshita and Ito, 2006), yet

the SINs provided the first mechanistic evidence for this information flow. In the mouse visual cortex a similar inhibitory interneuron with size filtering properties was recently described, suggesting the possibility such size filtering mechanisms might be conserved across species and brain regions (Adesnik et al., 2012 and see Figure 30 for comparison).

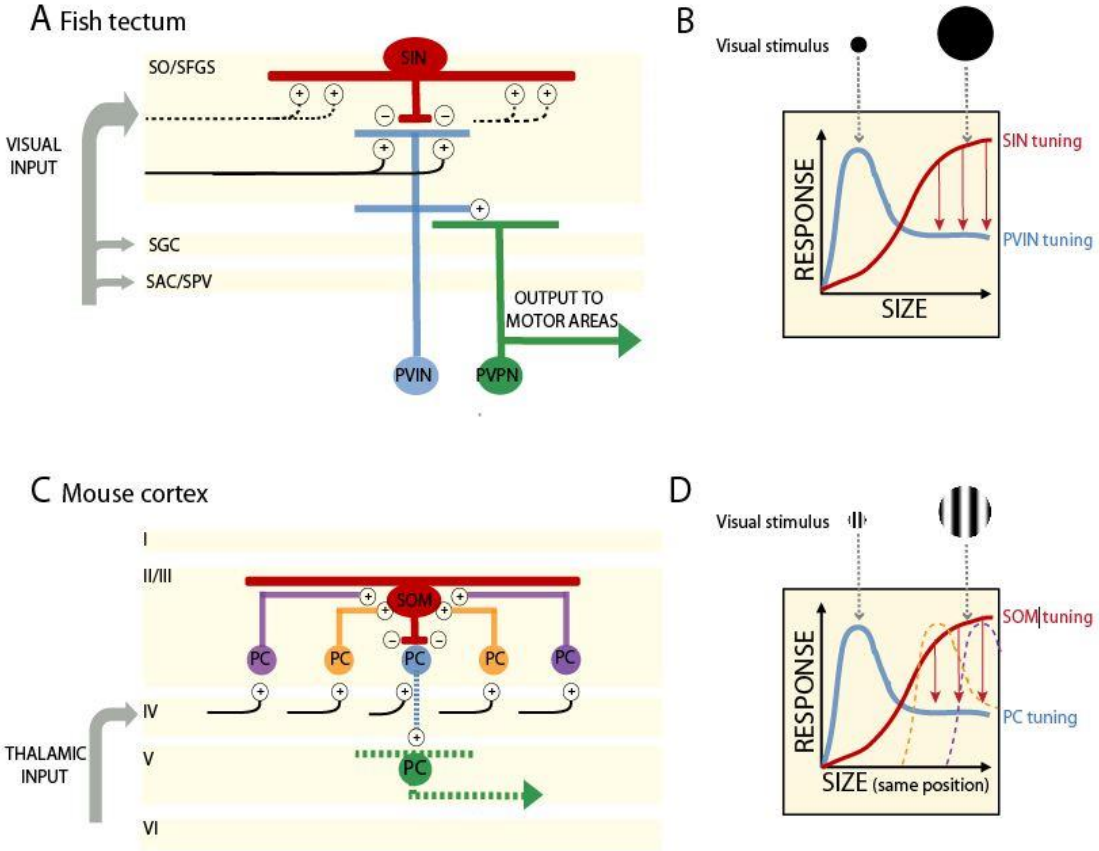

Figure 30: Similar inhibitory populations across species, SINs and SOMs. (A) SINs receive putative RGC input and are (B) SIN activity sharpens the tuning of PVINs. (C) In the mouse cortex, the somatostatin +, SOMs provide local inhibitory input to PCs while receiving input from many neighboring PCs. (D) Localized inhibition by the SOMs sharpens the tuning of individual PCs. [Figure reprinted from Barker and Baier 2013].

4.2 SINs contribute to large object avoidance and respond to changes in overall light level

We first tested the role of the SINs in size discrimination using the behavioral assay described in Chapter 2. Due to the labeling of other tectal neurons and several extratectal regions by the *Gal4s1156t* driver line we were unable to use *UAS* lines for ablation or silencing (e.g. *UAS:Nfsb-mChry* or *UAS:TeTxLC-CFP* as described in Chapter 2 and 3). Instead we employed a pulsed infrared (2-photon) laser to selective ablate single SINs. The main results of these experiments including changes in the size discrimination tuning curve resulting from SIN ablation have been described in detail in Chapter 3. Related experimental procedures will be discussed in Chapter 6. In this chapter, we highlight additional characterization that was undertaken to further map the response properties of the SINs. Increasing the number of SINs ablated increased deficits in the avoidance response measured by the R.I. (Figure 31A). For all fish ablated, we tested avoidance behaviors at 30° before and after ablation. Results for all fish are shown in Figure 31B. When subjecting SIN-ablated larvae to the full size discrimination tuning curve we observed a decrease in the R.I. at larger sizes (significant at 30°, see Figure 20, two-way ANOVA with Bonferroni correction, uncorrected p at 30° = 0.004).

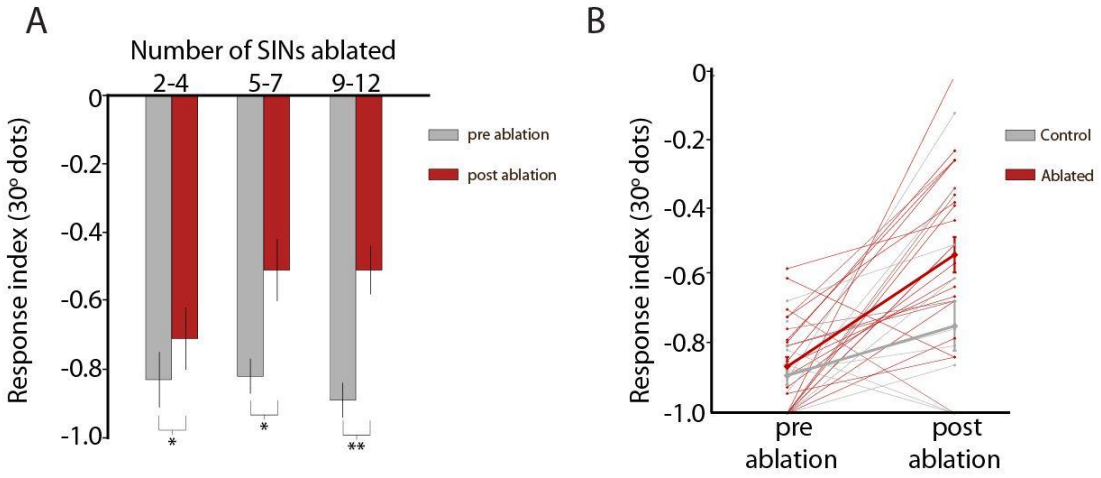

Figure 31: (**A**) Increasing the number of ablated SINs per larva, decreases the R.I. to 30° dots. R.I.s in the same larva are compared pre and post ablation. (p = 0.02, 0.04, 0.004, paired t test, n = 5, 7, 9 respectively). Error bars are ± SEM. (**B**) Individual pre and post R.I.s for all fish in (A).

SINs are responsive to overall luminance levels

In parallel to our behavioral experiments we developed a protocol for perfomring *in vivo* patch-clamp recordings in SINs while simultaneously presenting visual stimuli (Figure 32). In stable voltage-clamp recordings we observed an increased baseline activity in response to conditions of low-luminance, lights off. A representative example is shown in Figure 32. This strong effect biased any addditional size tuning mapping as recordings were performed in the dark to ensure the only illumination source was the screen presenting the visual stimuli. As the baseline activity in the dark was so high, it was difficult to extract changes in activity resulting

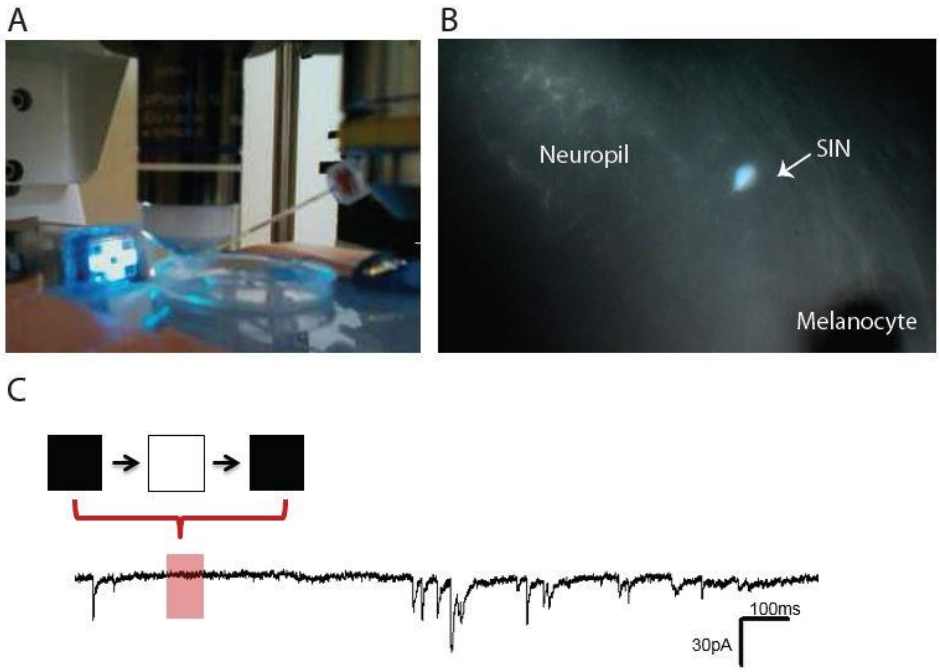

Figure 32: (**A**) Image of the experimental set-up for *in vivo* patch-clamp recordings in the larval zebafish. Visual stimuli are presented binocularly in front of the agarose-embedded fish. (**B**) Image of a SIN visualized under the fluorescent microscope (*Gal4s1156t, UAS:Kaede* fish; green fluorescence is Kaede +). Cell body of the SIN is ~ 8-10 µm and indicated with a white arrow. The neuropil is also labeled. Skin is peeled away gently to expose the brain, a melanotype in a section of intact skin is also labeled (lower right). (**C**) Example voltage-clamp recording of a SIN in response to a full field flash. Scale bar = 30pA and 100ms.

from the visual stimuli. However, preliminary analysis of our recordings revealed two striking features of SIN physiology. First, synaptic inputs to the SINs appeared to refine over time with the amplitude and frequency of EPSCs showing decreased variability at 9 dpf when compared to early timepoints (6 dpf; see Figure 33 for representative examples). Secondly, quantificaiton of the total synaptic current during “lights-on” versus “lights- off” (high vs. low luminance) conditions, showed a significant increase in the excitatory synaptic current in the dark (Figure 34, $p = 0.007$, paired t test). These results although, preliminary suggest several possibilities. One is that SINs receive selective input from OFF visual pathways either directly from RGCs or through relay neurons in the OFF pathway. We observed delays of around 100 ms between stimulus onset and the first recorded EPSCs. Monosynaptic inputs assessed by electrical stimulation from the retina to the thalmus have been reported in the 5 ms range (Usrey et al., 1998) and in the frog less than 1ms from retina to tectum (Matsumoto and Bando, 1980). However, average delays between visual stimlus onset and OFF RGC spiking have been reported to be between 60-100 ms (Gollisch and Meister, 2008), allowing for the possibility that SINs receive direct synaptic input from RGCs. Another intriguing possibility is that SINs may have an endogenous sensitivity to light (Fernandes et al., 2012; Fischer et al., 2013). Although further studies are required before any firm conclusions can be made.

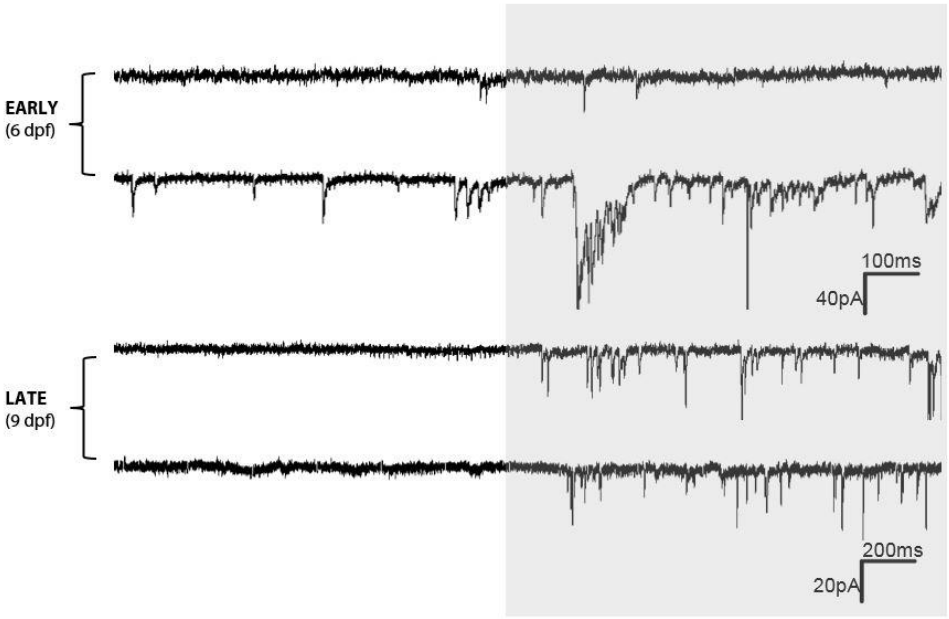

Figure 33: Excitatory synaptic input to SINs is increased under conditions of low luminance and shows developmental refinement. Two example traces for developmental time points 6 dpf (top) and 9dpf (bottom) are shown. At later time points, 9 dpf, the amplitude and frequency are less variable when compared to 6 dpf. Scale bar = 200 ms and 20 pA.

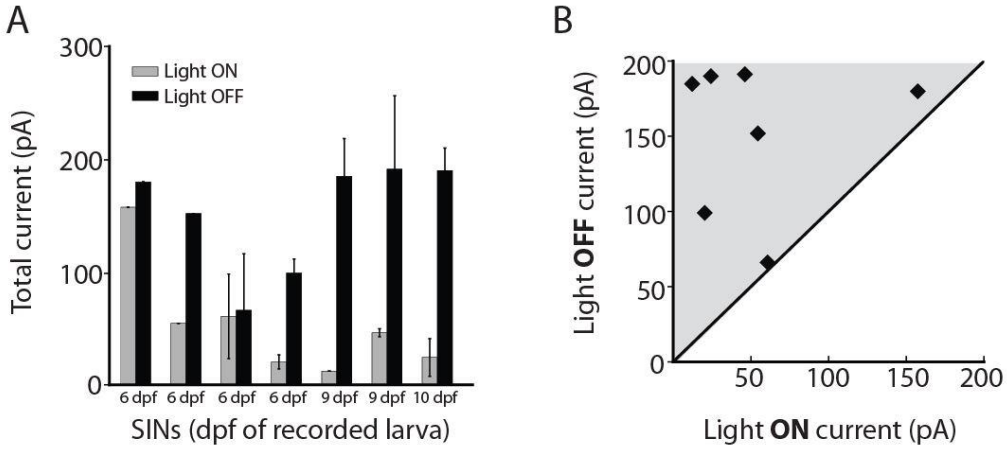

Figure 34: SINs receive greater synaptic input in conditions of low luminance. (A) When room lights were ON or OFF the synaptic input across all ages is increased in conditions of darkness (p = 0.007, paired t test). (**B**) Total current under light on conditions is plotted against total current for light off conditions. All cells fall above the unity line, displaying OFF tuning. n= 7 cells in 7 larvae.

4.3 Discussion

We found that SINs are responsive to overall luminance levels. How can we interpret these results in relation to previous studies suggesting SINs mediate size tuning? One important consideration is the visual stimulus. The size of a visual object can alter luminance and contrast profiles across the visual presentation area and it is likely that this confound contributed to different interpretations. The initial characterization of the SINs used a full screen flash (dark to light) and a vertical black bar moving across a lighter background. As the size of the black bar increases, so does the overall darkness across the visual stimulus. It is possible that the SINs respond to this change as opposed to the increase in the bar size. However, more detailed characterization using isoluminant stimuli is necessary.

A subsequent study identified subtypes of SINS with distinct size tuning (Preuss et al., 2014). It is difficult to compare this population of SINs with the SINs targeted in our experiments as both populations were targeted in different *Gal4* driver lines and therefore direct comparisons of the labelled populations cannot be made. This work demonstrated that SINs with more superficially stratified arbors are tuned to smaller objects and those with deeper stratified arbors are tuned to larger objects. This segregation of size tuning aligns with additional data reported in this study demonstrating that input from RGCs also displays a superficial to deep, small to large object size tuning. This result is in contrast with the original SIN study, which did not observe appreciable changes in the size tuning of retinal axons based on arborization layer. However, this is consistent with work by Semmelhack et al., which demonstrates RGC arbors optimally tuned to prey-like (small) stimuli arborize in the most superficial layers of the tectum (Semmelhack et al., 2014). How can these findings be reconciled? One possibility is the sensitivity of the calcium indicators. Earlier studies that did not observe RGC specific size layers used an early version of GCaMP (GCaMP1.6 vs. GCaMP3 and GCaMP6) with a much lower detection threshold (Chen et al., 2013; Nakai et al., 2001; Tian et al., 2009). Finally, despite a careful electrophysiological

characterization of subtypes, the most recent SIN study also did not control for overall contrast changes during the changing size stimulus. In future experiments it would be interesting to test if size tuning remained unchanged with overall changes in luminance or contrast of the visual stimulus.

Additional work will be needed to resolve the role of the SINs in visually mediated circuits. It is clear that some components of size filtering are disrupted in behavioral manipulations targeting SINs, but it remains uncertain if these defects arise from a loss of specific size-tuning properties or more general mechanisms for contrast and/or luminance calibration.

References

Adesnik, H., Bruns, W., Taniguchi, H., Huang, Z.J., and Scanziani, M. (2012). A neural circuit for spatial summation in visual cortex. Nature *490*, 226–231.

Barker, A.J., and Baier, H. (2013). SINs and SOMs: neural microcircuits for size tuning in the zebrafish and mouse visual pathway. Front. Neural Circuits *7*, 89.

Chen, T.-W., Wardill, T.J., Sun, Y., Pulver, S.R., Renninger, S.L., Baohan, A., Schreiter, E.R., Kerr, R.A., Orger, M.B., Jayaraman, V., et al. (2013). Ultrasensitive fluorescent proteins for imaging neuronal activity. Nature *499*, 295–300.

Del Bene, F., Wyart, C., Robles, E., Tran, A., Looger, L., Scott, E.K., Isacoff, E.Y., and Baier, H. (2010). Filtering of visual information in the tectum by an identified neural circuit. Science *330*, 669–673.

Fernandes, A.M., Fero, K., Arrenberg, A.B., Bergeron, S.A., Driever, W., and Burgess, H.A. (2012). Deep brain photoreceptors control light-seeking behavior in zebrafish larvae. Curr. Biol. CB *22*, 2042–2047.

Fischer, R.M., Fontinha, B.M., Kirchmaier, S., Steger, J., Bloch, S., Inoue, D., Panda, S., Rumpel, S., and Tessmar-Raible, K. (2013). Co-expression of VAL- and TMT-opsins uncovers ancient photosensory interneurons and motorneurons in the vertebrate brain. PLoS Biol. *11*, e1001585.

Gollisch, T., and Meister, M. (2008). Rapid neural coding in the retina with relative spike latencies. Science *319*, 1108–1111.

Kinoshita, M., and Ito, E. (2006). Roles of periventricular neurons in retinotectal transmission in the optic tectum. Prog. Neurobiol. *79*, 112–121.

Kinoshita, M., Ueda, R., Kojima, S., Sato, K., Watanabe, M., Urano, A., and Ito, E. (2002). Multiple-site optical recording for characterization of functional synaptic organization of the optic tectum of rainbow trout. Eur. J. Neurosci. *16*, 868–876.

Matsumoto, N., and Bando, T. (1980). Excitatory synaptic potentials and morphological classification of tectal neurons of the frog. Brain Res. *192*, 39–48.

Nakai, J., Ohkura, M., and Imoto, K. (2001). A high signal-to-noise Ca(2+) probe composed of a single green fluorescent protein. Nat. Biotechnol. *19*, 137–141.

Preuss, S.J., Trivedi, C.A., Vom Berg-Maurer, C.M., Ryu, S., and Bollmann, J.H. (2014). Classification of Object Size in Retinotectal Microcircuits. Curr. Biol. CB.

Scott, E.K., and Baier, H. (2009). The cellular architecture of the larval zebrafish tectum, as revealed by gal4 enhancer trap lines. Front. Neural Circuits *3*, 13.

Semmelhack, J.L., Donovan, J.C., Thiele, T.R., Kuehn, E., Laurell, E., and Baier, H. (2014). A dedicated visual pathway for prey detection in larval zebrafish. eLife *3*.

Tian, L., Hires, S.A., Mao, T., Huber, D., Chiappe, M.E., Chalasani, S.H., Petreanu, L., Akerboom, J., McKinney, S.A., Schreiter, E.R., et al. (2009). Imaging neural activity in worms, flies and mice with improved GCaMP calcium indicators. Nat. Methods *6*, 875–881.

Usrey, W.M., Reppas, J.B., and Reid, R.C. (1998). Paired-spike interactions and synaptic efficacy of retinal inputs to the thalamus. Nature *395*, 384–387.

Chapter 5: General Discussion

This work investigated the size classification of visual objects. From the perspective of the larval zebrafish the size of a novel object has immense consequences for survival. Potential predators will be large and potential food sources small. We explored this question from the level of sensory input to the level of behavioral output: investigating (1) how information about object size is organized in the brain to identify an object as “small” or “large” (2) how this classification is associated with a valence “good” vs. “bad” and finally (3) how object size and valence classification are used to generate a behavioral output (i.e.“approach” vs. “avoid”).

Several recent studies suggest that retinal inputs are exceptionally well-tuned to specific visual features when they arrive in the tectum (Gabriel et al., 2012; Nikolaou et al., 2012; Preuss et al., 2014; Semmelhack et al., 2014). These results raise an important question in relation to our work: to what extent is the classification of object size inherited from the retina versus generated *de* novo in the tectum? If the size tuning of tectal neurons can be attributed to pre-processing in the retina, how does the tectum contribute to size-mediated behavior? In several species, the tectum has demonstrated roles in determining object salience and location, and mediating orienting behavior and motor planning (Akert, 1949; Felsen and Mainen, 2012; Ingle, 1973; Krauzlis et al., 2013; Mysore and Knudsen, 2011; Salas et al., 1997). Importantly in the larval zebrafish ablations of the tectum inhibit prey capture (Gahtan et al., 2005), and visually-mediated escape (Temizer et al., 2015). Two recent studies characterize the response properties of RGCs to behaviorally relevant stimuli (optimal prey and looming objects), yet these studies do not ask how input from these retinal streams is further processed by the resident tectal neurons (Semmelhack et al., 2014; Temizer et al., 2015). In the case of Semmelhack et al, how, for example how do PVNs respond to prey stimuli? How are their tuning properties altered when AF7

RGC inputs are lost? Similarly two studies examining the activity in PVNs in response to prey capture stimuli do not link activity in these neurons to RGC activity (Bianco and Engert, 2015; Muto et al., 2013).

Experiments performed in this work provide a potential link. We confirm that loss of AF7-projecting RGCs results in a change in the overall size tuning profile of *Gal4mpn354* neurons, shifting the population tuning response to larger objects. The removal of *Gal4mpn354* neurons through genetically targeted ablation, results in a behavioral shift from approach to avoidance in response to small objects. Conversely, when activated *Gal4mpn354* neurons enhance approaches, but only to small sizes. A general approach enhancement pathway predicts increased approaches at all sizes. Restricted enhancement suggests the *Gal4mpn354* neurons are acting on pre-filtered information, (e.g. a “small object” pathway from the retina). As we were unable to shown a direct synaptic connection between RGCs and *Galmpn354* neurons it is possible that size information from the retina is further processed upstream of *Gal4mpn354* circuitry.

We hypothesize that the *Gal4mpn354* neurons act selectively on a “small object” classification circuit to enhance behavioral outputs for approach. This may be useful for the characterization of ambiguous stimuli. A miscalculation in the approach of a potential prey object is not life threatening, whereas the misclassification of a potential predator has potentially lethal consequences for the larval zebrafish. We propose one possible mechanism for *Gal4mpn354* action, providing a platform for future experiments (Figure 35).

Currently we are limited by techniques to further dissect intratectal circuitry. In the absence of reliable markers for tectal neurons or a classification of their inputs and outputs, it is difficult to further dissect the *Gal4mpn354* circuit components. The development of new tools such as virus tracing across synapses (Ginger et al., 2013) or the expansion of current tools such as Gal4 enhancer trapping lines (Asakawa and Kawakami, 2009; Scott et al., 2007) may contribute to

advancing our circuit dissection toolbox. However, the identification of the *Gal4mpn354* neurons provides a promising starting point for circuit analysis.

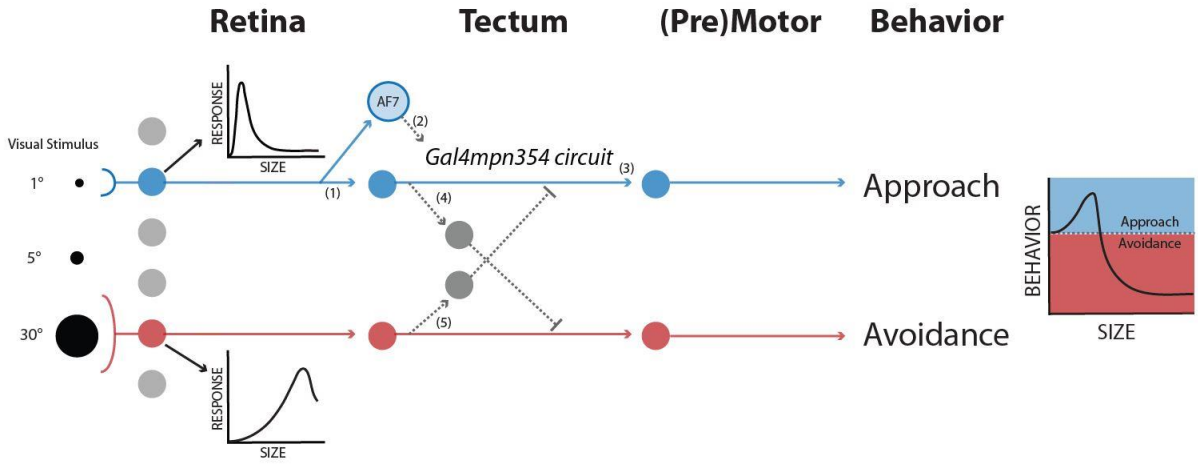

Figure 35: (1) *Gal4mpn354* neurons may receive input directly from RGCs or from tectal interneurons downstream of RGC input. Some of this input is likely from the AF7-projecting RGCs. (2) *Gal4mpn354* may also receive direct input, from resident neurons within AF7 sending projections to the tectum. (3) The *Gal4mpn354* circuit may act to enhance the filtering of small object information in the tectum or act directly to enhance the premotor circuitry for approach. (4) One mechanism for *Gal4mpn354* neuron action may be via reciprocal inhibition with a parallel avoidance pathway (5). The behavioral switch between, approach, and avoidance we observe in ablation experiments supports this hypothesis.

References

Akert, K. (1949) Der visuelle Greifreflex. Helv. Physiol. Pharmcol. Acta. 7, 112-134.

Asakawa, K., and Kawakami, K. (2009). The Tol2-mediated Gal4-UAS method for gene and enhancer trapping in zebrafish. Methods San Diego Calif *49*, 275–281.

Bianco, I.H., and Engert, F. (2015). Visuomotor transformations underlying hunting behavior in zebrafish. Curr. Biol. CB *25*, 831–846.

Felsen, G., and Mainen, Z.F. (2012). Midbrain contributions to sensorimotor decision making. J. Neurophysiol. *108*, 135–147.

Gabriel, J.P., Trivedi, C.A., Maurer, C.M., Ryu, S., and Bollmann, J.H. (2012). Layer-specific targeting of direction-selective neurons in the zebrafish optic tectum. Neuron *76*, 1147–1160.

Gahtan, E., Tanger, P., and Baier, H. (2005). Visual prey capture in larval zebrafish is controlled by identified reticulospinal neurons downstream of the tectum. J. Neurosci. Off. J. Soc. Neurosci. *25*, 9294–9303.

Ginger, M., Haberl, M., Conzelmann, K.-K., Schwarz, M.K., and Frick, A. (2013). Revealing the secrets of neuronal circuits with recombinant rabies virus technology. Front. Neural Circuits *7*, 2.

Ingle, D. (1973). Evolutionary perspectives on the function of the optic tectum. Brain. Behav. Evol. *8*, 211–237.

Krauzlis, R.J., Lovejoy, L.P., and Zénon, A. (2013). Superior colliculus and visual spatial attention. Annu. Rev. Neurosci. *36*, 165–182.

Muto, A., Ohkura, M., Abe, G., Nakai, J., and Kawakami, K. (2013). Real-time visualization of neuronal activity during perception. Curr. Biol. CB *23*, 307–311.

Mysore, S.P., and Knudsen, E.I. (2011). The role of a midbrain network in competitive stimulus selection. Curr. Opin. Neurobiol. *21*, 653–660.

Nikolaou, N., Lowe, A.S., Walker, A.S., Abbas, F., Hunter, P.R., Thompson, I.D., and Meyer, M.P. (2012). Parametric functional maps of visual inputs to the tectum. Neuron *76*, 317–324.

Preuss, S.J., Trivedi, C.A., Vom Berg-Maurer, C.M., Ryu, S., and Bollmann, J.H. (2014). Classification of Object Size in Retinotectal Microcircuits. Curr. Biol. CB.

Salas, C., Herrero, L., Rodriguez, F., and Torres, B. (1997). Tectal codification of eye movements in goldfish studied by electrical microstimulation. f. Neuroscience *78*, 271–288.

Scott, E.K., Mason, L., Arrenberg, A.B., Ziv, L., Gosse, N.J., Xiao, T., Chi, N.C., Asakawa, K., Kawakami, K., and Baier, H. (2007). Targeting neural circuitry in zebrafish using GAL4 enhancer trapping. Nat. Methods *4*, 323–326.

Semmelhack, J.L., Donovan, J.C., Thiele, T.R., Kuehn, E., Laurell, E., and Baier, H. (2014). A dedicated visual pathway for prey detection in larval zebrafish. eLife *3*.

Temizer, I., Donovan, J.C., Baier, H., and Semmelhack, J.L. (2015). A Visual Pathway for Looming-Evoked Escape in Larval Zebrafish. Curr. Biol. CB *25*, 1823–1834.

Chapter 6: Materials and Methods

6.1 Introduction

Techniques utilized in experiments described in this thesis are detailed in this chapter. In addition, general advances in neuroscience have made these experiments possible and will be reviewed briefly here.

Early work in neuroethology sought to link behavior to neural activity. Electrophysiological recordings provided information about the spiking properties of neurons in brain regions. Data collection was often limited to single units, in some cases clusters of neurons, and post hoc identification of these neurons was limited. The advent of molecular reporters and modulators of neural activity greatly expanded the number of neurons that could be simultaneously tracked and the specificity of which their identity can be assigned (Fenno et al., 2011; Nakai et al., 2001).

GCaMP: A genetically encodable sensor for neural activity

A landmark advance was the modification of the green fluorescent protein (GFP) to include a calcium sensitive domain. The resulting protein, GCaMP increased its fluorescence as a result of a conformational change induced by Ca^{+2} binding (Nakai et al., 2001). Previously calcium sensitive dyes have been and still are used to optically record neural activity, but the genetically-controllable expression GCaMP allowed for the possibility of cell type specific targeting. The newest versions of GCaMP are remarkably good, with the resolution of single spikes reported with a $99 \pm 0.2\%$ success rate (Chen et al., 2013). While these sensors lack the temporal resolution of direct electrical access to the neuron provided by electrophysiology they far exceed

these techniques in allowing for simultaneous imaging of network dynamics. This technology has been used to special advantage in the larval zebrafish, where the transparent brain of the larva and its relative numerically small size allowed for whole brain imaging during several behaviors (Kubo et al., 2014; Portugues et al., 2014).

Optogenetics: Methods for spatiotemporal activation and silencing of neuronal activity

In stride with advances in monitoring neural activity, technologies for controlling neural activity emerged. These technologies collectively described as “optogenetics” have taken advantage of light-gated ion channels, isolated from numerous microbes that can be genetically expressed in neurons. Light of discrete wavelengths is used to modulate the resting membrane potential of neurons expressing these light-gated pumps or channels and results in hyperpolarization or depolarization of the cell (Fenno et al., 2011). As with the genetically encoded calcium indicators (GECIs) current versions of the opsin driven actuators are very good at approximating neural activity with some versions able to sustain spike trains up to 200 Hz (Gunaydin et al., 2010).

Generating enhancer and gene trap transgenic lines: Targeted neuronal labeling

While the ability to control neurons is essential to the task of dissecting circuits, the question of which neurons to target and how to reliably do so is also pertinent. The zebrafish has proven remarkably tractable in generating transgenic lines using the *Tol2* system (Asakawa and Kawakami, 2009; Scott et al., 2007; Suster et al., 2009). This system uses the Tol2 transposon (isolated from medaka) to insert DNA sequences flanked by *Tol2* sites into the genome. In the zebrafish larvae, donor DNA and *Tol2* mRNA can be injected into the developing larva at the one cell stage, resulting in stable integration of target genes in a subset of injected larvae. This

technique has been utilized to create gene and enhancer trap lines, generating many transgenic Gal4 lines with sparse labeling of neuronal populations (Kawakami, 2007). Several of the transgenic lines used in this paper were generated by these techniques (Asakawa and Kawakami, 2009; Scott and Baier, 2009; Scott et al., 2007).

6.2 Experimental Procedures

Zebrafish maintenance and care. Zebrafish (*Danio rerio*) were maintained at 28°C on a 14hr light/10hr dark cycle using standard protocols (Westerfield, 2009). All animal procedures were performed in accordance with approved protocols. Transgenic lines were maintained in a TLN background (*Tüpel long-fin* (TL) wild-type strain carrying mutations in *mitfa* (nacre, N)). The following transgenic lines were used: *Tg(-7atoh7:GAL4-VP16)*, Et(Gal4-VP16)s1013t, Et(Gal4-VP16)s1038t, Et(Gal4-VP16)s1156t, *Tg(UAS:Kaede)*^{s1999t}, *Tg(UAS:nfsb-mCherry)*^{c264}, *Tg(UAS:Dendra-kras)*^{s1998t}, *Tg(UAS:GCaMP6s)mpn101, Tg(5xUAS:TeTxLCCFP)*^{zf85}, *Tg(UAS:GFP)mpn100, Tg(-2.7shha:GFP), BGUG Tg(pou4f3:GAL4, UAS:GAP43-GFP).* The *Gt*(*Gal4-FF)mpn354* line was identified in our lab by screening for genomic insertions of Gal4FF using the gene trap construct T2KSAGFF as described previously (Asakawa and Kawakami, 2009) . *Tg(vglut2a:loxP-DsRed-loxP-GFP)* (Satou et al., 2013) and *Tg*(*gad1b*: *loxP-DsRed-loxP-GFP*) (Satou et al., 2012) were acquired from S. Higashijima. All experiments were performed using larvae between 4 dpf and 15 dpf.

Reagents. All reagents were obtained from Sigma Aldrich or Invitrogen.

Size discrimination assay. A single larva was placed in a custom-built transparent plastic chamber (14 x 18 x 128 mm). The chamber was placed directly on an upward facing computer screen. Stimuli were generated on the screen using custom-written programs in Psychophysics toolbox (Brainard, 1997). A high-speed CCD camera (Guppy, Allied Vision Technologies), positioned above the behavioral chamber, recorded the larva's movements during the behavioral trial. Moving dots of maximal contrast (black dots on a white background) were presented in a pseudo-random order with both the position and size of the dots shuffled. The vertical distance between the screen and the larva was 15.8 mm and this value was used to calculate the visual angle subtended by the dot when positioned directly beneath the larva. Dot sizes calculated from these coordinates ranged from 1° to 50° of the larva's visual field. Nine dots of each size were presented during a single trial to ensure that a minimum of three larva-dot interactions was collected for analysis. Dots moved with a constant speed of 42°/s. Behavior was performed between 4 dpf and 15 dpf. For larvae in genetically targeted ablation experiments (using *UAS:Nfsb-mChry*, + MTZ), the behavioral assay was performed at 5 dpf prior to the addition of MTZ and again following ablation at 7 dpf. The level of water in the behavioral chamber was kept constant across experiments, and all experiments were performed with the room lights off, to ensure the only illumination was from the computer screen. Room temperature was maintained between 26 and 28°C. All behavioral experiments were performed during the natural light part of the larva's light/dark cycle. Video acquisition was performed with Active Dcam software (A&B Software) at 60 Hz. Images in Figure 6 were collected with a high-speed CMOS camera (Photonfocus) with StreamPix software (Norpix).

Calcium imaging. Calcium imaging was performed using a custom-built moveable objective microscope (MOM, Sutter Instruments) under a 20x objective (Olympus, 1.0NA). GCaMP6s was excited by a 920nm laser (Chameleon Ultra, Coherent). Larvae were embedded in 2.5% low

melting point agarose (Invitrogen) the day prior to imaging. Imaging was performed at 5 dpf or for AF7 ablation experiments at 6-7 dpf. Image acquisition was performed at 3.37 frames/s. ScanImage software was used for image acquisition and scanning control (Pologruto et al., 2003). Visual stimulation was presented on a miniature OLED screen (eMagin). To minimize light entering the PMTs, two magenta filters were placed on the screen. The visual stimulus was a gray bar moving across a black background. The speed of the bar was held constant for all trials (7.8°/s). Visual stimuli were generated using a custom-programmed graphical interface for Vision Egg (Straw, 2008). Visual stimuli were presented in a pseudo-random order to prevent habituation to stimuli. Each bar was presented for 4s, followed by a 2s period of visual stimulus off.

***BGUG* single cell labeling.** *Gt*(*Gal4-FF)mpn354, Tg(UAS:Nfsb-mchry)* fish were crossed to *Tg(pou4f3:GAL4, UAS:GAP43-GFP)* fish. Larvae were screened for double mCherry and GFP expression and single cells labeled in GFP were imaged (experiment repeated two times, n = 3 larvae with single cell labeling).

Confocal imaging. Confocal imaging was performed using Zeiss LSM700 or LSM780 microscopes with associated ZEN software. To confirm genetically targeted ablations, the same acquisition settings were used for pre- and post-ablation image collection. For all figures, where representative expression patterns are displayed, at least 5 larvae were imaged per condition.

Nitroreductase ablations. Larvae expressing *Tg(UAS:nfsb-mCherry)*^{c264}, were treated with 10mM metronidazole (MTZ, Sigma Aldrich) in Danieau's solution at 5 dpf for 12 h in a light protected chamber, as previously described (Pisharath et al., 2007). MTZ solution was removed

and larvae allowed to recover for 24 h before imaging or behavioral experiments were performed (see Figure 36).

Single cell laser ablations. Targeted laser ablations were performed using a Chameleon Ultra, Coherent laser (850 nm wavelength) at ~40 mW power after the objective. ScanImage software was used for image acquisition and scanning control (Pologruto et al., 2003). For ablations the laser was scanned over the target cell for ~10 ms in a 16 x 16 pixel window, zoom 50-100. *Gals1156t*, *UAS:Kaede* larvae were used to visualize SINs for ablation (see Figure 37). For targeted ablations of *Gal4mpn354* neurons (see Figure 22), cells were targeted in a *Gal4mpn354, UAS:GCaMP6s* (TLN, *nacre*) background.

Optogenetic manipulations. *Gal4mpn354, UAS:GCaMP6s* larvae were in crossed and injected with *Tg*(*Tol2-UAS:ChR2(H134R)-mCherry)s1986t* and transposase mRNA at the one-cell stage. Embryos were screened for mCherry expression in the *Gal4mpn354* pattern. Positive embryos and wild type controls were used in behavioral experiments with the size discrimination assay (as described above). A custom-made blue light (475 nm) LED array surrounded the behavioral chamber. LEDs were pulsed at 10 Hz (20% duty cycle) during the behavioral experiments. LEDs were acquired from www.leds.de (Cree XP-E 2, blue).

AF7 ablations. Ablations were performed as previously described (Semmelhack et al., 2014 and see Figure 27B), except a protocol was chosen to cause more extensive damage to RGC axons in the AF7 neuropil. In brief, ablations were performed using a 40x objective, at 850nm (Chameleon Ultra, Coherent, ~40 mW power after the objective). Ablations were performed in 5 dpf or 6 dpf larvae, either uni- or bi-laterally. In some cases size tuning was acquired prior to and

following ablation. Calcium imaging was performed at 6 dpf or 7 dpf. Cells were classified as imaged in “intact AF7” conditions if the ipsilateral AF7 was intact at the time of imaging, or “ablated AF7” conditions if the ipsilateral AF7 was ablated at the time of imaging. Ablations were confirmed visually by confocal imaging 12-24 h after ablation. Analysis of calcium imaging was performed as described below.

Calcium imaging. Raw fluorescence values were extracted using the Time Series Analyzer V2.0 plug-in for ImageJ (Schneider et al., 2012). Z scores were calculated from dF/F values obtained from the raw fluorescence traces. To calculate each Z score a minimum of three trials was averaged. For each trial, an average pixel intensity was extracted across all frames in the time series, within a designated ROI. (The same ROI size (2µm x 2µm) was used for each cell). ROIs were taken at the cell body, or where the cell could not be clearly identified, from the proximal dendrite. Fluorescence was averaged across the stimulus presentation period of 4 seconds, with the 2s stimulus-off preceding each stimulus used to calculate baseline fluorescence. Raw dF/F traces are presented across trials to show trial-to-trial variability in Figure 25C-E, Figure 26B, C. Background from the stimulus presentation was subtracted from all frames prior to analysis on a frame-by-frame basis using raw fluorescence values from a ROI outside of the biological sample. For data shown in Figure 26D, E and 27C, D, the assignment of size tuning was defined by the Z score. Cells with a Z score of 0.8 or greater were counted as “tuned” to the given size. In *Gal4mpn354, UAS:GCaMP6s* larvae, 27.8 (SEM $\pm$ 2.87) cells were labeled in the combined optic tecta. Of these 45% (SEM $\pm$ 0.05%) responded across three trials. Cells were further excluded from analysis if all trials did not result in a minimum dF/F value of 0.10. For Z score heat maps displayed in Figures 25-27, cells were ordered by size. Cells were binned into groups based on the smallest size, which generated a Z score of greater than 0.8. Within these bins, cells were ordered by highest to lowest Z score.

Behavioral analysis. All video recordings were blinded before analysis by an independent observer and unblinded after data analysis was complete. A minimum of three dot-larva interactions was required for each size. Data for behavioral trials was averaged for each fish and then averaged as a population. An avoidance was scored when the larvae generated a rapid movement away from a moving dot entering the central 200° of its visual field. An approach was scored when the larvae made directed movements toward a dot within the central 200° of its visual field. A neutral interaction, i.e., no response, was scored when a dot entering the central 200° visual field did not cause the larva to change its direction of swimming or if the larva remained stationary. For ablation experiments, larvae were only included if they showed an R.I. of ≤-0.6 to 30° dots prior to the ablation procedure.

Statistics. For the size discrimination assay, two-way ANOVA tests with Bonferroni or Tukey's correction for multiple comparisons were used. One-sample t tests were used to test if responses to any size were significantly different from 0. To test the normality and the homoscedasticity of the behavioral tuning curves, we used the D'Agostino and Pearson test ($p = 0.0316$ for Figure 9A) and Bartlett's test ($p = 0.0872$ for Figure 9A, (excluding 5°)) respectively. These results met the criteria for parametric statistical testing. For statistics performed on data represented by the V.I., the Fisher's exact test was used. For normalized population responses, summed Z scores for each size (positive Z score values only) were normalized to the maximum value, and comparisons between the two populations were made using the Mann-Whitney U test. Statistical tests were performed using programs in GraphPad Prism 6.0 or the statistical toolbox in Matlab 2014b. In all figures, * indicates $p < 0.05$; ** indicates $p < 0.005$; *** indicates $p < 0.0005$. All t tests are two-tailed. All error bars are $\pm$ SEM. n = number of larvae unless otherwise indicated.

Optomotor response (OMR). OMR was tested in the same behavioral set-up used for the size discrimination assay. Visual stimuli consisted of moving gratings of 136° spatial frequency. Gratings were presented in opposing directions for a minimum of three trials. The OMR index was calculated as the amount of time the larva spent swimming in the direction of the gratings minus the amount of time spent swimming against the gratings, divided by the total amount of time the larva was swimming. A value of 1 indicated an OMR that was perfectly correlated to the direction of the moving gratings and a value of -1, a response that was perfectly anti-correlated to the direction of the moving gratings.

Enucleation: Enucleation was performed on 4 or 5 dpf larvae (wild type, TL background). Larvae were anesthetized with 0.02% tricaine and mounted in 2% low melting point agarose (Invitrogen). A 25G sterile needle and #55 forceps (Fine Science Tools) were used to gently remove the eyes. Larvae were removed from the agarose and allowed to recover overnight. Mobility was tested on the following day and if unimpaired behavioral experiments were performed the next day at 7 dpf.

Electrophysiology: Whole-cell patch clamp recordings were performed on 4 -10 dpf larvae following standard protocols (Arrenberg et al., 2009; Engert et al., 2002). Larvae were anesthetized on ice and mounted in 2% low melting point agarose in external solution. A small incision was made at the base of the tectum with a sharp glass electrode and a small piece of skin was peeled away to expose an area for recording where SINs were visible. SINs were targeted for recordings in *Gals1156t*, *UAS:Kaede* larvae under a Zeiss Axioscope2. The following recording solutions were used: External solution (in mM): 115 NaCl, 2 KCl, 10 HEPES, 2 $CaCl_2$, 10 Glucose, 1.5 $MgCl_2$, pH 7.4; Internal solution (in mM): 110 Potassium gluconate ($C_6H_{11}KO_7$),

10 KCl, 5 NaCl, 1.5 $MgCl_2$, 20 HEPES, 0.5 EGTA, pH 7.3. Patch pipettes (8–10 MΩ resistance) were pulled from Borosilicate glass (O.D. 1.5 mm, I.D. 0.86 mm; Sutter Instruments BF 150-86-10). Data were low-pass filtered (2 kHz, Axopatch 200B, Axon Instruments) and digitized (10kHz, Digidata 1440A, Axon Instruments). Data was analyzed with pClamp software (Molecular Devices). Visual stimulation was presented on a miniature OLED screen (eMagin).

Paramecium capture assay: For paramecium, capture experiments 10-20 paramecia (*Paramecium multimicronucleatum*, Carolina Biological Supply Company, Burlington, NC) were added to a single well of a 24-well dish along with a single larva in 1mL of Danieau's solution. Paramecia in each dish were counted at 15 minute intervals for two hours, at which point 50% of the paramecia were lost in positive control conditions.

6. 3 Figures related to Experimental Procedures

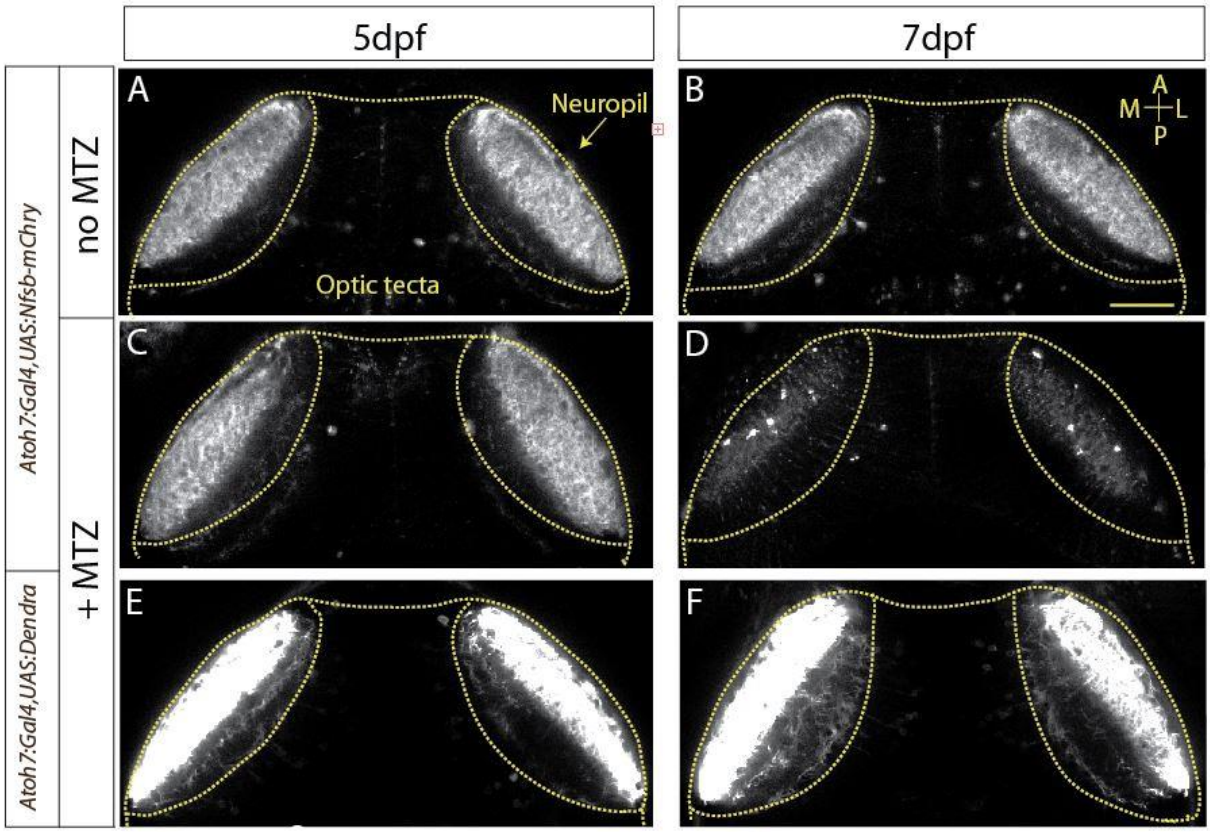

Figure 36: Effectiveness and specificity of cell ablations. (**A-F**) Nitroreductase-mediated ablation of RGCs. Top views of the optic tectum at 5 dpf (**A, C, E**) and at 7 dpf (**B, D, F**). (**A, B**) shows an untreated *Atoh7*:*Gal4, UAS:Nfsb-mChry* larva. (**C, D**) shows an MTZ-treated *Atoh7*:*Gal4, UAS:Nfsb-mChry* larva. Note almost complete loss of RGC arbors within the tectal neuropil. Remaining fluorescent blebs are remnants of degenerated axons. (**E, F**) shows an MTZ-treated *Atoh7*:*Gal4, UAS:Dendra* larva. MTZ (10mM) was given for 12 hours at 5 dpf, followed by a recovery period. \ Scale bar for (A-F) = 50µm. A = anterior, P = posterior, M = medial, L = lateral. Hatched yellow lines denote the neuropil of the optic tecta for each image in (A-F) (also denoted with arrow in (A)).

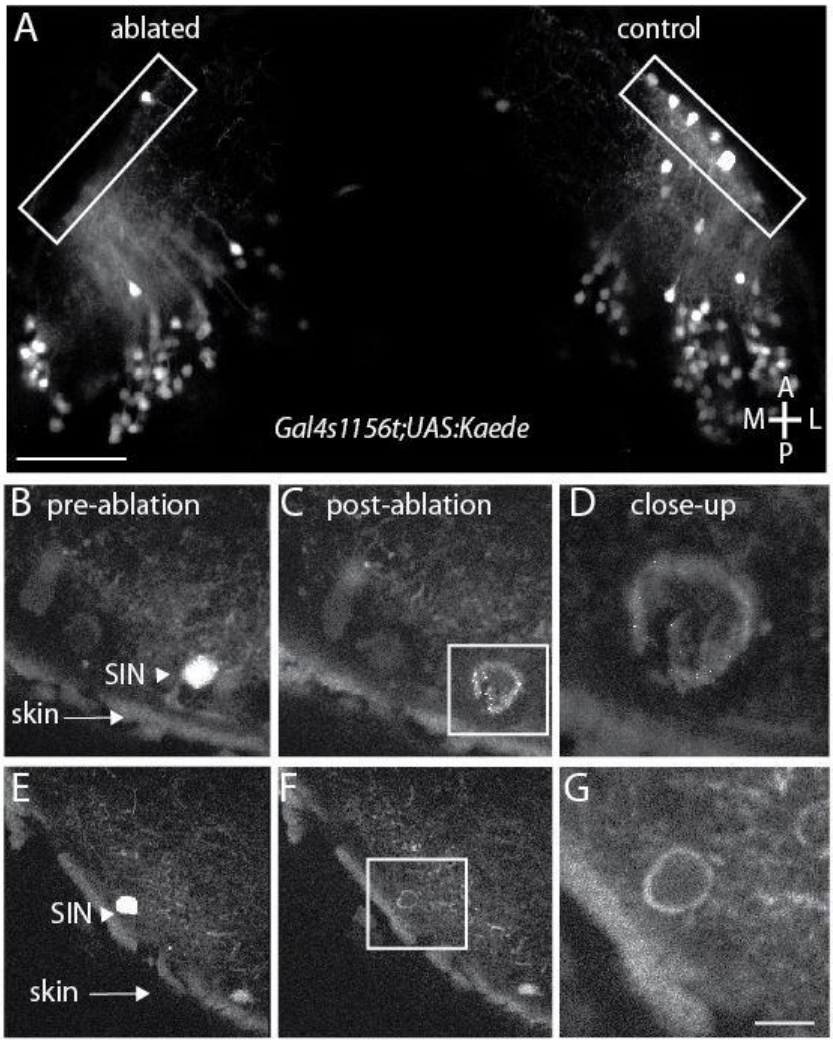

Figure 37: (**A-G**) Two-photon targeted ablations of SINs. (**A**) Following targeted ablations of SINs in *Gal4s1156t, UAS:Kaede* 6 dpf larva, fish were allowed to recover overnight and then subjected to the behavioral assay. Imaging at 7 dpf demonstrates near complete ablation of SINs in the left ('ablated') tecta but not in the right ('control') tecta. The superficial area of the tectal neuropil where the SIN cell bodies are located is enclosed by a white box. (**B-G**) Two examples of pre and post ablations. (**B**) and (**E**) SINs are superficially located within the tectum, autofluorescence from the skin is indicated with an arrow, white arrowheads indicate SINs prior to ablation. (**C**) and (**F**) immediately following ablation the cells in (B) and (E) are imaged again. Corresponding close-ups are shown in (**D**) and (**G**) and display cellular debris remaining from ablation with the focused beam of the 2-photon laser. Damage is restricted to the targeted cell and does not spread to neighboring tissue. Scale bar for (A) = 50µm, for (G) = 10 µm. A = anterior, P = posterior, M = medial, L = lateral.

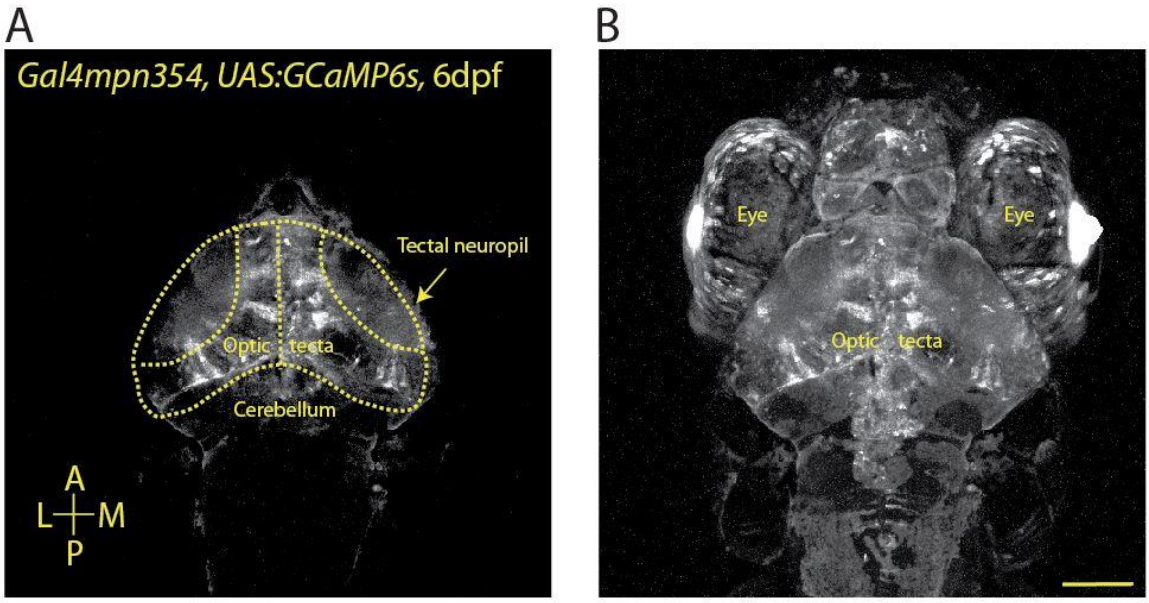

Figure 38: (**A**) 10x image of *Gal4mpn354* driving expression of *UAS:GCaMP6s* in a 6 dpf larva. (**B**) Maximum fluorescence projection of image in (A) through the entire larva. Eyes and skin are visible due to autofluorescence. Eyes are labeled in (B). A = anterior, P = posterior, M = medial, L = lateral; Scale bar = 100 µm**.**

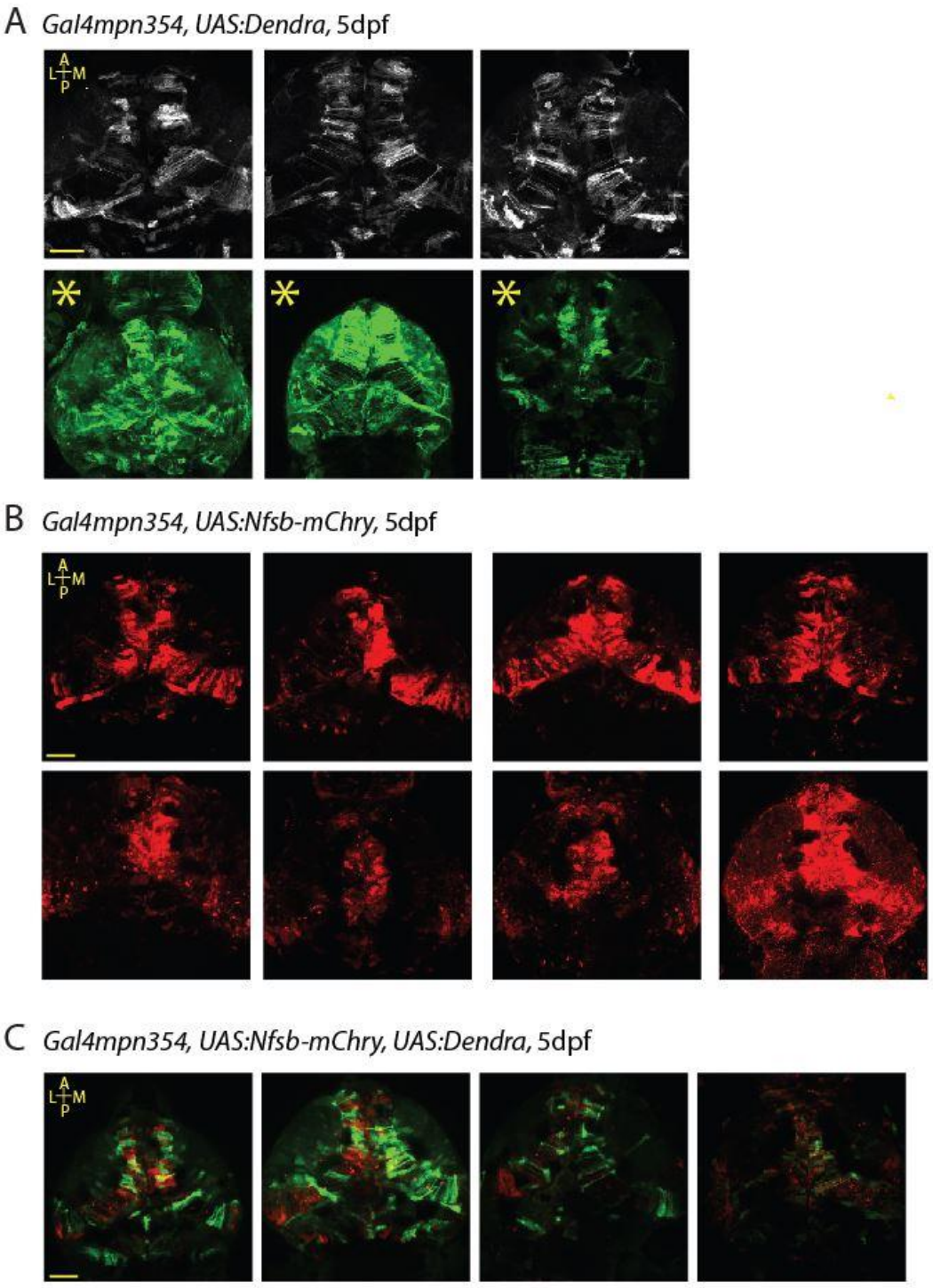

Figure 39: Expression of *Gal4mpn354* driver line in multiple UAS lines. (**A**) Examples of six fish with *Gal4mpn354* driving expression in *UAS:Dendra* (white or green pseudocolor). Yellow asterisks indicate expression patterns that were excluded from behavioral experiments due to extratectal expression when observed in any UAS line. (**B**) Examples of the expression pattern in eight fish with *Gal4mpn354* driving *UAS:Nfsb-mCherry.* (**C**) Examples of 4 fish with *Gal4mpn354* expression driving *UAS:Dendra* and *UAS:Nfsb-mCherry*. All fish are 5 dpf. All fish shown in (B) were used in behavioral experiments. A = anterior, P = posterior, M = medial, L = lateral; Scale = 50 µm.

References

Arrenberg, A.B., Del Bene, F., and Baier, H. (2009). Optical control of zebrafish behavior with halorhodopsin. Proc. Natl. Acad. Sci. U. S. A. *106*, 17968–17973.

Asakawa, K., and Kawakami, K. (2009). The Tol2-mediated Gal4-UAS method for gene and enhancer trapping in zebrafish. Methods San Diego Calif *49*, 275–281.

Brainard, D.H. (1997). The Psychophysics Toolbox. Spat. Vis. *10*, 433–436.

Chen, T.-W., Wardill, T.J., Sun, Y., Pulver, S.R., Renninger, S.L., Baohan, A., Schreiter, E.R., Kerr, R.A., Orger, M.B., Jayaraman, V., et al. (2013). Ultrasensitive fluorescent proteins for imaging neuronal activity. Nature *499*, 295–300.

Engert, F., Tao, H.W., Zhang, L.I., and Poo, M. (2002). Moving visual stimuli rapidly induce direction sensitivity of developing tectal neurons. Nature *419*, 470–475.

Fenno, L., Yizhar, O., and Deisseroth, K. (2011). The development and application of optogenetics. Annu. Rev. Neurosci. *34*, 389–412.

Gunaydin, L.A., Yizhar, O., Berndt, A., Sohal, V.S., Deisseroth, K., and Hegemann, P. (2010). Ultrafast optogenetic control. Nat. Neurosci. *13*, 387–392.

Kawakami, K. (2007). Tol2: a versatile gene transfer vector in vertebrates. Genome Biol. *8 Suppl 1*, S7.

Kubo, F., Hablitzel, B., Dal Maschio, M., Driever, W., Baier, H., and Arrenberg, A.B. (2014). Functional architecture of an optic flow-responsive area that drives horizontal eye movements in zebrafish. Neuron *81*, 1344–1359.

Nakai, J., Ohkura, M., and Imoto, K. (2001). A high signal-to-noise Ca(2+) probe composed of a single green fluorescent protein. Nat. Biotechnol. *19*, 137–141.

Pisharath, H., Rhee, J.M., Swanson, M.A., Leach, S.D., and Parsons, M.J. (2007). Targeted ablation of beta cells in the embryonic zebrafish pancreas using E. coli nitroreductase. Mech. Dev. *124*, 218–229.

Pologruto, T.A., Sabatini, B.L., and Svoboda, K. (2003). ScanImage: flexible software for operating laser scanning microscopes. Biomed. Eng. Online *2*, 13.

Portugues, R., Feierstein, C.E., Engert, F., and Orger, M.B. (2014). Whole-brain activity maps reveal stereotyped, distributed networks for visuomotor behavior. Neuron *81*, 1328–1343.

Satou, C., Kimura, Y., and Higashijima, S. (2012). Generation of multiple classes of V0 neurons in zebrafish spinal cord: progenitor heterogeneity and temporal control of neuronal diversity. J. Neurosci. Off. J. Soc. Neurosci. *32*, 1771–1783.

Satou, C., Kimura, Y., Hirata, H., Suster, M.L., Kawakami, K., and Higashijima, S. (2013). Transgenic tools to characterize neuronal properties of discrete populations of zebrafish neurons. Dev. Camb. Engl. *140*, 3927–3931.

Schneider, C.A., Rasband, W.S., and Eliceiri, K.W. (2012). NIH Image to ImageJ: 25 years of image analysis. Nat. Methods *9*, 671–675.

Scott, E.K., and Baier, H. (2009). The cellular architecture of the larval zebrafish tectum, as revealed by gal4 enhancer trap lines. Front. Neural Circuits *3*, 13.

Scott, E.K., Mason, L., Arrenberg, A.B., Ziv, L., Gosse, N.J., Xiao, T., Chi, N.C., Asakawa, K., Kawakami, K., and Baier, H. (2007). Targeting neural circuitry in zebrafish using GAL4 enhancer trapping. Nat. Methods *4*, 323–326.

Semmelhack, J.L., Donovan, J.C., Thiele, T.R., Kuehn, E., Laurell, E., and Baier, H. (2014). A dedicated visual pathway for prey detection in larval zebrafish. eLife *3*.

Straw, A.D. (2008). Vision egg: an open-source library for realtime visual stimulus generation. Front. Neuroinformatics *2*, 4.

Suster, M.L., Kikuta, H., Urasaki, A., Asakawa, K., and Kawakami, K. (2009). Transgenesis in zebrafish with the tol2 transposon system. Methods Mol. Biol. Clifton NJ *561*, 41–63.

Westerfield M. (2009). Essential zebrafish methods: cell and developmental biology (Amsterdam: Elsevier).

Publishing Agreement

It is the policy of the University to encourage the distribution of all theses, dissertations, and manuscripts. Copies of all UCSF theses, dissertations, and manuscripts will be routed to the library via the Graduate Division. The library will make all theses, dissertations, and manuscripts accessible to the public and will preserve these to the best of their abilities, in perpetuity.

Please sign the following statement:

I hereby grant permission to the Graduate Division of the University of California, San Francisco to release copies of my thesis, dissertation, or manuscript to the Campus Library to provide access and preservation, in whole or in part, in perpetuity.

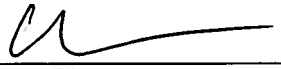

Author Signature

11/9/15

Date